

AD-A266 411

51



National
Defence

Défense
nationale



INTERFEROMETRIC GPS ATTITUDE: A STOCHASTIC ERROR MODEL (U)

by

J. Chris McMillan

DTIC
ELECTE
JUL 02 1993
S A D

This document has been approved
for public release and sale; its
distribution is unlimited.

DEFENCE RESEARCH ESTABLISHMENT OTTAWA
REPORT NO. 1168

Canada

February 1993
Ottawa

80
pgs

93-15132

98 7





National
Defence Défense
nationale

DMIC QUALITY INSPECTED 5

INTERFEROMETRIC GPS ATTITUDE: A STOCHASTIC ERROR MODEL (U)

by

J. Chris McMillan
*Communication and Navigation Section
Electronics Division*

Accession For	NTIS CR&EI	✓
DMIC	148	<input type="checkbox"/>
Unsolicited		<input type="checkbox"/>
Justification		
By		
Distribution		
Availability Codes		
Dist	Avail. 100% or S. 100%	<input type="checkbox"/>
A-1		

DEFENCE RESEARCH ESTABLISHMENT OTTAWA
REPORT NO. 1168

PCN
041LJ

February 1993
Ottawa

ABSTRACT

During the August 1992 sea trial off the west coast of Vancouver Island, onboard the CFAV Endeavour, data was collected from a relatively new type of GPS (Global Positioning System) receiver which measures attitude (heading, pitch and roll) as well as the usual GPS measurements of position and velocity. GPS attitude has the potential to provide rapid and precise attitude for a relatively low cost. Attitude is conventionally determined using inertial equipment, which for precise work is very expensive, large and requires a long "settling time" after turn-on. The receiver being evaluated on this sea trial was an Ashtech Three-Dimensional Direction Finding System (3DF). This report provides some general background on GPS attitude technology, presents the attitude errors observed during this sea trial and characterizes these errors as stochastic processes.

RÉSUMÉ

Au mois d'août 1992, lors d'un essai en mer au large de la côte ouest de l'Ile de Vancouver, à bord du CFAV Endeavour, des données ont été mesurées à l'aide d'un système relativement nouveau de récepteur SPG (Système de position globale) qui mesure l'attitude (direction, inclinaison et roulement) en plus des mesures SPG normales de position et de vitesse. L'attitude SPG peut permettre de donner rapidement et précisément l'attitude à un coût relativement bas. L'attitude est déterminée conventionnellement en utilisant l'équipement inertiel, qui, lorsqu'employé pour un travail de précision, s'avère très dispendieux, est encombrant et nécessite une longue période de réchauffement après l'allumage. Le récepteur évalué lors de cet essai en mer était un Système à trois-dimensions pour déterminer la direction de Ashtech. Ce rapport présente de l'information générale sur la technologie de l'attitude SPG ainsi que les erreurs d'attitude observées durant l'essai en mer. Il caractérise ces erreurs comme étant des procédures stochastiques.

EXECUTIVE SUMMARY

During the August 1992 sea trial off the west coast of Vancouver Island, onboard the CFAV Endeavour, data was collected from a new type of GPS (Global Positioning System) receiver which measures attitude (heading, pitch and roll) as well as the usual GPS measurements of position and velocity. This type of receiver uses GPS carrier phase difference measurements between pairs of antennas (using interferometric techniques). This method has been discussed in the literature since the late 1970's but is only now becoming practical due to recent developments in receiver hardware technology.

Attitude is conventionally determined using inertial equipment, which for precise work is very expensive, very large and heavy, requires a long "settling time" after turn-on and has high latitude limitations. This new type of GPS receiver however has the potential to provide rapid and precise attitude for a relatively low cost. Of course inertial attitude also has several advantages over GPS, such as providing high bandwidth output (high data rates) and being unaffected by jamming, spoofing, multipath, or loss-of-signal. It would seem that the best solution in many cases would be an integrated system with GPS attitude combined with a low cost inertial system. To investigate the potential performance of such an integrated system it is necessary to characterize the errors of the GPS attitude in a stochastic model.

The receiver being evaluated on this sea trial was an Ashtech Three-Dimensional Direction Finding System (3DF), which is a 24 channel, C/A code receiver with four antennas. For this trial the antennas were configured as a roughly level square with 10 metre sides. Precise position and attitude reference data was available throughout the trial from the DIINS (Dual Inertial Integrated Navigation System) equipment, which was also onboard. The accuracy of the raw inertial reference attitude was at least about 0.07 degrees in heading and 0.03 degrees in pitch and roll (rms). More importantly, the noise and other short-correlation-time errors of the reference system are much smaller than that of the 3DF. The reference data was available at 0.16 second intervals throughout the 7 day trial, providing almost four million data sets. Post processing the inertial reference data with differential GPS position measurements improved the reference attitude accuracy to about 0.01 degrees (rms).

The GPS attitude was generally available at one second intervals, but about 10% of the data was not available and a further 10% was flagged as invalid (carrier phase cycle ambiguity not resolved) and in fact had very large errors. In this case the 3DF sets the pitch and roll to zero and the heading is based on code phase measurements (which are much noisier than carrier phase measurements).

The accuracy of the valid GPS attitude data was first measured at the discrete one second points for which it was available and was found to be about 0.5 degrees in heading and 1.2 degrees in pitch and roll (rms). However this was due to a small amount of poor data (less than one percent) and perhaps a better measure of performance is the 95 percentile, which was 0.1 degrees for heading and 1.2 degrees for pitch and roll. Furthermore, most of these pitch and roll errors were dominated by biases, which presumably could have been removed by proper calibration. When these biases were removed the remaining pitch and roll errors were

significantly reduced to about 0.1 degrees (95%). As mentioned, these numbers are based on the comparison of only the available (at one second intervals) and valid GPS data with the corresponding reference data and are therefore referred to as "discrete-dynamic" errors. Thus the discrete-dynamic attitude accuracy in this configuration appears to be about 2 milliradians at the 95% level.

The true "continuous-dynamic" performance is somewhat worse when consideration is taken of the changes in the platform attitude between the one second GPS data points. This performance is measured by comparing the (unextrapolated) GPS data to all of the 0.16 second reference data. The rms errors, again dominated by a small amount of very poor data, were at the 0.6 degree level for heading and 1.3 degree level for pitch and roll. The 95 percentile continuous-dynamic accuracy of the GPS attitude was found to be about 0.4 degrees in heading and 1.9 degrees in pitch and roll. With the biases removed, these continuous-dynamic pitch and roll errors were reduced to 0.9 degrees (95%). The GPS receiver under evaluation is supposed to be capable of a slightly higher output rate (2 Hz). Although higher rates may lead to increased noise, they could also presumably reduce the continuous-dynamic errors, and in any case, if this were used to aid an inertial system the continuous-dynamic errors would not be relevant.

The stochastic behaviour of the attitude errors collected over this week-long trial could be modeled quite accurately as the sum of three independent components: a constant bias, uncorrelated white noise and a first order Markov process. The bias was on the order of one degree and is likely an installation/calibration error which could be quite easily removed. The noise and Markov processes were each at about the 0.03 degree level (0.5 milliradian), one sigma. For applications where this is not acceptable, or where better bandwidth is required (such as for fire control) then integration with even a low cost inertial system could provide very good sub-milliradian attitude data.

Considerable care must be taken when extending these results to other situations. In the static situation, such as artillery pointing, the noise may be reduced by longer sampling periods, however the multipath errors may create worse temporally correlated errors (i.e. Markov). In the marine environment these multipath errors are partially randomized or "whitened" by the wave-induced motion of the ship.

This type of receiver therefore shows considerable promise as an aid to navigation, either by itself if high bandwidth and continuous data is not essential, or integrated with an inertial system.

TABLE OF CONTENTS

	page
ABSTRACT	iii
EXECUTIVE SUMMARY	v
LIST OF FIGURES	ix
LIST OF TABLES	xi
1. INTRODUCTION	1
2. BACKGROUND	3
3. SEA TRIAL METHODOLOGY	10
3.1 Equipment	11
3.2 Expected 3DF Performance	12
3.3 Reference System Performance	15
4. RAW DATA	18
5. MEASURED 3DF ERROR BEHAVIOUR	23
5.1 Discrete-Dynamic Performance	23
5.2 Continuous-Dynamic Performance	25
6. STOCHASTIC ERROR MODEL	37
6.1 Autocorrelation Functions	38
6.2 Cross-Correlation Functions	43
6.3 Kalman Filter Model	44
7. ACKNOWLEDGMENTS	50
8. CONCLUSIONS	51
REFERENCES	53
APPENDIX A. PLATFORM DYNAMICS	55
APPENDIX B. DAILY ERROR PLOTS	57

LIST OF FIGURES

	page
FIGURE 1. INTERFEROMETER PRINCIPLE	3
FIGURE 2. ACCURACY VS BASELINE LENGTH	7
FIGURE 3. ACCURACY VS SAMPLE PERIOD	8
FIGURE 4. AREA OF OPERATION	10
FIGURE 5. GPS ANTENNA ARRAY INSTALLATION	11
FIGURE 6. GPS ANTENNA ARRAY GEOMETRY	12
FIGURE 7. VIEW OF ANTENNA ARRAY	14
FIGURE 8. AVAILABILITY	19
FIGURE 9. RAW 3DF HEADING	20
FIGURE 10. RAW 3DF PITCH	20
FIGURE 11. RAW 3DF ROLL	20
FIGURE 12. DETAIL OF 3DF & REFERENCE HEADING	21
FIGURE 13. DETAIL OF 3DF & REFERENCE PITCH	21
FIGURE 14. DETAIL OF 3DF & REFERENCE ROLL	21
FIGURE 15. 3DF MRMS	22
FIGURE 16. 3DF BRMS	22
FIGURE 17. DISCRETE HEADING ERROR VS TIME	27
FIGURE 18. DISCRETE PITCH ERROR VS TIME	27
FIGURE 19. DISCRETE ROLL ERROR VS TIME	27
FIGURE 20. DISCRETE HEADING ERROR VS TIME (rescaled)	28
FIGURE 21. DISCRETE PITCH ERROR VS TIME (rescaled)	28
FIGURE 22. DISCRETE ROLL ERROR VS TIME (rescaled)	28
FIGURE 23. DETAILED VIEW OF HEADING ERROR	29
FIGURE 24. DETAILED VIEW OF PITCH ERROR	29
FIGURE 25. DETAILED VIEW OF ROLL ERROR	29
FIGURE 26. DISCRETE HEADING ERROR PERCENTILES	30
FIGURE 27. DISCRETE PITCH ERROR PERCENTILES	30
FIGURE 28. DISCRETE ROLL ERROR PERCENTILES	30
FIGURE 29. DISCRETE HEADING ERROR PERCENTILES (rescaled)	31
FIGURE 30. DISCRETE PITCH ERROR PERCENTILES (rescaled)	31
FIGURE 31. DISCRETE ROLL ERROR PERCENTILES (rescaled)	31
FIGURE 32. CONTINUOUS HEADING ERROR VS TIME	32
FIGURE 33. CONTINUOUS PITCH ERROR VS TIME	32
FIGURE 34. CONTINUOUS ROLL ERROR VS TIME	32
FIGURE 35. CONTINUOUS HEADING ERROR VS TIME (rescaled)	33
FIGURE 36. CONTINUOUS PITCH ERROR VS TIME (rescaled)	33
FIGURE 37. CONTINUOUS ROLL ERROR VS TIME (rescaled)	33
FIGURE 38. DETAILED VIEW OF HEADING ERROR	34
FIGURE 39. DETAILED VIEW OF PITCH ERROR	34
FIGURE 40. DETAILED VIEW OF ROLL ERROR	34

FIGURE 41. CONTINUOUS HEADING ERROR PERCENTILES	35
FIGURE 42. CONTINUOUS PITCH ERROR PERCENTILES	35
FIGURE 43. CONTINUOUS ROLL ERROR PERCENTILES	35
FIGURE 44. CONTINUOUS HEADING ERROR PERCENTILES (rescaled)	36
FIGURE 45. CONTINUOUS PITCH ERROR PERCENTILES (rescaled)	36
FIGURE 46. CONTINUOUS ROLL ERROR PERCENTILES (rescaled)	36
FIGURE 47. HEADING ERROR AUTOCORRELATION FUNCTION	45
FIGURE 48. PITCH ERROR AUTOCORRELATION FUNCTION	45
FIGURE 49. ROLL ERROR AUTOCORRELATION FUNCTION	45
FIGURE 50. HEADING ERROR AUTOCORRELATION FUNCTION DETAIL	46
FIGURE 51. PITCH ERROR AUTOCORRELATION FUNCTION DETAIL	46
FIGURE 52. ROLL ERROR AUTOCORRELATION FUNCTION DETAIL	46
FIGURE 53. HEADING ERROR AUTOCORRELATION (Fine Detail)	47
FIGURE 54. PITCH ERROR AUTOCORRELATION (Fine Detail)	47
FIGURE 55. ROLL ERROR AUTOCORRELATION (Fine Detail)	47
FIGURE 56. HEADING/PITCH CROSS-CORRELATION FUNCTION	48
FIGURE 57. HEADING/ROLL CROSS-CORRELATION FUNCTION	48
FIGURE 58. PITCH/ROLL CROSS-CORRELATION FUNCTION	48
FIGURE 59. HEADING/PITCH CROSS-CORRELATION FUNCTION (detail)	49
FIGURE 60. HEADING/ROLL CROSS-CORRELATION FUNCTION (detail)	49
FIGURE 61. PITCH/ROLL CROSS-CORRELATION FUNCTION (detail)	49
FIGURE B1. DAY1 DISCRETE HEADING ERROR VS TIME	58
FIGURE B2. DAY2 DISCRETE HEADING ERROR VS TIME	59
FIGURE B3. DAY3 DISCRETE HEADING ERROR VS TIME	60
FIGURE B4. DAY4 DISCRETE HEADING ERROR VS TIME	61
FIGURE B5. DAY5 DISCRETE HEADING ERROR VS TIME	62
FIGURE B6. DAY6-7 DISCRETE HEADING ERROR VS TIME	63
FIGURE B7. DAY1 DISCRETE PITCH ERROR VS TIME	64
FIGURE B8. DAY1 DISCRETE ROLL ERROR VS TIME	64
FIGURE B9. DAY2 DISCRETE PITCH ERROR VS TIME	65
FIGURE B10. DAY2 DISCRETE ROLL ERROR VS TIME	65
FIGURE B11. DAY3 DISCRETE PITCH ERROR VS TIME	66
FIGURE B12. DAY3 DISCRETE ROLL ERROR VS TIME	66
FIGURE B13. DAY4 DISCRETE PITCH ERROR VS TIME	67
FIGURE B14. DAY4 DISCRETE ROLL ERROR VS TIME	67
FIGURE B15. DAY5 DISCRETE PITCH ERROR VS TIME	68
FIGURE B16. DAY5 DISCRETE ROLL ERROR VS TIME	68
FIGURE B17. DAY6-7 DISCRETE PITCH ERROR VS TIME	69
FIGURE B18. DAY6-7 DISCRETE ROLL ERROR VS TIME	69

LIST OF TABLES

	page
TABLE 1. GENERAL CHARACTERISTICS OF INS vs GPS	2
TABLE 2. SUMMARY OF LITERATURE RESULTS	6
TABLE 3. EXPECTED SYSTEM PERFORMANCE	12
TABLE 4. DISCRETE-DYNAMIC 3DF ATTITUDE ERRORS	24
TABLE 5. CONTINUOUS-DYNAMIC 3DF ATTITUDE ERRORS	26
TABLE 6. DISCRETE 3DF ERROR MODEL PARAMETERS	41

1. INTRODUCTION

A sea trial was conducted in August 1992 by the Navigation Group of the Electronics Division of the Defence Research Establishment Ottawa. One of the secondary objectives of this trial was to evaluate the performance of a new type of GPS (Global Positioning System) receiver, which is designed to measure attitude (heading, pitch and roll) as well as the usual GPS measurements of position and velocity. This type of receiver can compute attitude by taking double-difference carrier phase measurements from several (at least three) GPS satellite signals at several (at least three) different antennas. Since the antennas are usually more than one wavelength apart, there is a significant cycle-ambiguity problem to solve as well. Sometimes a fourth antenna is used to assist in this ambiguity resolution. This technique is adequately described in the literature (see for example references [1] to [10]) and is summarized in Section 2 below.

This new GPS technology has many potential applications. It could partially replace, or at least complement, the very large and costly marine inertial systems currently used to measure attitude on ships. It could provide rapid and precise alignment of artillery pieces. It could provide heading information at extremely high latitudes where inertial systems cannot. It could also be used to precisely align sensors on airborne or spaceborne platforms.

Platform attitude is required for fire control purposes and/or sensor alignment on most military platforms, and in particular for naval vessels. This is generally considered a mission critical function, so that highly accurate, reliable and timely (i.e. low latency) attitude data is required. The inertial sensors currently used to provide this data are very costly, massive and power consuming. A marine INS (Inertial Navigation System) typically costs several hundred thousand dollars, weighs several hundred kilograms and consumes hundreds of watts of power. For high latitude operations it is important to recognize that the heading accuracy of an inertial system will be seriously degraded, increasing roughly as $\sec(\text{latitude})$, thus becoming essentially useless in the immediate vicinity of the pole. The attitude determining GPS receiver, by comparison, costs less than \$80K (potentially much less), weighs less than 10 kg, consumes only about 12 watts and is not degraded at high latitudes.

Unfortunately there are also expected to be shortcomings with the GPS technology in the area of performance (accuracy, availability, reliability, data latency). Of course GPS relies on external line-of-sight signals and is therefore subject to jamming, spoofing, shading and multipath. GPS attitude determination also requires the installation of several antennas (at least three), with associated cables.

It may be possible, however, to overcome most if not all of these shortcomings by properly integrating the GPS attitude receiver with a lower cost (and therefore lower performance) inertial system or AHRS (attitude and heading reference system). The degree to which this will meet the accuracy performance requirements will depend upon the error characteristics of the INS and of the GPS attitude, the latter of which is the subject of this report. The reliability and environmental requirements would also require special consideration, but these are not addressed here.

Table 1 below compares the general characteristics of the two competing technologies, for the purpose of attitude determination in the marine environment.

TABLE 1. GENERAL CHARACTERISTICS OF INS vs GPS

FACTOR	MARINE INERTIAL	GPS
Cost (\$K)	> 250	< 80
Environmental	full mil spec.	commercial rugged
Heading Accuracy (degrees RMS)	< 0.05 x secant(lat.)	TBD ($\cong 0.1$)
Pitch, Roll Accuracy (degrees RMS)	< 0.025	TBD ($\cong 0.1$)
Data Rate	400 Hz	1 Hz
Time to First Fix	hours	seconds
Size (m ³)	> 0.3 (0.5 x 0.5 x 1.5)	$\cong 0.004$ (0.2 x 0.2 x 0.1)
Weight (kg)	> 300	< 5
Power (watts)	> 500	12
Other Considerations	self-contained	cabling, antennas with clear view of sky, multipath, jamming, denial

Comparison with ground based or airborne inertial systems will be quite different, with the INS being considerably smaller, lighter, less expensive, less power consuming, and requiring less alignment time, but also having lower accuracy. The GPS error characteristics will also be different in the land and air environment, since these errors will depend largely on the platform dynamics, the antenna baseline lengths and the multipath environment. In particular static accuracy can be significantly better than dynamic accuracy (provided that multipath is carefully avoided) and longer baselines will produce better accuracy than shorter ones.

The purpose of this report is therefore to produce an initial characterization of the dynamic attitude performance of an Ashtech Three-Dimensional Direction Finding System (3DF) in the marine environment, as well as to provide some general background on this general class of GPS receiver equipment. The Ashtech 3DF is a 24-channel single frequency GPS receiver with four micro strip antennas. References [6] and [10] provide a more complete description.

2. BACKGROUND

The determination of heading and attitude from GPS has been discussed in the literature for some time. Written over fifteen years ago, reference [1] describes the general principles behind attitude determination using phase comparison between pairs of antennas. The basic concept is as shown in Figure 1.

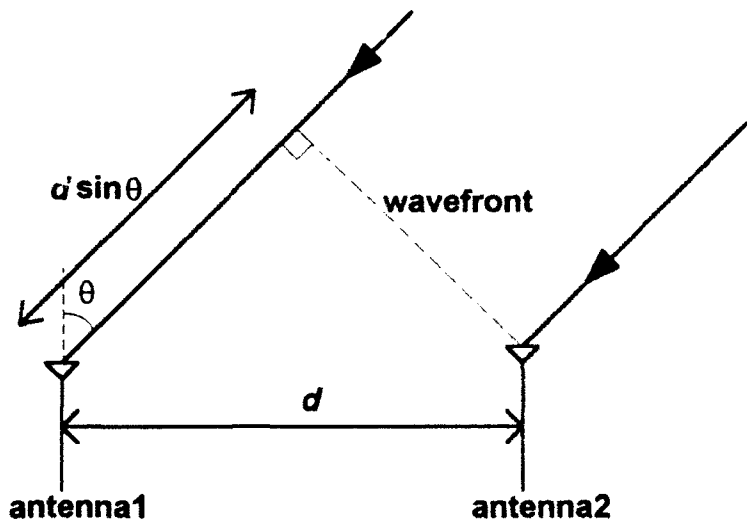


FIGURE 1. INTERFEROMETER PRINCIPLE

The fundamental interferometer equation, derived from Figure 1, relates the measured phase difference ϕ at the two antennas to the angle of incidence θ of the signal to the antenna baseline:

$$d \sin \theta = n\lambda + \phi \lambda / 2\pi \quad (1)$$

where d is the baseline length, λ is the signal wavelength (where in the case of C/A code GPS $\lambda \approx 19$ cm) and n is the integer number of wavelengths (phase ambiguity) needed to ensure that measured phase difference ϕ is in the range $-\pi < \phi < \pi$. This phase ambiguity can arise when $d > \lambda/2$, which is usually the case as we shall see.

Assuming that this phase ambiguity has been resolved, then from equation 1 it can be seen that a phase measurement error of $\delta\phi$ will result in an angular measurement error of $\delta\theta$ where:

$$\delta\theta = \left(\frac{\lambda}{2\pi d \cos \theta} \right) \delta\phi \quad (2)$$

This shows how the phase error $\delta\phi$, due to either receiver phase measurement error or

multipath error, will cause an error in the angular measurement. Thus the important factors to control when determining the angular measurement error $\delta\theta$ are the phase error $\delta\phi$, the baseline length d (since λ is a constant and θ is determined by the satellite geometry which cannot be controlled) and of course the phase ambiguity resolution. Incidentally, the satellite geometry, represented by the $\cos\theta$ term, is generally such that horizontal angular measurements (heading) are more accurate than vertical angular measurements (pitch and roll) by a factor of 1.5 to 2, just as the horizontal GPS position measurements are generally more accurate than the vertical GPS position measurements, by the same amount.

In 1977 it was suggested in reference [1] that this type of receiver could attain accuracies of 2 to 20 minutes of arc (0.03 to 0.33 degrees) with measurement rates of 10 per second. This was an analytical discussion, in the context of an airborne platform, assuming a three antenna interferometer (the minimal configuration). The general discussion in this reference illustrates how the expected attitude errors due to phase measurement error and multipath error (the two dominant sources of error) are inversely proportional to the baseline length. This discussion assumed a GPS carrier phase measurement accuracy of 0.6 degrees. Since the wavelength of the L1 carrier signal is 19.0 cm, this is equivalent to $19 \times 0.6 / 360 = 0.03$ cm. This also assumed four metre baselines between three antennas. The suggested application of this technique was to eliminate the long alignment times required by inertial systems on moving platforms (i.e. on an aircraft carrier or in flight). This paper also foresaw the integration of this type of receiver with an inertial system.

Reference [2], apparently from 1981, provides a more complete discussion of error sources and provides simulation results suggesting that an accuracy of 50 μ rad (0.003 degrees) may be achievable. However this assumed a static three antenna baseline, *no multipath error*, four GPS satellites visible and *15 minutes of Kalman filtering with an INS* (1 nautical mile per hour type). Ignoring multipath, especially in a static situation, will result in significantly underestimated errors. The Kalman filter based integration with an INS as briefly described here, is an excellent idea, especially in the dynamic situation. (The assumed baseline lengths were 1 metre and the GPS carrier phase measurement accuracy was assumed to be 0.36 degrees.) This paper also concludes that 0.06 degrees heading accuracy can be achieved with 5 minutes of filtering.

In 1983 DREO sponsored a proof of concept study to investigate the feasibility of measuring azimuth (heading) using this technique with the older Transit satellite system. The technique used, called AZTRANS (AZimuth from TRANSit), was originally developed by the Applied Physics Lab in 1971, and was adapted by JMR Instruments Ltd. in 1983. Using a JMR-A1 receiver with two antennas on a static four metre baseline, it was shown in reference [3] that one degree azimuth accuracies (rms) could easily be obtained, and 0.5 degree accuracy (rms) was feasible. Note that since Transit operates at 400 MHz, its carrier wavelength λ is about four times longer than that of the GPS L1 carrier (which is at 1540 MHz), leading to proportionally larger Transit attitude errors $\delta\theta$ for a given phase measurement error $\delta\phi$, according to equation 2 above.

Later in 1983, reference [4] provided another discussion of this technique as applied to GPS, with simulations suggesting that 2.4 mrad (0.14 degrees) rms attitude accuracy can be

achieved with 2 metre baselines, a 5.0 mm phase measurement accuracy, and three antennas. It also suggests that 0.6 mrad (0.03 degrees) rms attitude accuracy can be achieved with 20 metre baselines.

As described in reference [5], an attitude GPS receiver was actually developed to the ADM stage in 1986 by Starnav Corporation of Ottawa (with support from the National Research Council of Canada), which demonstrated 0.6 degree attitude error standard deviation (plus some bias) in static mode. This used a 3 antenna array with 1 metre baselines. The failure of this receiver to enter production was blamed on the Challenger disaster of 1986, which set back the GPS satellite launch schedule, delaying market demand for receiver equipment.

The receiver evaluated on this trial is the Ashtech 3DF. The manufacturer has published, in reference [6], a paper describing the 3DF system and presenting some performance test results. Most of the results are from static tests and indicate accuracies consistent with Figure 2. For example the claimed static accuracy was as good as 0.006 degrees (0.1 mrad). However this used a baseline length of 110 metres and apparently also used heavy temporal filtering. It therefore cannot be applied to the dynamic situation. Shorter baselines of one metre produced accuracies of about 0.3 degrees, again in static mode, with heavy temporal filtering. The only dynamic data presented by the manufacturer was not conclusive because of poor reference data, however it suggests an accuracy of between 0.4 degrees and 0.05 degrees. The text of [6] suggests the latter figure but the data presented does not appear to support this conclusion and in fact suggests something closer to 0.2 degrees. Again there seems to be some temporal filtering involved, which hides some of the true dynamic error. In fact, as mentioned in [6], three small Kalman filters (2 states each) are used to smooth the heading, pitch and roll measurements respectively.

Reference [7], from 1991, describes an attitude determining system built by Adroit Systems Inc. in 1990, designed for static pointing of artillery. This system uses a modified Texas Instruments TI-420 receiver with three co-linear antennas to measure azimuth and elevation (heading and pitch) only. The antennas form one short (about 14 centimeters) sub-wavelength baseline for phase ambiguity resolution, and one longer (one metre) baseline for attitude measuring. Since this was a static implementation, the measured performance could be improved by extending the measurement interval. The azimuth accuracy varied from about 0.6 degrees for a one second sample to 0.3 degrees (standard deviation) for 30 second processing to (apparently) 0.1 degree for 360 second measurements. (Reference [7] in most cases presents the average errors rather than the rms errors, which is not very useful.) This reference also presents some results from two competing receivers of the same class (static, two dimensional), one from Magnavox and one from Texas Instruments. Because of different implementation decisions the error characteristics of the three competing designs were somewhat different, for example with the Magnavox errors having somewhat larger biases but smaller standard deviations.

In reference [8] some 1992 experimental results are presented comparing an Ashtech 3DF to a Litton LTN90/100 strapdown inertial system. This dynamic test was performed on a pickup truck over straight and smooth highways, so that there were actually very little dynamics. Care was also taken to avoid multipath, and time of day was chosen to maximize

GPS satellite coverage: five satellites with Position Dilution of Precision (PDOP) between 2 and 4. Thus the limited data presented in reference [8] (about 40 minutes of data) may have produced optimistic results for this 1 to 2 metre antenna baseline configuration.

These results from the literature are summarized in Table 2 below.

TABLE 2. SUMMARY OF LITERATURE RESULTS

REF.	# OF ANTEN -NAS	SIMUL- ATED OR REAL	STATIC OR DYNA- MIC	BASELINE LENGTH (metres)	PHASE MEASUREMENT ACCURACY (mm)	SAMPLE PERIOD (sec.)	ATTITUDE ACCURACY (degrees rms*)	
							HEADING	PITCH/ROLL
1	3	S	S	4	0.3	0.1	0.03 - 0.33	
2	3	S	S	1	0.2	300	0.06	-
4	3	S	S	2-20	5.0	720	0.14-0.03	0.14-0.03
5	3	R	S	1			0.6	-
6a	4	R	S	1	0.2	1	0.14	0.25
6b	4	R	S	110	0.2	1	0.002	0.004
6c	4	R	D	50	0.2	1	0.05-0.2 ¹	-
7	3	R	S	1		30	0.3	0.6
8	4	R	D	1.5	0.2	1	0.2 ²	0.4

* Not all references provided rms error statistics, and some that do appear to have confused rms with standard deviation, as discussed in the two notes below.

NOTE 1. Concerning the heading accuracy for reference 6c in Table 2: The dynamic attitude errors of the 3DF system presented in reference [6] (0.4 degrees) is a *mean* rather than an rms error. The rms of course is generally larger than the mean (according to the Minkowski inequality). Reference [6] also suggests that most of this mean error (0.34 degrees) is due to an error in the calibration of the reference gyro rather than to the 3DF system, and goes on to discuss the resulting error in the mean (of 0.05 degrees) as though this were the dynamic error. Unfortunately this "error in mean" is not a good measure of performance since it completely ignores the noise. Furthermore, when the mean (i.e. the bias) is removed in this way, basically all that remains is noise, which from the plotted data shown in reference [6] visually appears to be at about the 0.2 degree rms level, suggesting an rms value of about 0.2 degrees. (Alternatively this could be quoted as the standard deviation value, in which case the mean is removed by definition.)

NOTE 2. Concerning the accuracy results for reference 8 in Table 2: The rms statistics given for reference [8] appear to be *standard deviation* statistics (i.e. with biases removed), because in many cases the "rms" error statistic given is smaller in magnitude than the corresponding mean error statistic (which is mathematically impossible).

Table 2 suggests that performance can be improved simply by extending the antenna baseline lengths and the sample period. In fact the basic relationship of equation 2 above has led various authors, such as in reference [9] and the manufacturer of the equipment under test (in reference [6]), to publish graphs showing a direct relationship between baseline length and accuracy, as shown in Figure 2 (which incidentally excludes multipath-type errors, which could be very significant). Reference [10] contains a similar plot with an additional line representing the expected performance *with* multipath, indicating errors which are larger, by a factor of about 2.5, than the non-multipath errors.

Unfortunately there are often problems with extending the baseline length on many platforms. First there is the limitation of the platform size, and second there is the limitation of baseline stability. The true antenna baseline lengths must be known and preferably must be very stable under temperature fluctuations and mechanical vibrations. Flexing on a large platform can therefore cause difficulties, although it has been suggested that this technique can be used to actually measure this flexing, as discussed in reference [10].

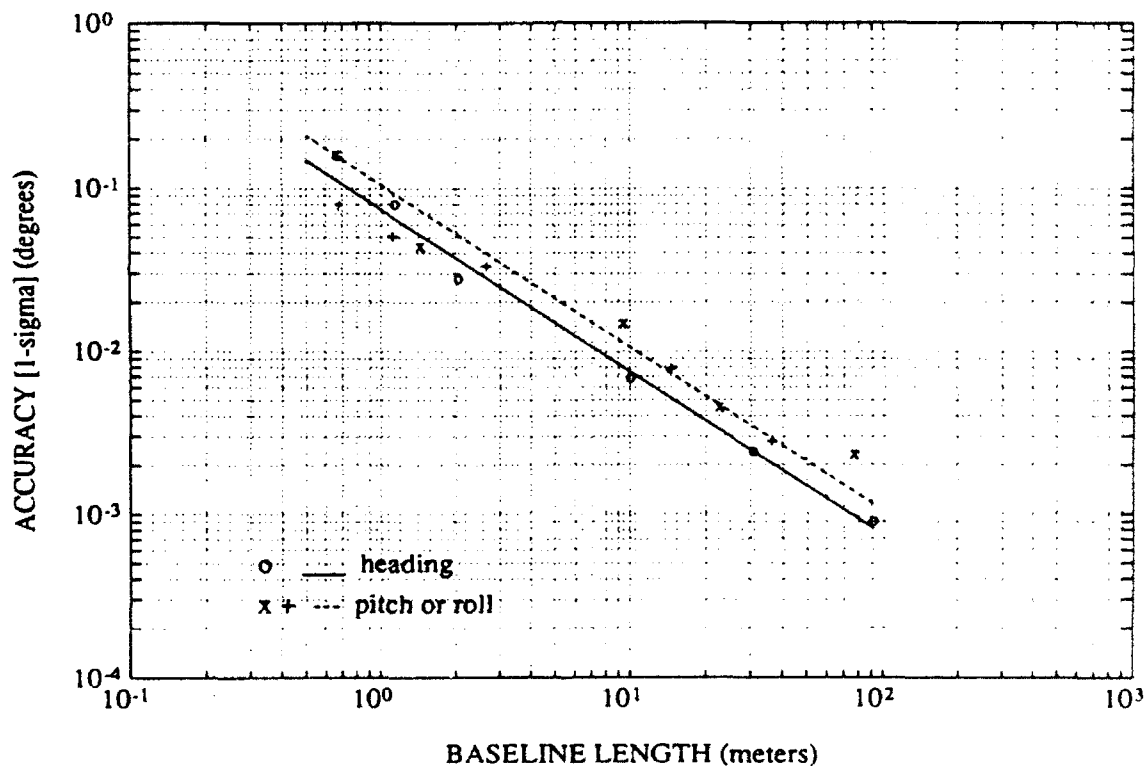


FIGURE 2. ACCURACY VS BASELINE LENGTH

Another method of improving accuracy is to extend the sample period, allowing many different measurements to be combined using some averaging or filtering technique to reduce

the phase measurement error. This is only possible when the attitude can be assumed constant, as in the static situation, such as for artillery alignment, or if inertial-type aiding is available.

The effectiveness of extending the sample period (using temporal filtering) is also strongly determined by the degree to which the phase errors are temporally uncorrelated. For example uncorrelated white noise can be easily removed through filtering whereas a bias (totally correlated) cannot. Although true biases can be removed by an installation calibration, errors which vary slowly in time cannot be removed by either calibration or averaging. In the static situation, multipath can produce these types of errors which are significantly correlated in time, limiting the effectiveness of this filtering.

Reference [7] shows the expected relationship between sample period and accuracy, for a one meter antenna baseline, as reproduced here in Figure 3.

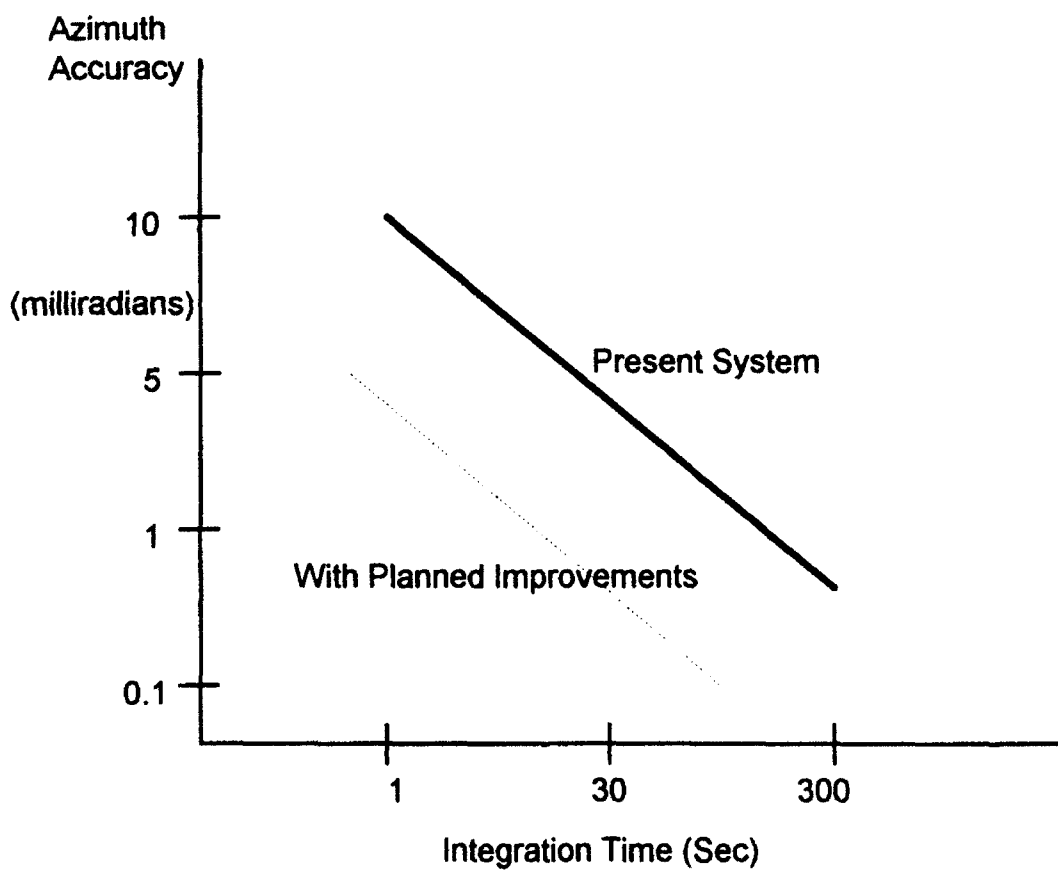


**FIGURE 3. ACCURACY VS SAMPLE PERIOD
(1 meter baseline)**

One question which comes to mind when reviewing this literature is the long time from concept to realization. The likely explanation for this long delay between the theoretical derivation of this technique (1977) and its practical implementation (1992) is that the extreme miniaturization of receiver hardware, with receiver-on-a-chip and multichannel chips, has only recently made it economical to build into the same receiver the large number of receiver channels necessary to implement multi-antenna attitude determination. This delay could thus be partially blamed on the slow implementation of the GPS Space Segment (i.e. the Shuttle disaster), which delayed the consumer demand.

3. SEA TRIAL METHODOLOGY

The general execution of this sea trial is discussed more fully in reference [11]. The duration of the trial was two weeks including installation and removal of equipment, from August 14 to 28, 1992. Seven days were spent at sea collecting data. The 3DF data set extends from 22:09 on day 230 to 16:19 on day 237 (Greenwich mean time). There were no indications of any unusual conditions of the GPS space or control segments at that time.

The area of operation was as illustrated in Figure 4, which shows the ship's track over the entire trial, from the differential GPS reference data. The sea trial was conducted on the CFAV Endeavour, which is a 75 meter, 1600 ton research vessel operated by the Defence Research Establishment Pacific, in Esquimalt B.C.

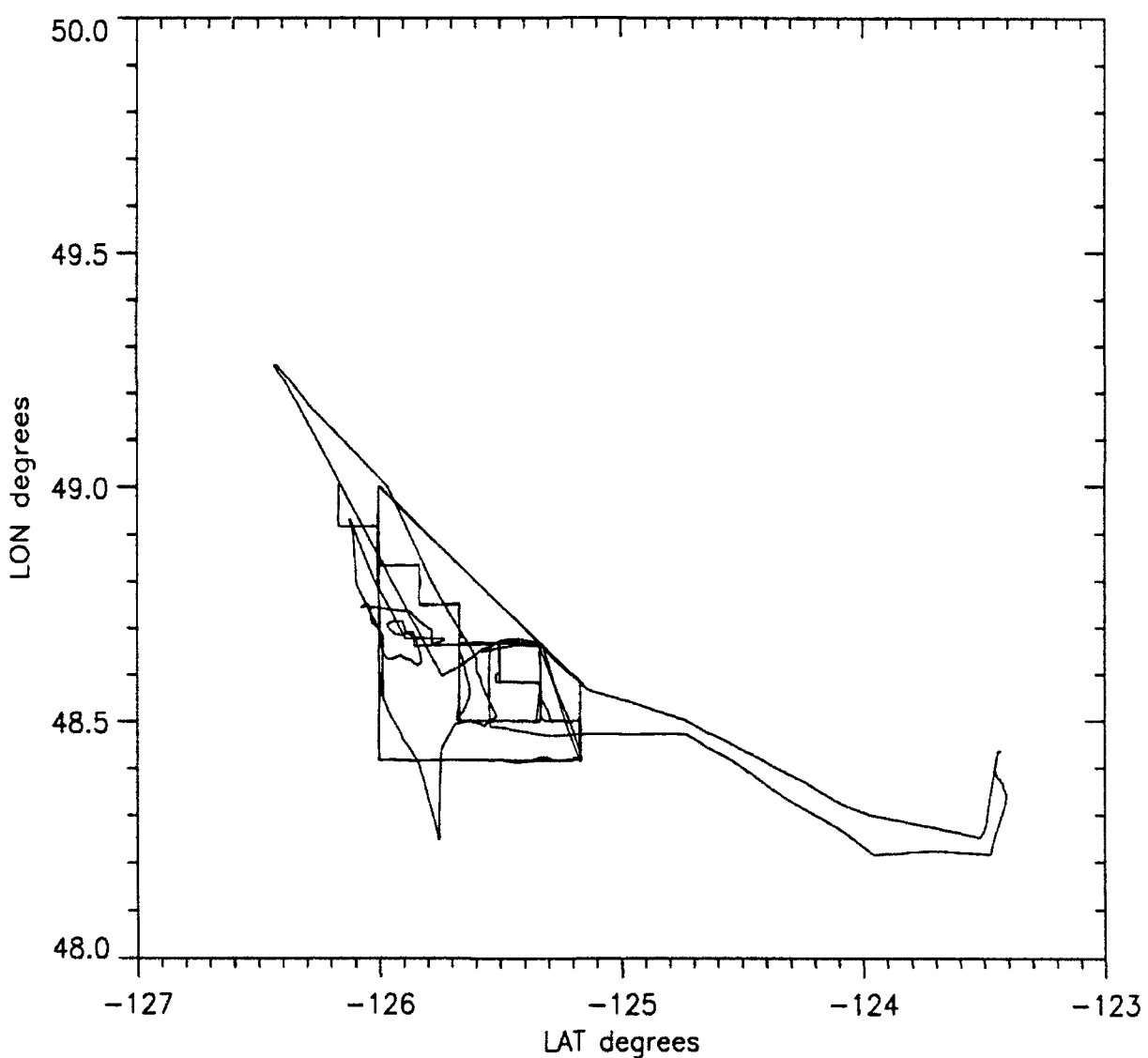


FIGURE 4. AREA OF OPERATION

3.1 Equipment

Since the primary purpose of the trial was to collect sensor data for DIINS (Dual Inertial Integrated Navigation System) development (see reference [12]), the navigation sensor complement included a relatively high performance marine inertial navigation system, referred to here as INS1. This provides a continuous reference for heading, pitch and roll with an expected accuracy significantly better than the expected GPS attitude accuracy, essentially no noise or transients, and a data rate about six times faster. There was also a lower quality airborne INS, referred to here as INS2, which nevertheless had highly predictable errors (RLG based, strapdown, free inertial).

There was also a differential GPS receiver (DGPS) providing position reference accurate to about 5 metres. With the DIINS software, it is possible to integrate this accurate position data with either of the INSs to provide further enhanced attitude data. This has the added advantage of providing covariance information (from the DIINS Kalman filter) to indicate more precisely the expected accuracy of the integrated attitude solutions.

The Ashtech 3DF 4-antenna array was installed at the stern of the ship, as illustrated in Figure 5. These antennas formed an approximately square horizontal array with 10 metre baselines in both the longitudinal direction (heading and pitch measuring) and lateral direction (heading and roll measuring), with the exact dimensions given in Figure 6.

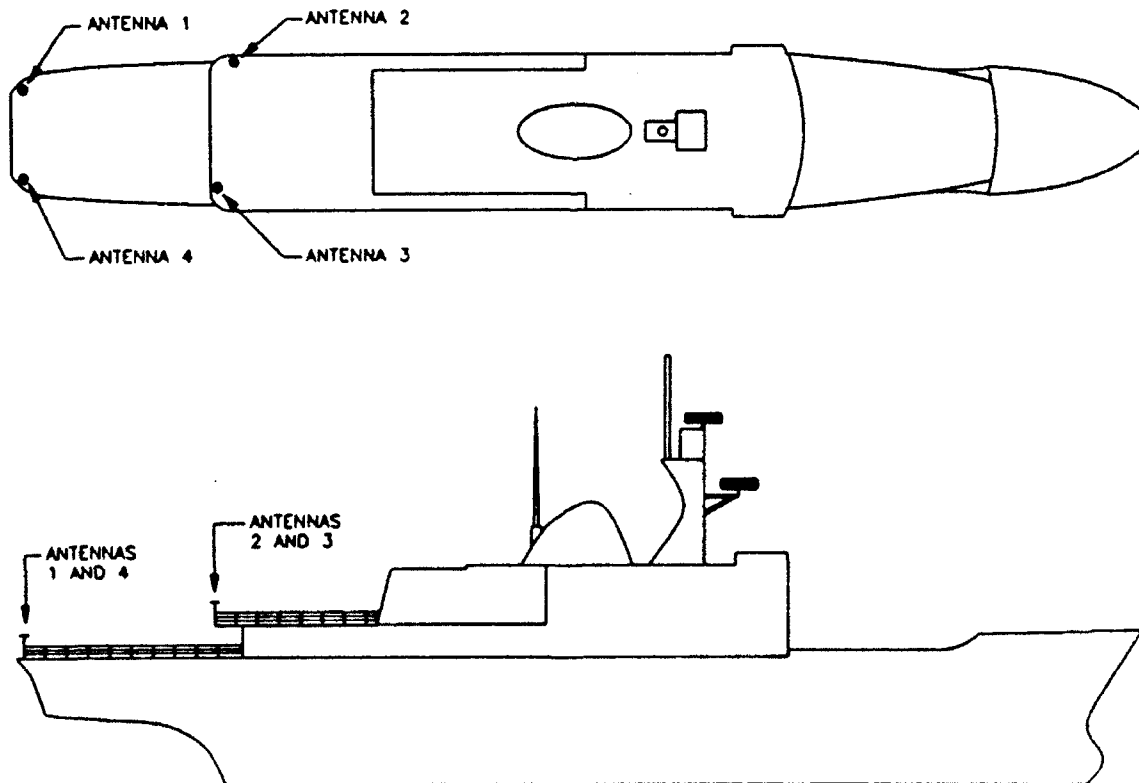


FIGURE 5. GPS ANTENNA ARRAY INSTALLATION

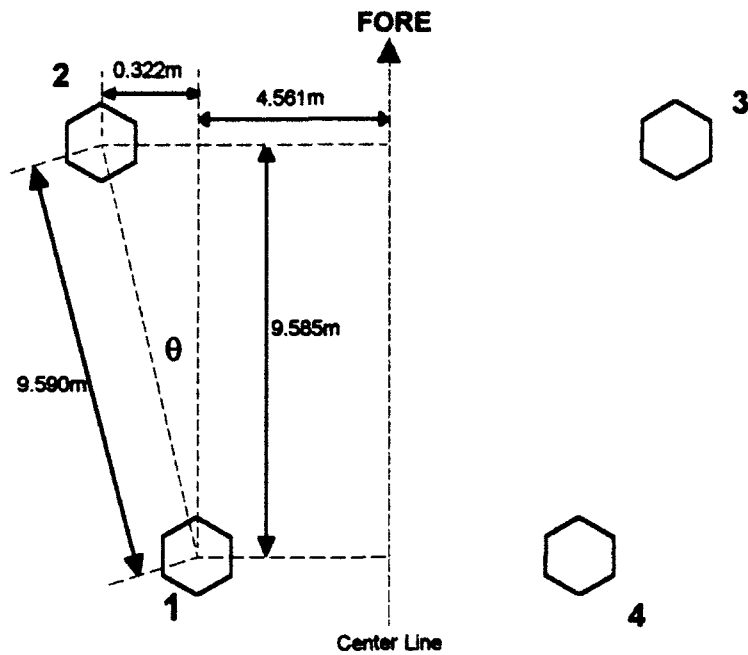


FIGURE 6. GPS ANTENNA ARRAY GEOMETRY

Table 3 provides a list of the systems relevant to this report, giving their resolutions, data rates and their expected attitude accuracies. Of course there is at this time no real specification for the accuracy of the 3DF attitude measurements, especially in a dynamic environment. The general factors having an effect on this accuracy are discussed in Section 2 above, while the expected accuracy of this specific installation is discussed in Section 3.2 below, where θ is heading, ϕ is pitch, ψ is roll and $\epsilon \equiv 10^{-16}$.

TABLE 3. EXPECTED SYSTEM PERFORMANCE

SENSOR	RESOLUTION (degrees)		DATA RATE (sec.)	EXPECTED RMS ERROR (degrees)	
	θ	ϕ, ψ		θ	ϕ, ψ
3DF	ϵ	ϵ	1.0	$\cong 0.1$	$\cong 0.15$
INS1	0.005	0.003	0.16	<0.07	<0.03
INS2	0.005	0.005	0.51	0.10	0.05
INS1/DGPS	ϵ	ϵ	0.16	0.01	0.01
INS2/DGPS	ϵ	ϵ	0.51	0.01	0.01

The resolution, ϵ , of the binary 3DF attitude data on output (which uses double precision, or 64 bits) is so much better than the accuracy as to be irrelevant. The same is true of the output from the INS/GPS integration filters.

The expected rms errors given in Table 3 for INS2 are as specified for the USAF Standard Form, Fit and Function (F³) Medium Accuracy Inertial Navigation Unit (SNU 84-1), which is basically a one nautical mile per hour unit.

The approximate accuracy performance figures given for the INS/DGPS integrated solution in Table 3 are based on the Kalman filter covariance values. The validity of this covariance information has been verified to a great extent by simply verifying the error models upon which it is based. This was done by a detailed examination of all filter inputs and outputs (for example by verifying the consistency of the residuals with the residual covariances).

3.2 Expected 3DF Performance

Since baselines were of the same length in both lateral and longitudinal directions, as seen from Figure 6, the pitch and roll errors should be statistically of the same magnitude (by symmetry). However they should be larger than the heading errors by a factor of about 1.5 to 2, due to the difference in vertical and horizontal satellite geometry, as discussed in section 2 above (see equation 2). The most relevant data from the literature is from references [6c] and [8]. However the reference [6c] data was very limited and apparently did not have a good reference system, whereas the reference [8] data was collected on a truck driving down a straight, smooth road, under close to ideal GPS reception conditions. Since this Endeavour data was collected 24 hours a day for seven days, on a gently pitching and rolling ship, with some degree of superstructure masking, we can perhaps expect more spurious data and more dynamically induced errors. On the other hand the antenna baselines used here were about six times longer than those of reference [8], (but five times shorter than those of reference [6]) so that on balance the nominal errors should be roughly in line with the corresponding rows (6c and 8) of Table 2: around the 0.1 to 0.2 degree level.

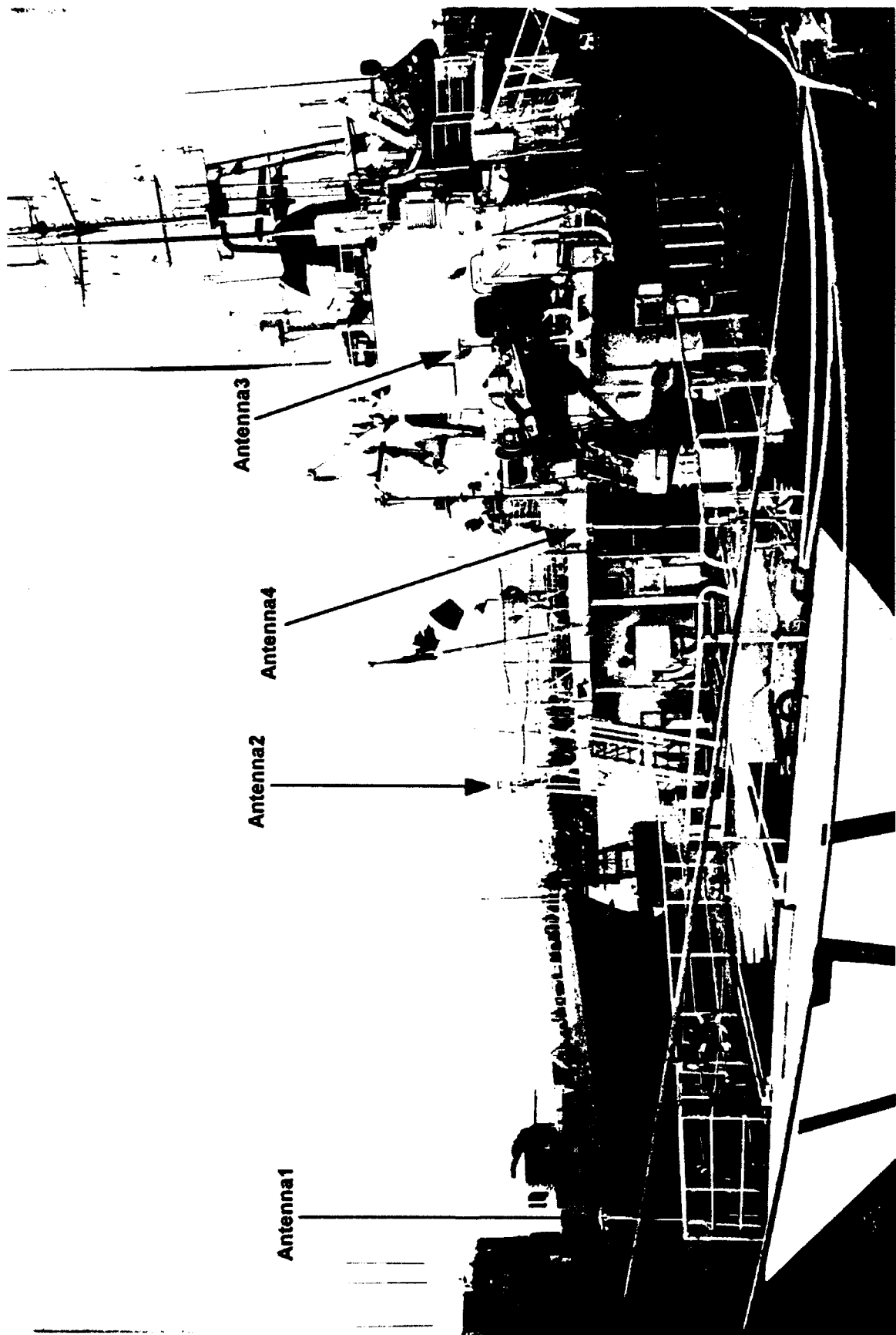


FIGURE 7. VIEW OF ANTENNA ARRAY

3.3 Reference System Performance

As mentioned, various sensors were available to provide reference data. The INS1 inertial navigation system by itself should provide sufficiently accurate pitch and roll reference data, as indicated by Table 3. For heading reference however the raw INS1 may not be adequate. In this case the INS1/DGPS data may be required, which is certainly accurate enough.

Another consideration is that the INS1 (and INS1/DGPS) accuracies listed in Table 3 actually apply to the discrete data points at their time of validity. This data was taken from the digital interface of INS1 at a 0.16 second rate, which was the slowest recording rate available. Since this reference data was not synchronized with the one second GPS attitude times, comparison of these two discrete data sets required some *data registration*, to match corresponding data. This data registration process introduces two additional sources of error: latency error and interpolation error.

It could be mentioned that the INS1 data was available at considerably higher rates from the digital interface (and essentially continuously from the synchro outputs). However this was not considered necessary, as explained below, and with limited data recording capacity on a seven day trial, was not practical.

3.3.1 Latency Error

Precise absolute time tagging of all sea trial reference data, and in particular INS1 and INS2 data, was accomplished by using GPS clocks with IRIG B output. These clocks allow the recording systems to time tag the data with the time of receipt of the first byte of each message to an accuracy of several microseconds. However there was some uncertainty in the exact time of *validity* of the data (as opposed to its time of recording). Even after the recording times are corrected for the known latencies (which for the INS1 reference data were on the order of tens of milliseconds) there was still a time uncertainty of a few milliseconds. (It should perhaps be mentioned that the synchro output from INS1, which has negligible latency, could have been used if necessary.) The attitude error introduced by this timing error will be determined by the angular rate of the platform.

For the attitude reference system (INS1) for example, the uncertainty in latency of the attitude data is δt where:

$$\delta t \leq 0.002 \text{ seconds} \quad (3)$$

During this time the attitude θ will have changed by $\delta\theta$, where:

$$\delta\theta = \delta t \partial\theta/\partial t \quad (4)$$

where $\partial\theta/\partial t$ is the time rate of change of the attitude angle. Thus this uncertainty in timing δt will cause an attitude error $\delta\theta$, as given by equation 4, which is determined by the platform angular rate $\partial\theta/\partial t$. To place a limit on this latency error we must place a limit on this angular

rate.

As discussed in Appendix A, (equation A8) the dynamics of the platform during this trial were such that a maximum angular rate of less than $\partial\theta/\partial t = 4.2$ degrees/second is expected. Substituting in equation 4 this indicates a data latency error bound of

$$|\delta\theta| < 0.008 \text{ degrees} \quad (5)$$

which is not significant.

Unfortunately the 3DF data itself was time tagged internally, and not by the data collection device (i.e. not at its output times), so that nothing could be said about its data latency, which is important for use by a dynamic control system.

3.3.2 Interpolation Error

Since the reference data, recorded at 0.16 second intervals, is not synchronized with the one second 3DF data, it was necessary to interpolate the reference data, introducing an interpolation error. With linear interpolation we estimate the angle θ to be

$$\hat{\theta}(t + \Delta t) = \theta(t) + \Delta t \times \frac{\partial\theta}{\partial t}(t) \quad (6)$$

where in this case

$$-0.08 \text{ seconds} \leq \Delta t \leq 0.08 \text{ seconds} \quad (7)$$

The magnitude of the resulting attitude error $|\delta\theta|$ will be approximately that of the next term in the Taylor expansion, namely $\Delta t^2/2$ times the angular acceleration $\partial^2\theta/\partial t^2$.

$$|\delta\theta| \approx \frac{\Delta t^2}{2} \left| \frac{\partial^2\theta}{\partial t^2} \right| \quad (8)$$

Now the magnitude of the interpolation interval $|\Delta t|$ is at most 0.08 seconds in this case. Thus to place a limit on this error it is necessary to examine the angular acceleration of the platform. From Appendix A (equation A9) we see that the magnitude of the angular acceleration is less than 4.4 degrees/sec.². Thus from equation 8 we see that the interpolation error can be bounded by:

$$\begin{aligned} |\delta\theta| &< (0.08 \text{ sec})^2 (0.5) (4.4 \text{ degrees/sec}^2) \\ &\approx 0.014 \text{ degrees} \end{aligned} \quad (9)$$

which is also not very significant.

3.3.3 Total Reference System Error

When considering the ultimate accuracy of the reference data used, it is important to note that the latency and interpolation errors are both going to vary sinusoidally in magnitude, and are 90 degrees out of phase, since one is proportional to angular rate and the other to angular acceleration. Thus the bound on the sum of these two errors is much less than the sum of the bounds.

As already mentioned, another option if a more accurate reference or more confidence in the reference data were required, would be to run the raw INS1 or INS2 data through a Kalman filter with the differential GPS position measurements. This would improve the attitude estimates as well as provide error covariance information indicating quantitatively what the accuracy is, as a function of time. This would also provide residual and residual covariance information to verify that the INS errors during this sea trial did in fact conform to the error models upon which the Kalman filter is based (and upon which the INS performance figures of Table 3 are based). This would not by itself remove the small errors due to INS data latency uncertainty or to interpolation, and so the performance would be limited to about 0.005 degrees, as shown in Table 3. A higher order interpolation method however could have reduced those errors, but since they were not significant this was not done.

In fact the INS1/DGPS filter was run, to verify that the raw INS1 pitch and roll data was sufficiently accurate (which it was) and to provide corrections to the raw INS1 heading, so that it would also be adequate as reference for the 3DF data.

Another important aspect of the reference system errors is their behaviour in time in terms of the associated autocorrelation function. Inertial system errors are quite well understood (see for example reference [13]) and their temporal behaviour is distinctly different from the behaviour of the errors attributed here to the 3DF data. Because of this, any inertial errors which are present will not contribute significantly to the error model parameters attributed to the 3DF measurements. Neither will any (constant) data latency error, for the same reason, as will be explained in Section 6 below.

4. RAW DATA

The 3DF data set consisted of 520,255 data points, collected at a one Hz rate over the duration of the trial, which was 586,800 seconds long (almost 7 days). Thus there was 11% of the trial for which there was no 3DF data, primarily because of gaps in the GPS coverage (agreeing closely with the 11% missing differential GPS reference data). There were also brief periods, once a day, when the 3DF data recording was shut down to close off data files.

A further 10% of the available data was not "valid". Figure 8 shows the attitude reset flag values throughout the trial, as received from the 3DF receiver. This flag is "0" if the phase ambiguities have been resolved and a carrier phase attitude has been computed. It is "1" if the phase ambiguity has not been solved, in which case the pitch and roll are set to zero and a codephase (as opposed to carrier phase) heading estimate is given. For purposes of this report, only carrier phase attitude data has been analyzed. This "valid" data constituted about 90% of the available data (469,590 of the one second 3DF data points were flagged "0", out of the total 520,255 3DF data points). Thus the breakdown is as follows:

Total trial period	586,800 seconds	(100%)
Total 3DF data	520,255 seconds	(89%)
Valid 3DF data	469,590 seconds	(80%)

Figures 9 to 11 show the raw inertial heading, pitch and roll respectively, throughout the trial. These plots are included simply to provide an indication of the dynamics experienced during this trial. The trajectory plot of Figure 4 also gives an indication of the various headings assumed.

Figures 12 to 14 show the 3DF attitude (at 1 Hz) in comparison to the reference attitude (at 6.25 Hz), for a brief (100 second) interval. These illustrate the short term dynamics, due largely to wave motion, and at the same time give a first impression of the quality of the 3DF data. An appreciation of these short term dynamics is important when analyzing and interpreting the performance of the 3DF data, and these plots will be referred to again below.

Figure 15 shows the MRMS, which is the average double difference carrier phase residual, as supplied by the 3DF receiver. This is supposed to be typically 2 to 3 millimeters. Thus Figure 15 seems to indicate that there were no unusual problems with these phase measurements.

Figure 16 shows the BRMS, which is the RMS error for the differences between calibrated baseline magnitudes and computed baseline magnitudes for the three vectors formed by Antenna 1 to the other three antennas. This is supposed to be typically 1 to 3 centimeters, increasing under high PDOP conditions. Thus Figure 16 seems to indicate that there were no serious problems with PDOP or with these calibration values.

FIGURE 8a: AVAILABILITY

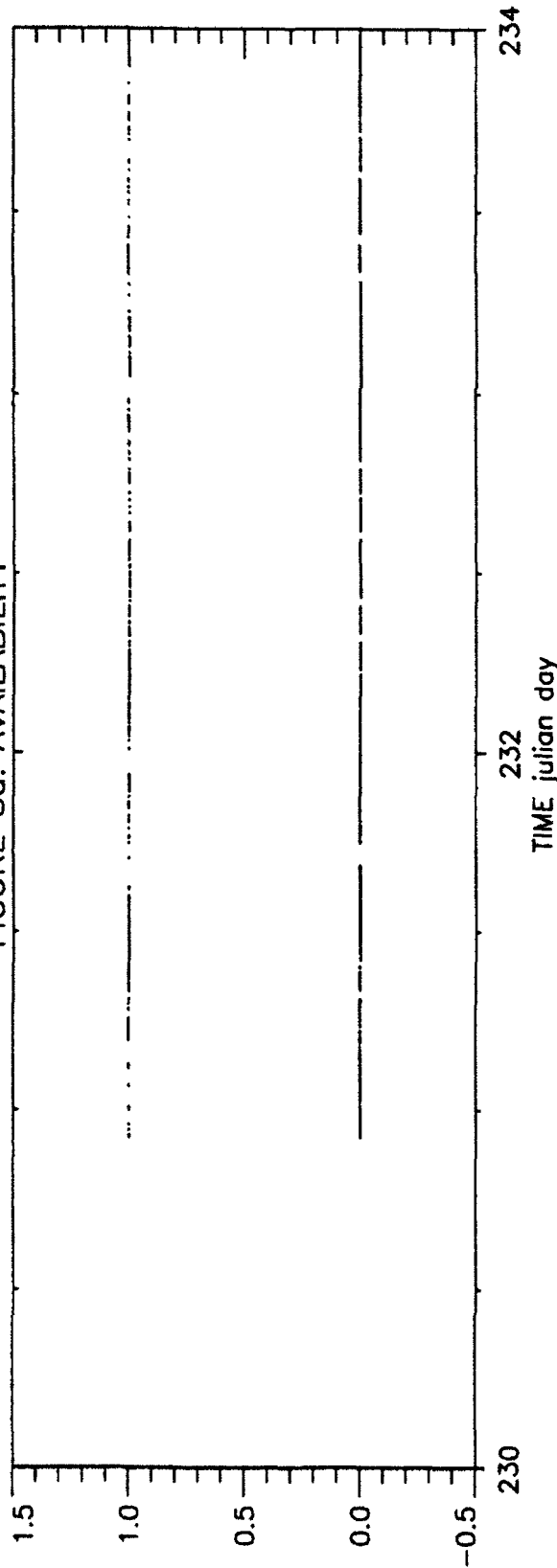


FIGURE 8b: AVAILABILITY

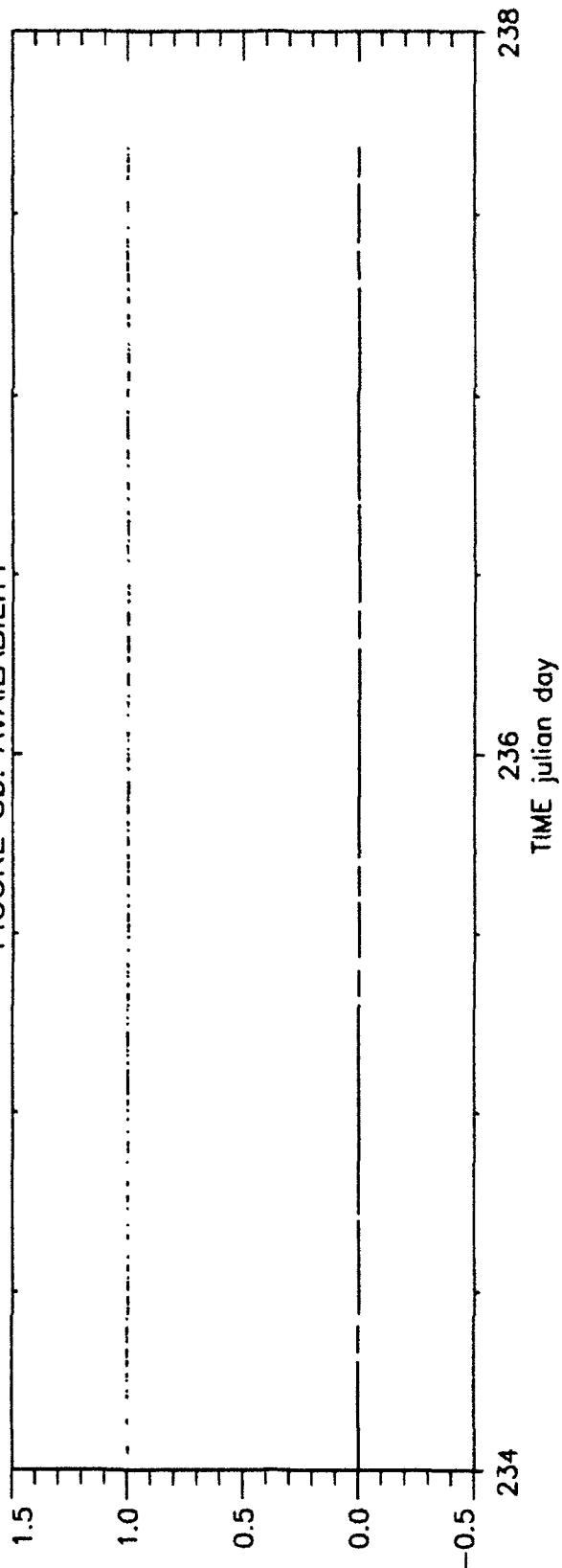


FIGURE 9: HEADING

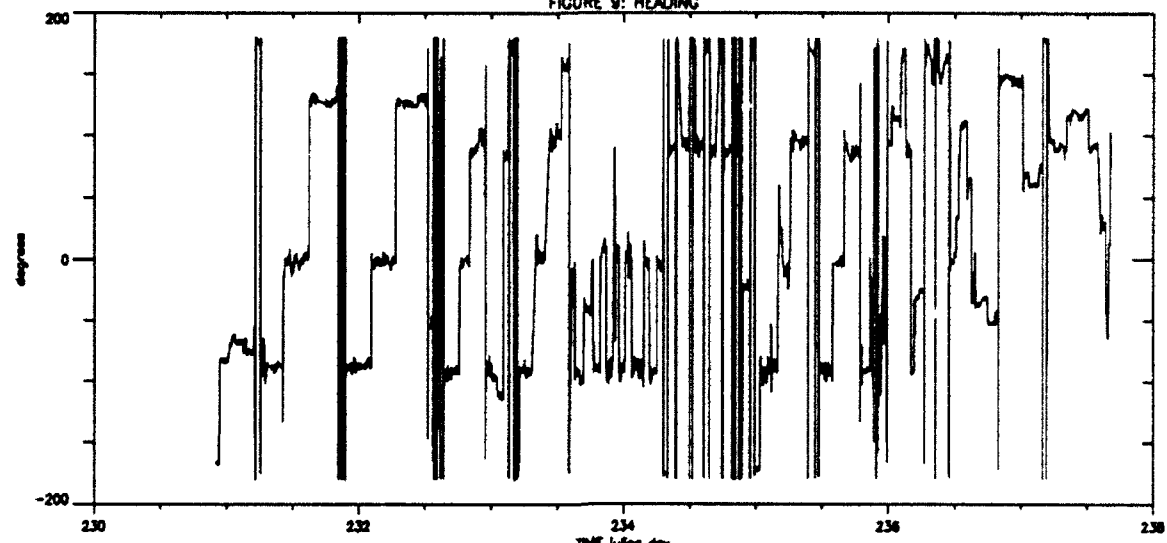


FIGURE 10: PITCH

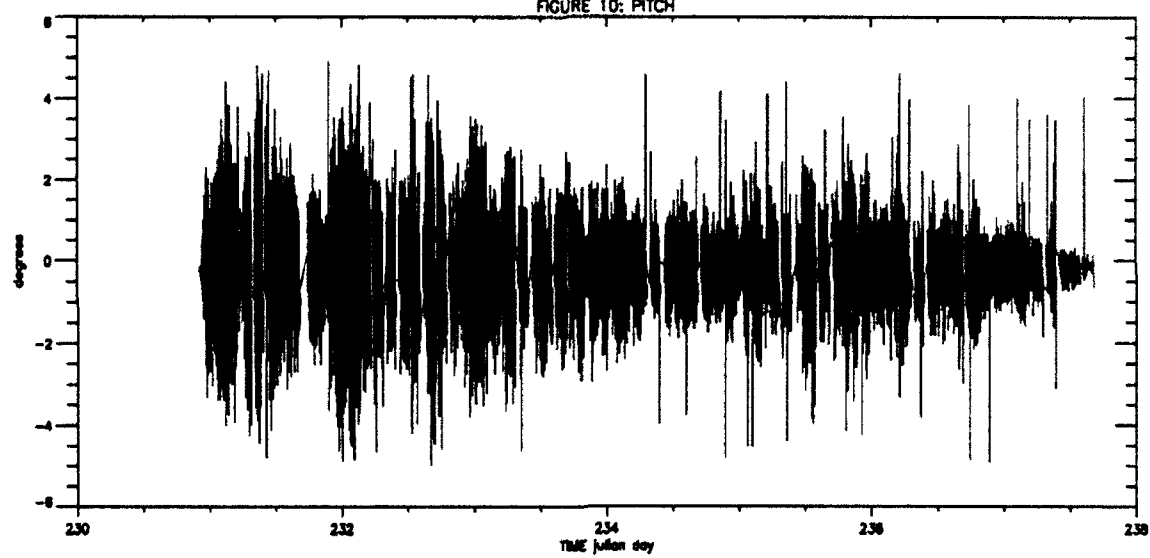


FIGURE 11: ROLL

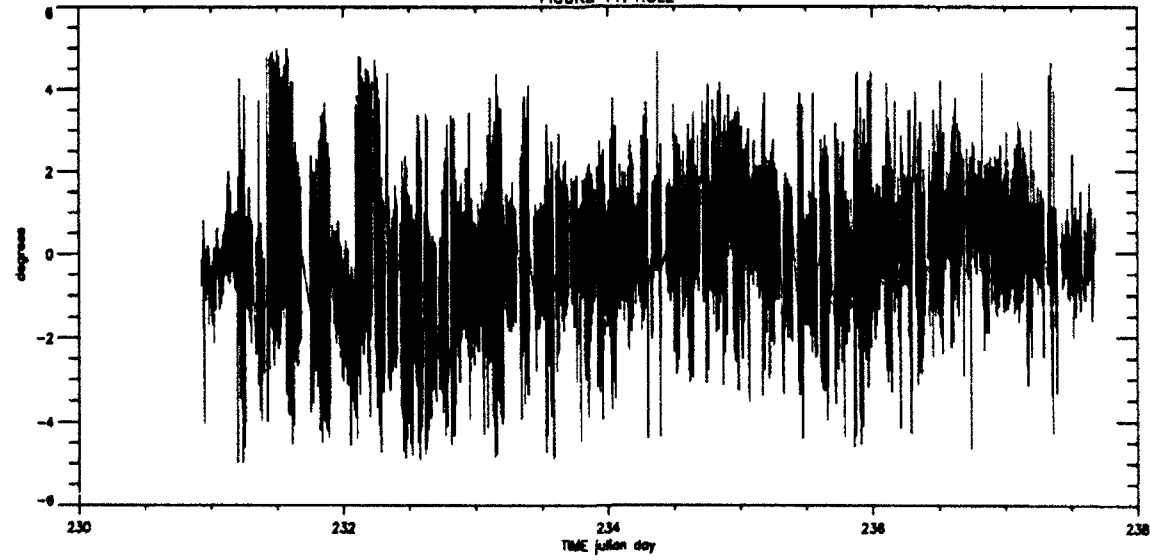


FIGURE 12: DETAIL OF 3DF & REFERENCE HEADING

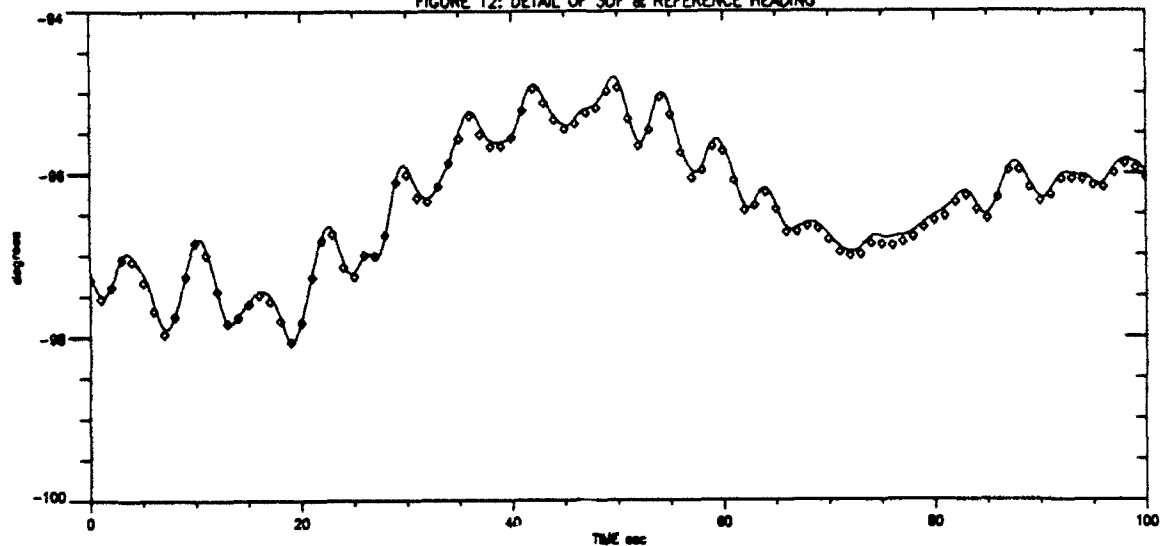


FIGURE 13: DETAIL OF 3DF & REFERENCE PITCH

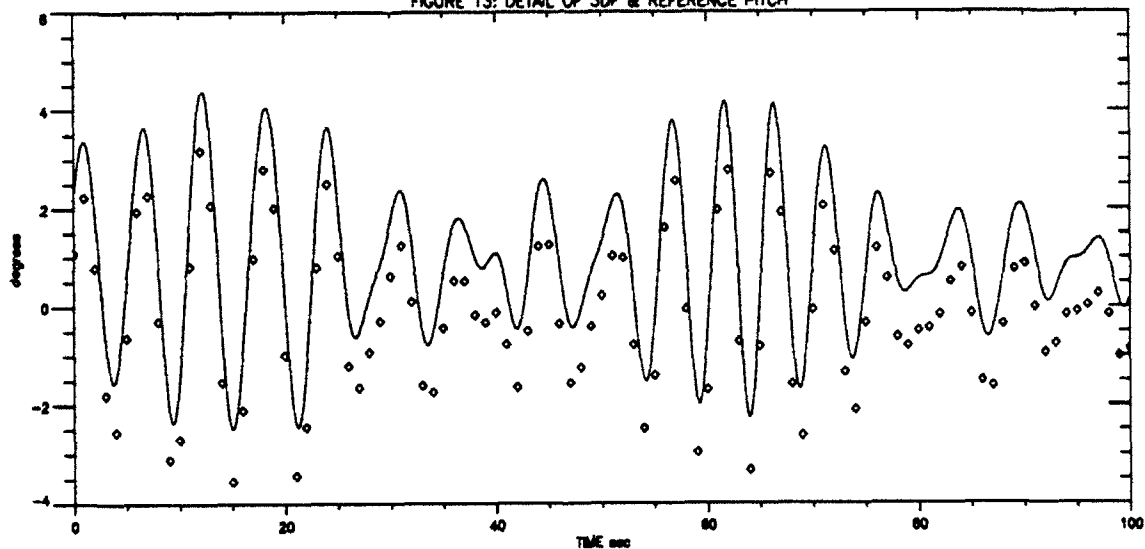


FIGURE 14: DETAIL OF 3DF & REFERENCE ROLL

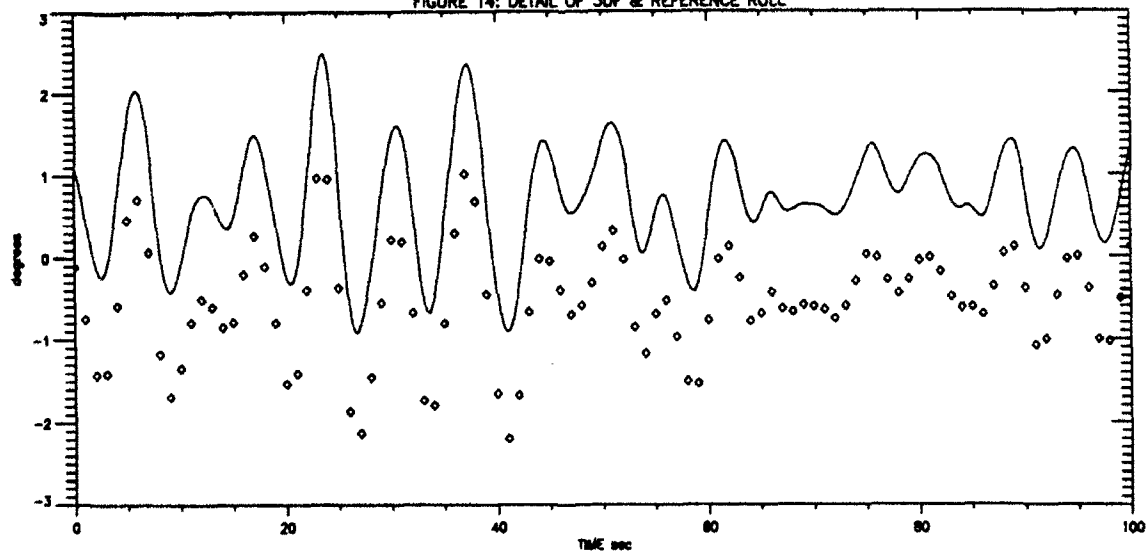


FIGURE 15: 3DF MRMS

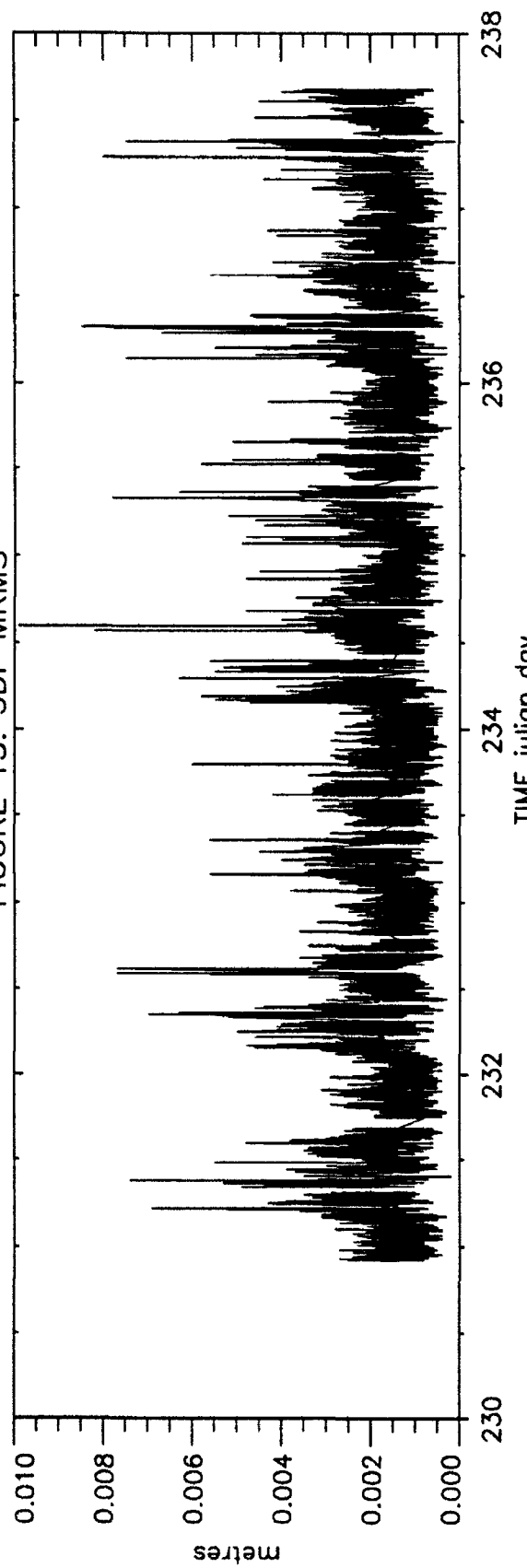
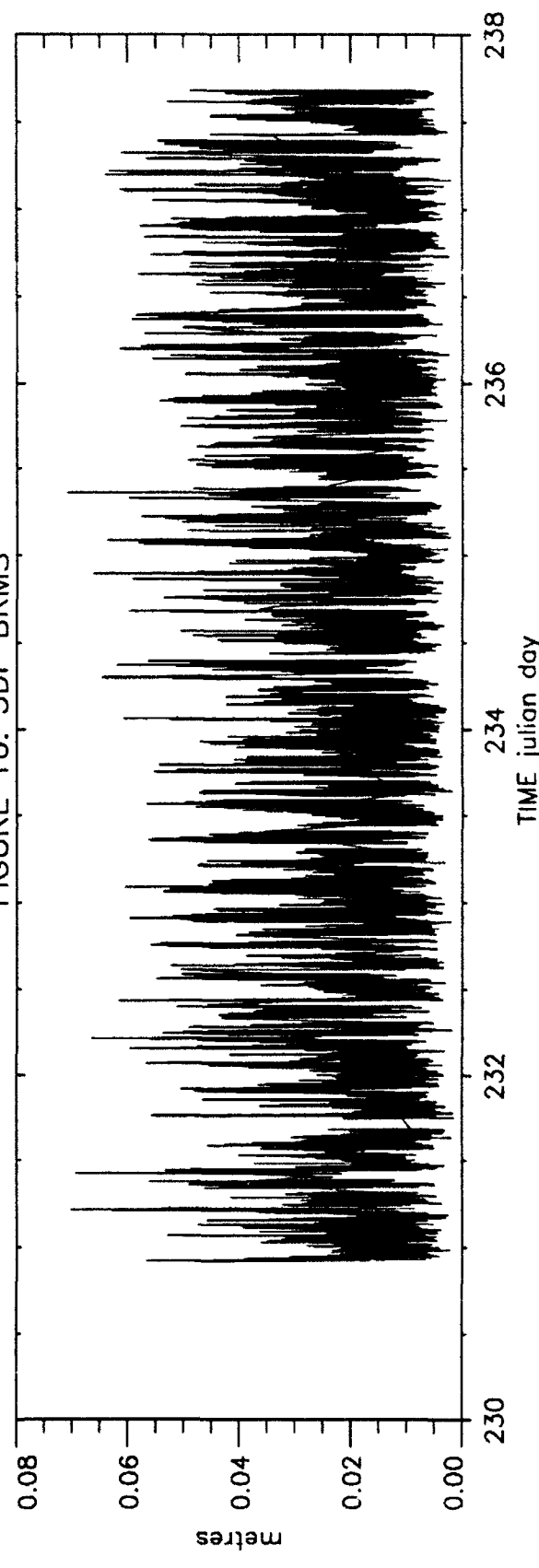


FIGURE 16: 3DF BRMS



5. MEASURED 3DF ERROR BEHAVIOUR

During this trial there were 14 Block II GPS satellites plus 4 Block I satellites operational. The full GPS operational capability is expected in 1995, at which time the GPS constellation will consist of 24 (Block II) satellites. Since the constellation was not fully operational at the time of this trial, some brief periods of poor satellite geometry were experienced, causing some abnormally large errors. Indeed about 9.7% of the 3DF attitude data was flagged as invalid, as illustrated in Figure 8. This data was therefore removed and all statistical results shown here are based on the remaining data.

Since this report is dealing with the *real-time* dynamic performance of a system which only provides discrete output, care must be taken to define what errors are being examined. For example data interpolation is not possible in real time. Therefore to indicate the potential 3DF performance, we have attempted to separate the actual measurement errors from the errors due to changes in the attitude between measurements.

We therefore first look only at the errors in the 3DF measurements at the one second marks. These one second errors will be referred to as the *discrete dynamic* errors. These can be interpreted as the errors seen by a user who did not require continuous attitude data, such as an integrated system with an inertial component. They could also be seen as an upper bound on the potential performance of such an integrated system which used a very low cost INS (or AHRS). However these figures can be very misleading for real-time dynamic applications, as discussed below.

These discrete dynamic errors however do not account for the very real dynamic limitations in the one second measurements. For example, if attitude data was being used *in real-time* at a 50 Hz rate but was only updated once a second, then any change in attitude over the one second update intervals (due to platform dynamics) would effectively be a real error in the estimate, even if it were perfectly accurate at the one second marks. This effect can be seen Figures 12 to 14, in the case of the 3DF system on a ship at sea. Here the platform dynamics between 3DF samples can be clearly seen. Since the reference data was recorded at a higher rate (about 6 Hz), a more honest evaluation of the continuous 3DF performance is found by comparing the single 3DF value for each one second interval with the reference values over the entire interval. Errors found in this way will be referred to as the *continuous dynamic* errors. Since this accurately reflects the real-time dynamic performance, it depends strongly on the platform dynamics and the measurement update rate. The results found here therefore apply only to a particular platform (small ship) and rate (1 Hz), and are intended primarily to illustrate how misleading the discrete dynamic performance can be.

5.1 Discrete-Dynamic Performance

The discrete dynamic errors of the 3DF heading, pitch and roll are shown in Figures 17 to 19, where the time histories throughout the trial are shown. Only valid carrier phase derived attitude data is shown. From these plots it is evident that the pitch and roll errors are dominated by constant biases, presumably due to misalignment.

Figures 20 to 22 show the same data on a smaller scale, so that the nominal data can be more easily seen. From these it can be seen that the pitch and roll errors are dominated by noise, while the heading error has a more complex behaviour, with some drifting components and sudden shifts in "bias". Appendix B presents this data on an expanded time scale for clearer viewing, showing daily plots. This appendix also shows the heading errors with some smoothing, so that the drifting errors and changes in the "bias" are not obscured by the noise.

The statistics derived from this data are presented in Table 4. Since the pitch and roll errors are obviously dominated by biases, presumably due to installation/calibration errors, statistics have also been derived from data with these biases removed, to better illustrate the stability and the potential accuracy performance.

As a cautionary note, it should be mentioned that, since the errors obviously have a large component of noise, the amount of data compressed onto the plots of Figures 17 to 22 makes it difficult to visually judge the rms values or standard deviations. With a plotting resolution of 300 dots per inch, presenting 469,577 data point against an 8 inch scale means that at each time pixel about 200 data points are superimposed, so that only the two extreme points from each set are visible. This of course has a magnifying effect on the apparent size of the errors.

Figures 23 to 25 present a detailed view of the discrete attitude errors, for the time period corresponding to Figures 12 to 14.

TABLE 4. DISCRETE-DYNAMIC 3DF ATTITUDE ERRORS

SOURCE	RMS ERROR (degrees)	STANDARD DEVIATION (degrees)	PERCENTILE (degrees)				
			raw		bias removed		
	68%	95%	68%	95%	100%		
HEADING	0.47	0.47	0.08	0.13	0.04	0.08	56.7
PITCH	1.14	0.27	1.13	1.20	0.05	0.11	4.5
ROLL	1.28	0.26	1.27	1.34	0.05	0.11	6.5

The rms and standard deviation numbers in Table 4 are based on 469,577 samples, taken at a one Hz rate over seven days (all available carrier phase based attitude measurements). The percentiles are based on samples taken every 20 seconds over the seven days.

Figures 26 to 28 show the complete set of percentile values for the valid data (with biases removed). This is simply a plot of all error magnitudes, sorted by magnitude. It can be interpreted as a sample cumulative probability density function as follows. If the values of the

percentile function for $|\delta\theta|$ is $V(p)$ for percentiles $0 < p \leq 100$, then

$$\text{Prob}\{|\delta\theta| \leq V\} = p/100 \quad (10)$$

Also noteworthy is the fact that the rms and standard deviation statistics in Table 4 are very large when compared to the percentile values: for normally distributed data the rms value should correspond to the 68 percentile. As can be seen from the percentile plots, the large rms values are due to a very small number of relatively large errors. If this were filtered with inertial data then these spurious points could be eliminated. In fact when the worst 1% of the errors are removed, then the standard deviation of the remaining data is 0.045 degrees in heading and 0.054 degrees in pitch and roll, which very closely matches the 68 percentiles (bias removed), as would be expected. Figures 29 to 31 show the error percentiles rescaled, so that the more meaningful values can be clearly seen.

The percentile statistics are therefore perhaps the most significant. These illustrate the nominal performance of about 0.05 degrees (or about one milliradian) at the one sigma level and about 0.1 degree (or about two milliradians) at the two sigma (95%) level. These discrete-dynamic errors are examined in more detail in Section 6 below.

5.2 Continuous-Dynamic Performance

For real-time use, as a stand-alone system on a moving platform, the continuous-dynamic performance is probably the most relevant. The continuous dynamic errors of the 3DF heading, pitch and roll are shown in Figures 32 to 34, where the time histories throughout the trial are shown. These results are of course highly dependent on the platform dynamics, which in this case were quite benign, and the measurement rate, which at 1 Hz was quite slow. As seen in Figures 9 to 14, the ship experienced fairly low amplitude (less than about 4 degrees) attitude oscillations with about a 5 to 10 second period.

As with the discrete data, only valid carrier phase derived attitude data is shown. Figures 35 to 37 show the same data on a smaller scale, so that the nominal data can be more easily seen. The statistics derived from this data are presented in Table 5. Since the pitch and roll errors are obviously dominated by biases, presumably due to installation/calibration errors, statistics have also been derived from data with these biases removed. Comparing these results with the discrete-dynamic statistics of Table 4, it becomes clear that the continuous-dynamic errors are dominated by the "extrapolation error" between the one second measurements.

Figures 38 to 40 present a detailed view of these attitude errors, for the time period corresponding to Figures 12 to 14. These illustrate the significant error growth between one second measurement updates, due to platform dynamics. Clearly an increased update rate, if possible, and/or a careful extrapolation method, would be desirable.

Figures 41 to 43 show the complete set of percentile values for the valid data (with biases removed). As with the discrete data, the statistics here are skewed by a very small number of bad data points (less than 1%). Thus, as with the discrete results, the percentiles are perhaps the most significant statistics to quote and Figures 44 to 46 show these error

percentiles rescaled, so that the more meaningful values can be clearly seen.

TABLE 5. CONTINUOUS-DYNAMIC 3DF ATTITUDE ERRORS

SOURCE	RMS ERROR (degrees)	STANDARD DEVIATION (degrees)	PERCENTILE (degrees)				
			raw		bias removed		
	68%	95%	68%	95%	100%		
HEADING	0.62	0.61	0.13	0.37	0.13	0.37	56.1
PITCH	1.24	0.56	1.21	1.90	0.28	0.91	8.1
ROLL	1.35	0.50	1.34	1.93	0.26	0.84	7.8

The rms and standard deviation numbers in Table 5 are based on 2,974,775 samples, taken at 0.16 second intervals over seven days. As with the discrete results, the percentiles are based on every 20th sample taken, (which in this case is every 3.2 seconds) over the seven days.

Since the characteristics of the continuous errors can be derived from those of the discrete errors if the platform dynamics are known, these continuous errors will not be further examined.

FIGURE 17: DISCRETE HEADING ERROR VS TIME

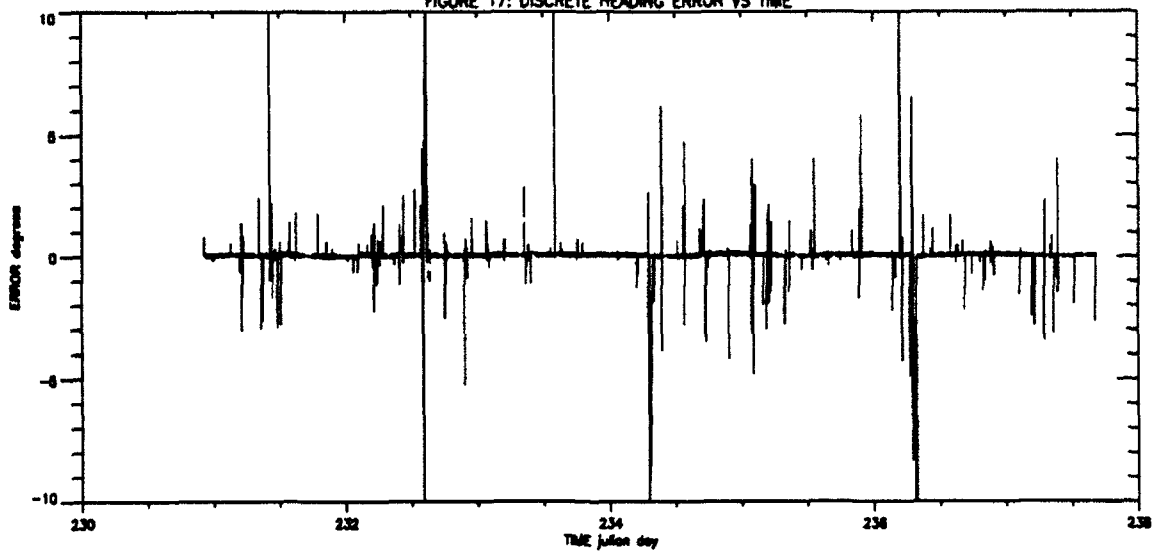


FIGURE 18: DISCRETE PITCH ERROR VS TIME

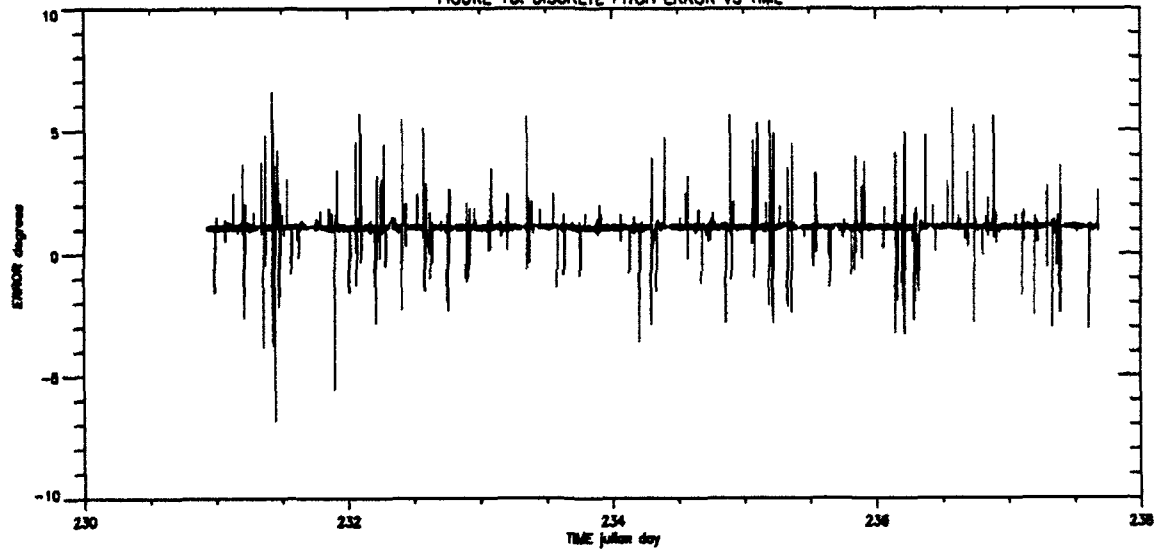


FIGURE 19: DISCRETE ROLL ERROR VS TIME

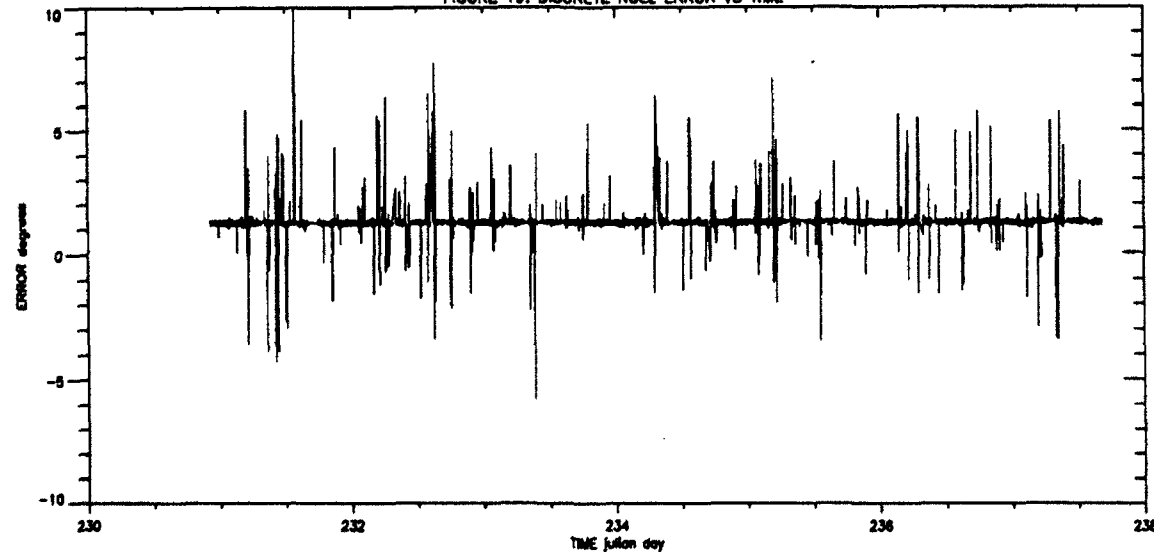


FIGURE 20: DISCRETE HEADING ERROR VS TIME

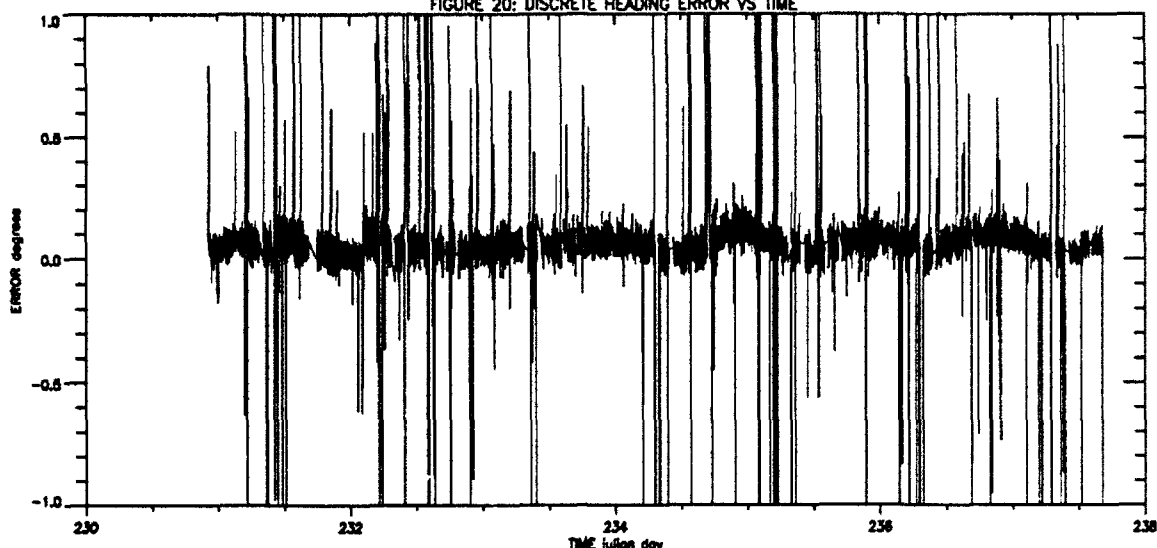


FIGURE 21: DISCRETE PITCH ERROR VS TIME

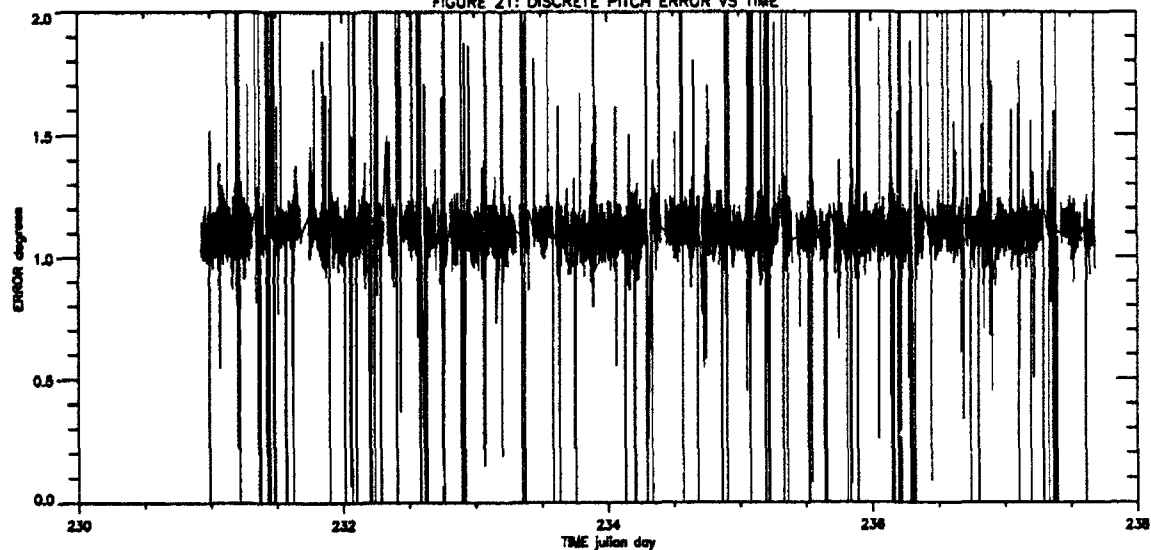


FIGURE 22: DISCRETE ROLL ERROR VS TIME

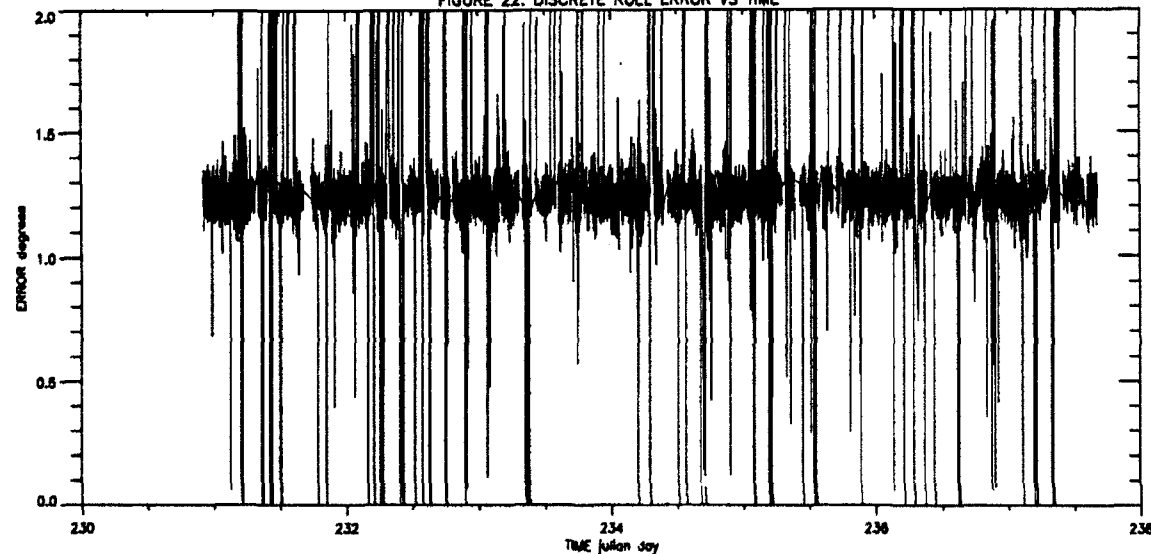


FIGURE 23: DETAILED VIEW OF HEADING ERROR

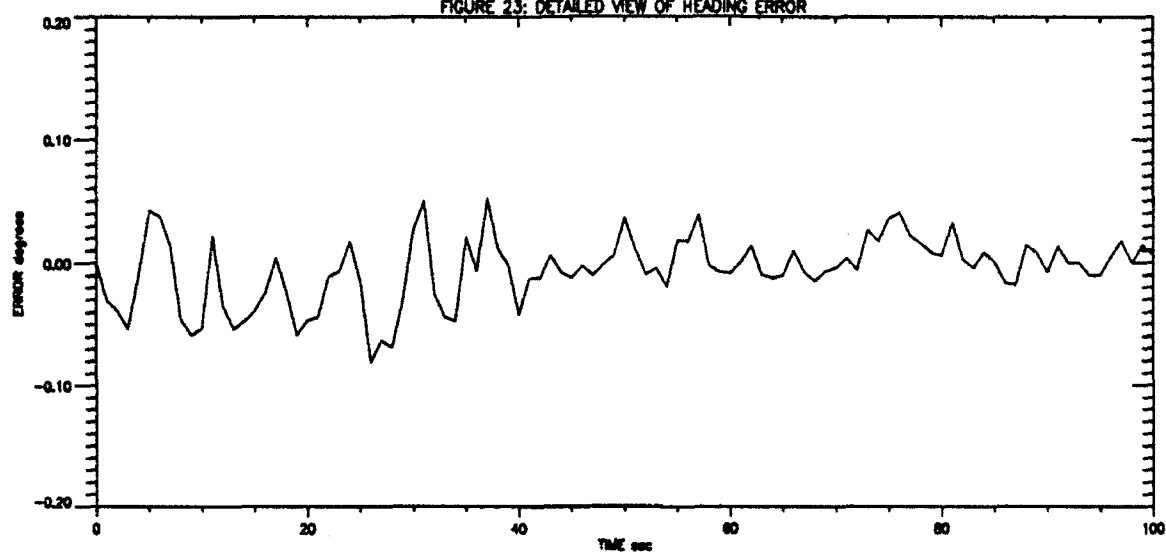


FIGURE 24: DETAILED VIEW OF PITCH ERROR

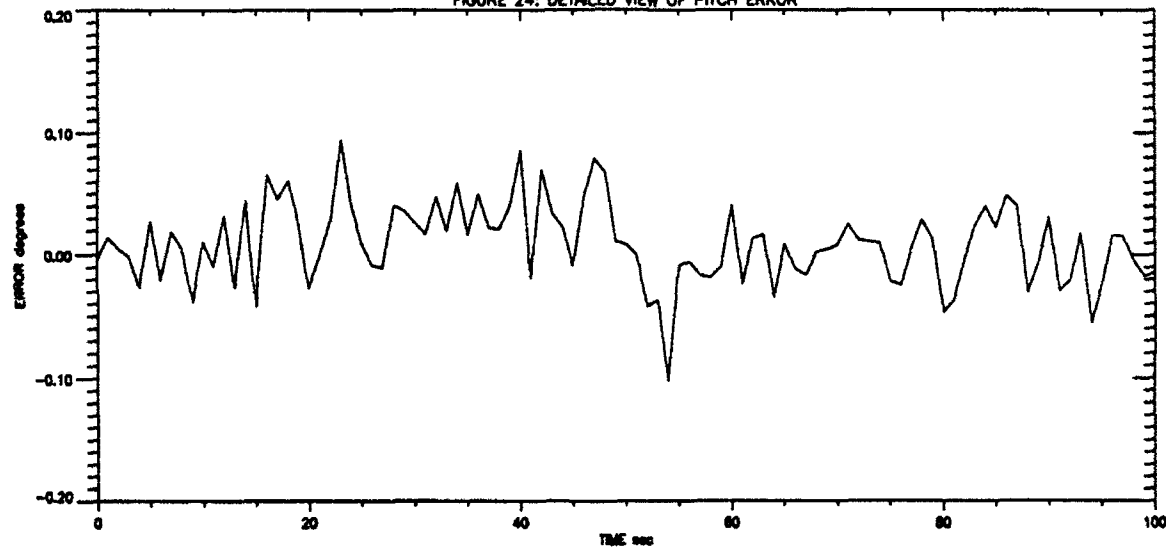


FIGURE 25: DETAILED VIEW OF ROLL ERROR

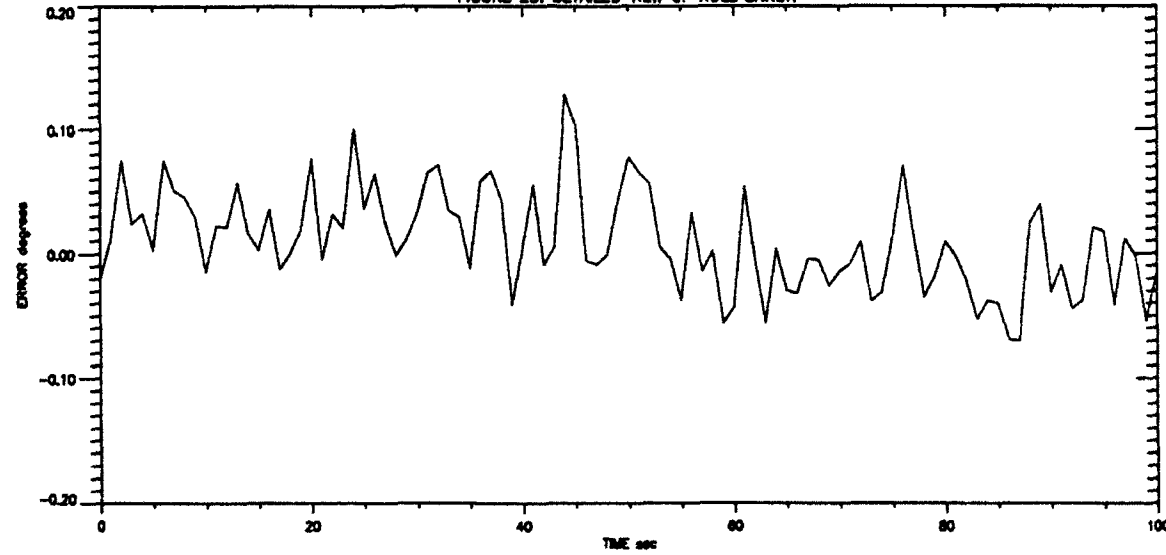


FIGURE 26: DISCRETE HEADING ERROR PERCENTILES

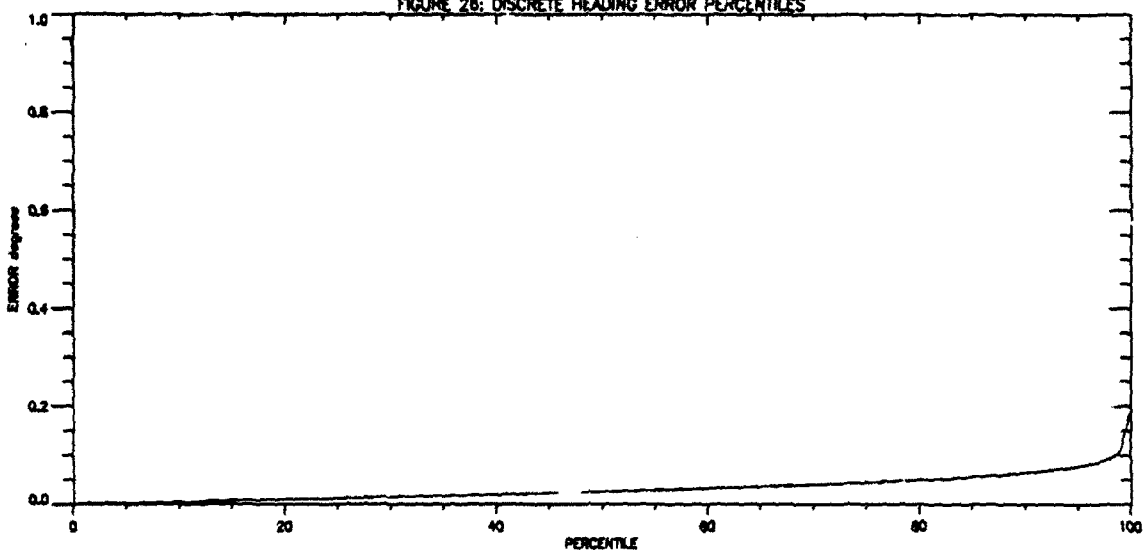


FIGURE 27: DISCRETE PITCH ERROR PERCENTILES

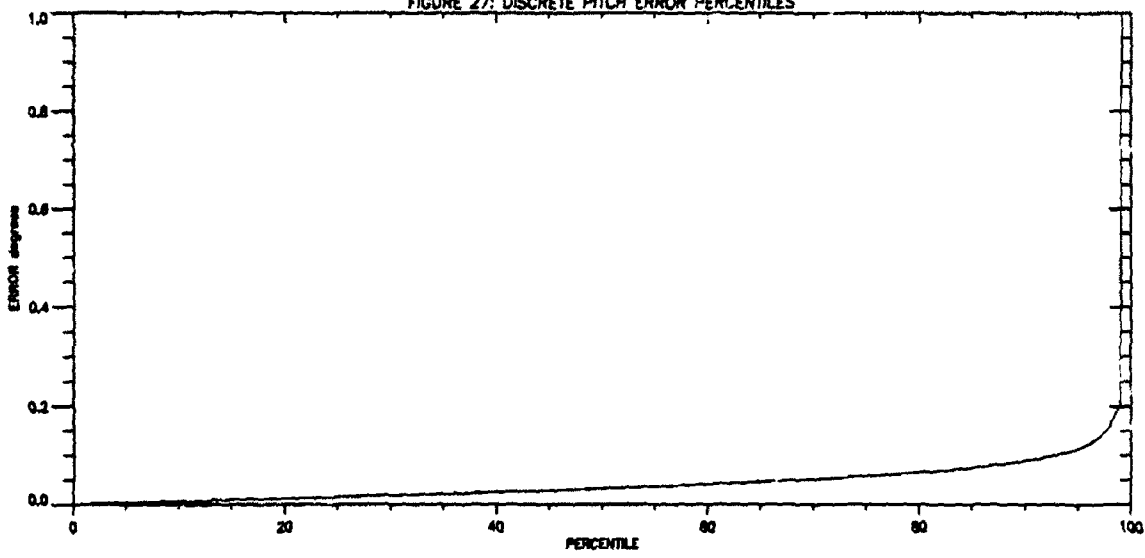


FIGURE 28: DISCRETE ROLL ERROR PERCENTILES

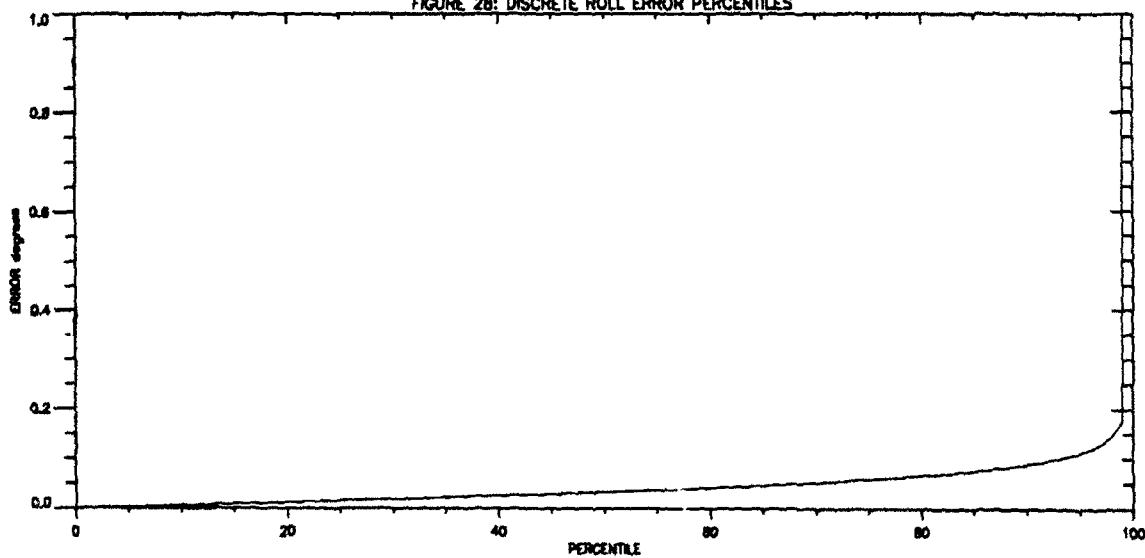


FIGURE 29: DISCRETE HEADING ERROR PERCENTILES

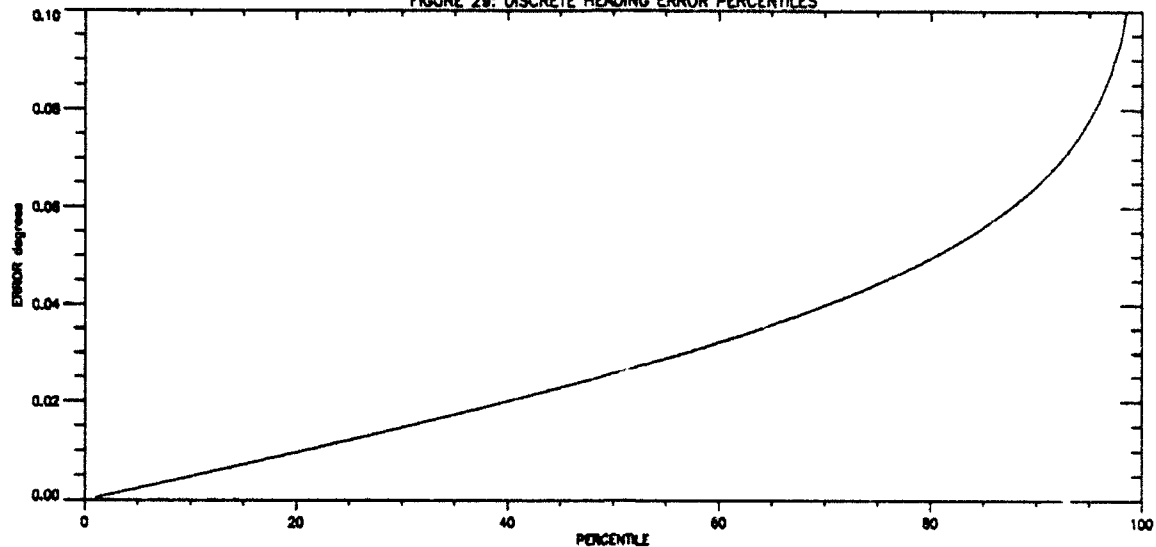


FIGURE 30: DISCRETE PITCH ERROR PERCENTILES

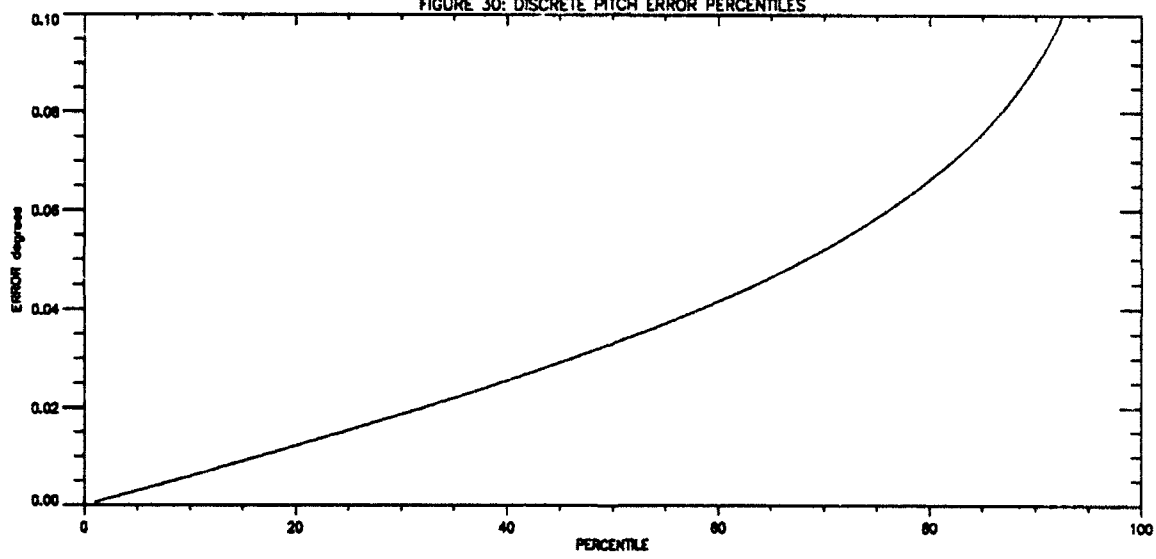


FIGURE 31: DISCRETE ROLL ERROR PERCENTILES

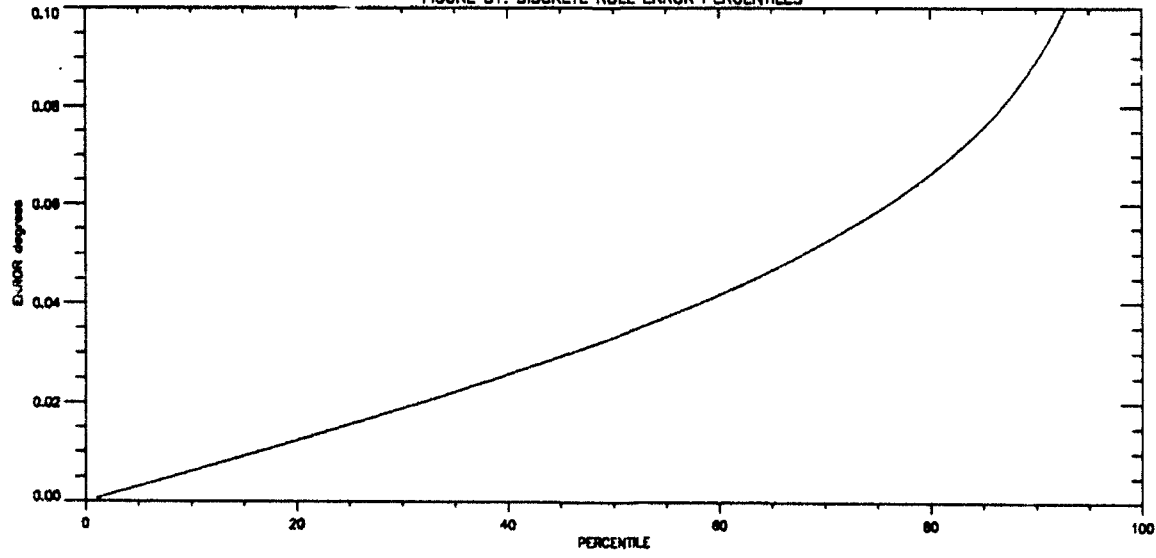


FIGURE 32: CONTINUOUS HEADING ERROR VS TIME

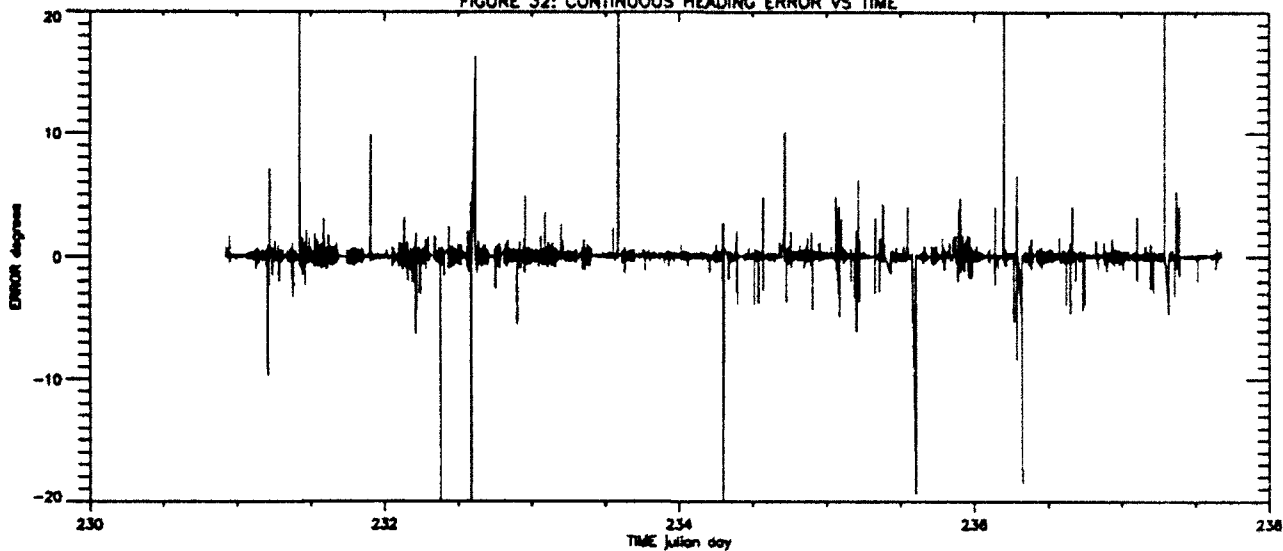


FIGURE 33: CONTINUOUS PITCH ERROR VS TIME

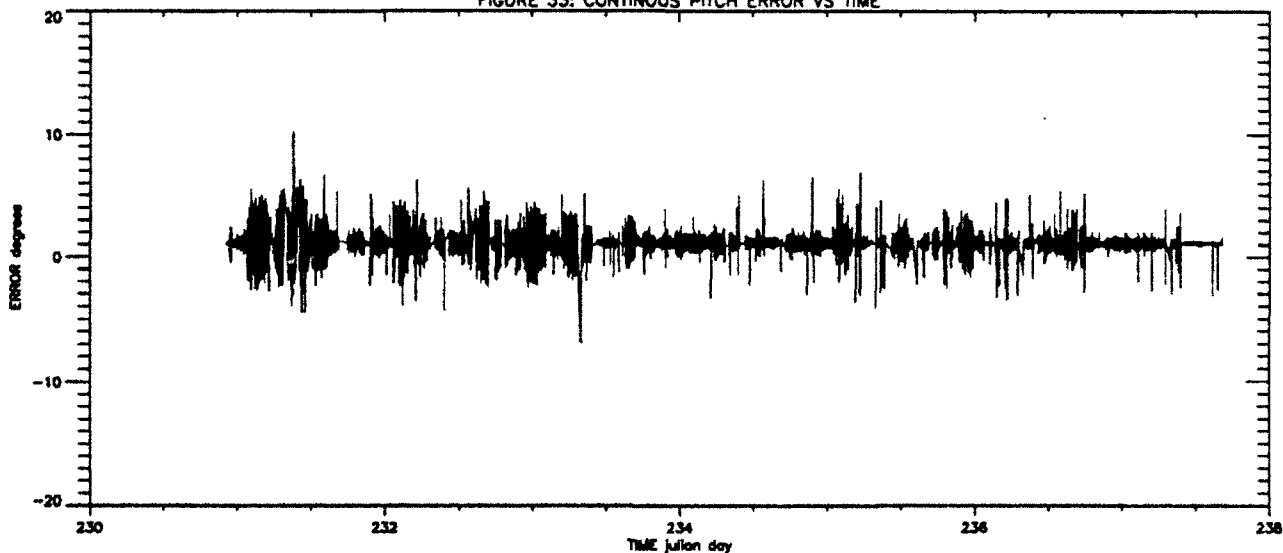


FIGURE 34: CONTINUOUS ROLL ERROR VS TIME

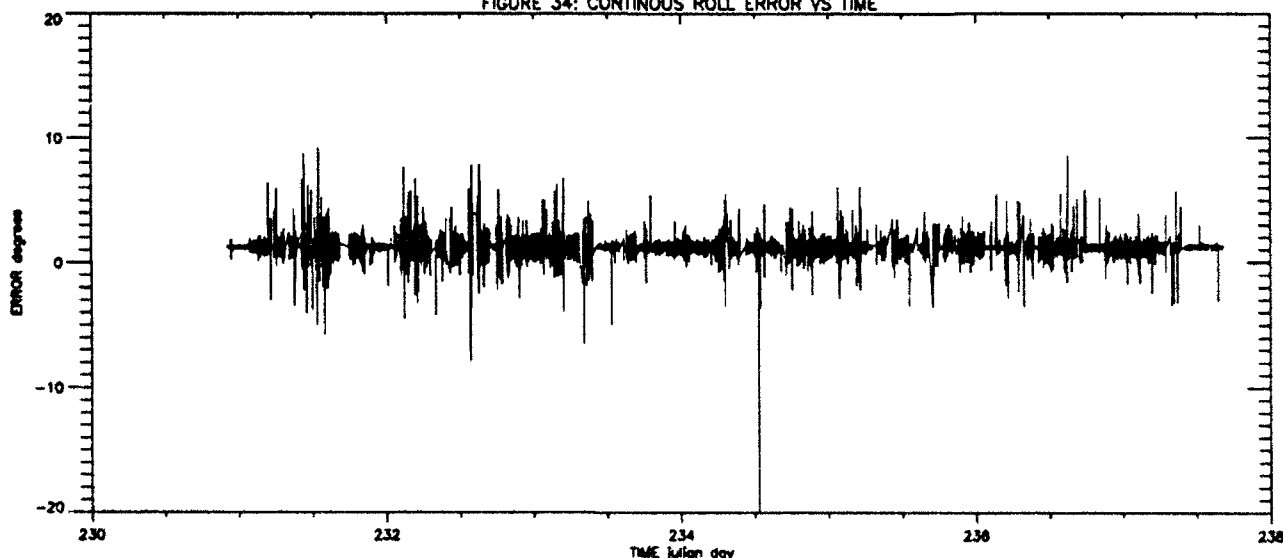


FIGURE 35: CONTINUOUS HEADING ERROR VS TIME

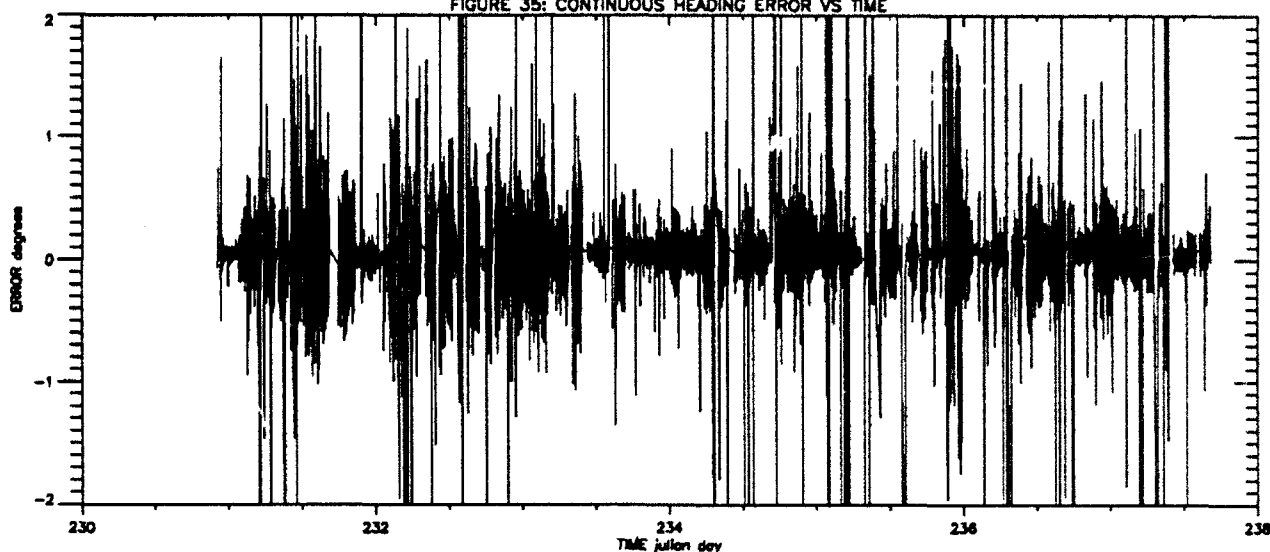


FIGURE 36: CONTINUOUS PITCH ERROR VS TIME

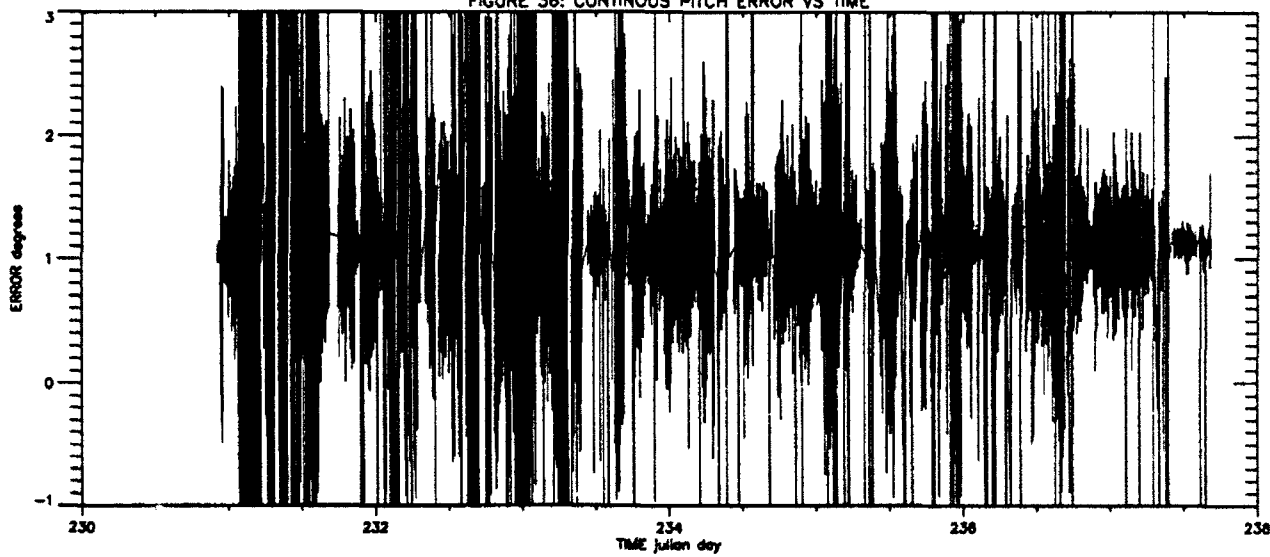


FIGURE 37: CONTINUOUS ROLL ERROR VS TIME

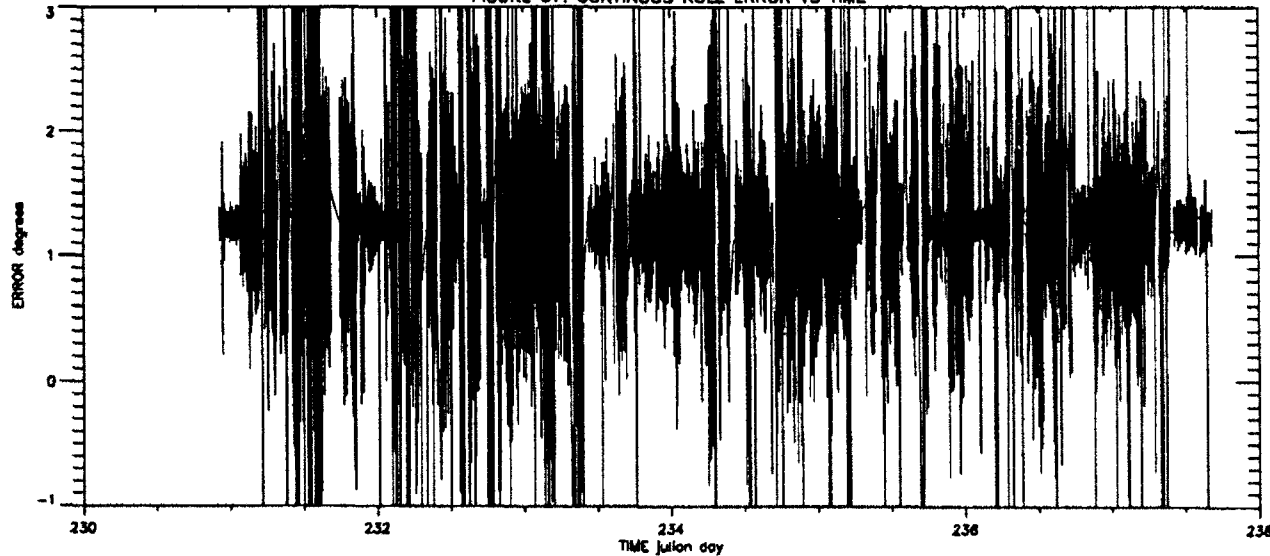


FIGURE 38: DETAILED VIEW OF HEADING ERROR

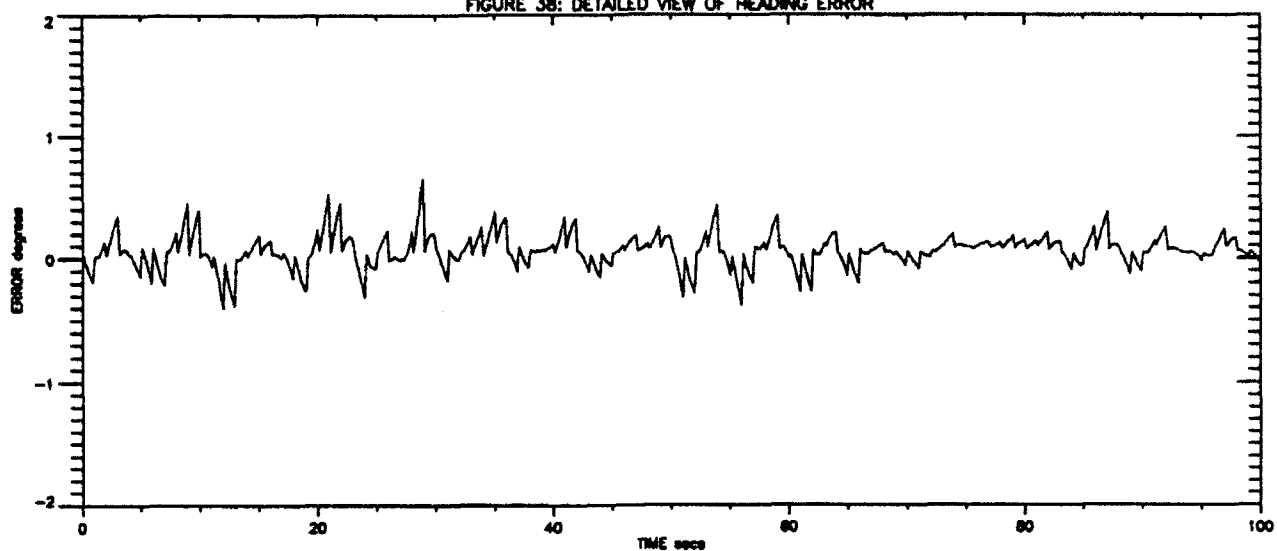


FIGURE 39: DETAILED VIEW OF PITCH ERROR

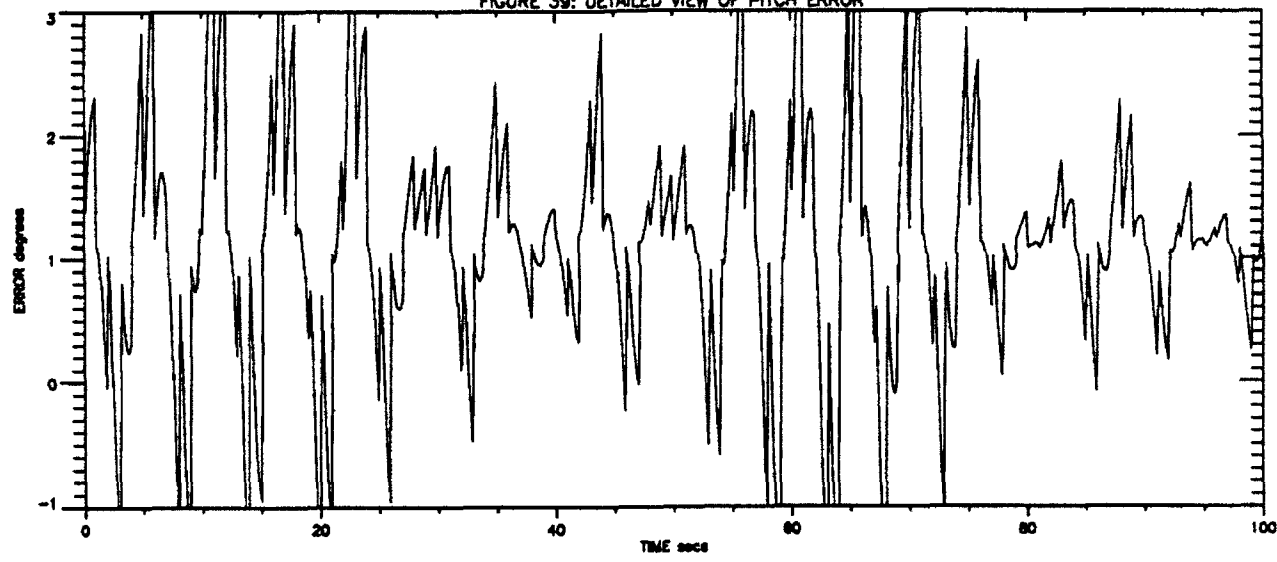


FIGURE 40: DETAILED VIEW OF ROLL ERROR

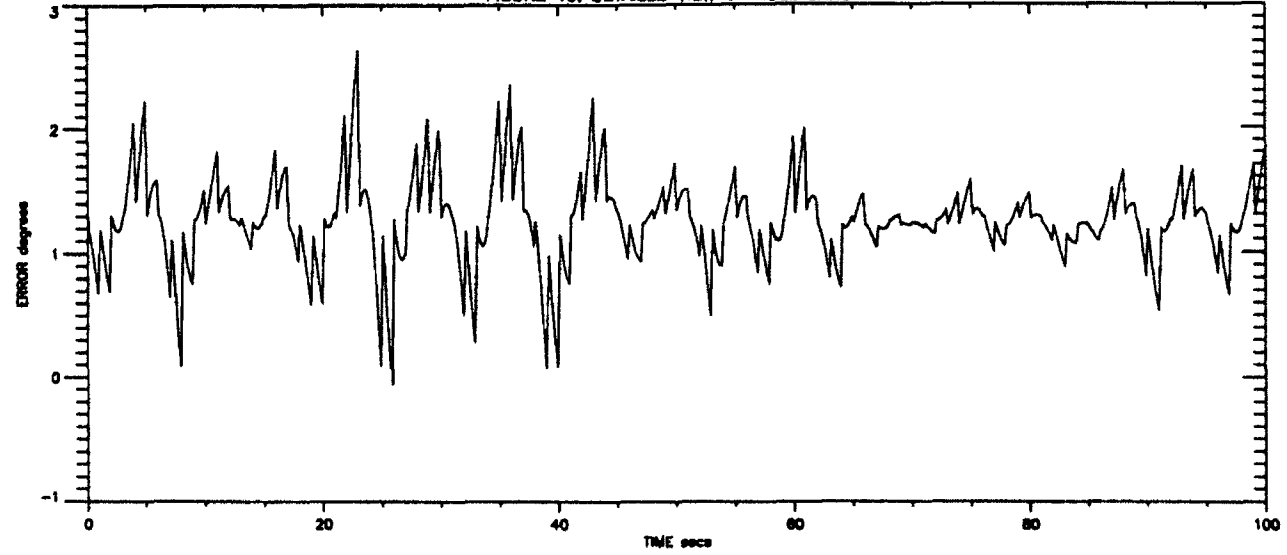


FIGURE 41: CONTINUOUS HEADING ERROR PERCENTILES

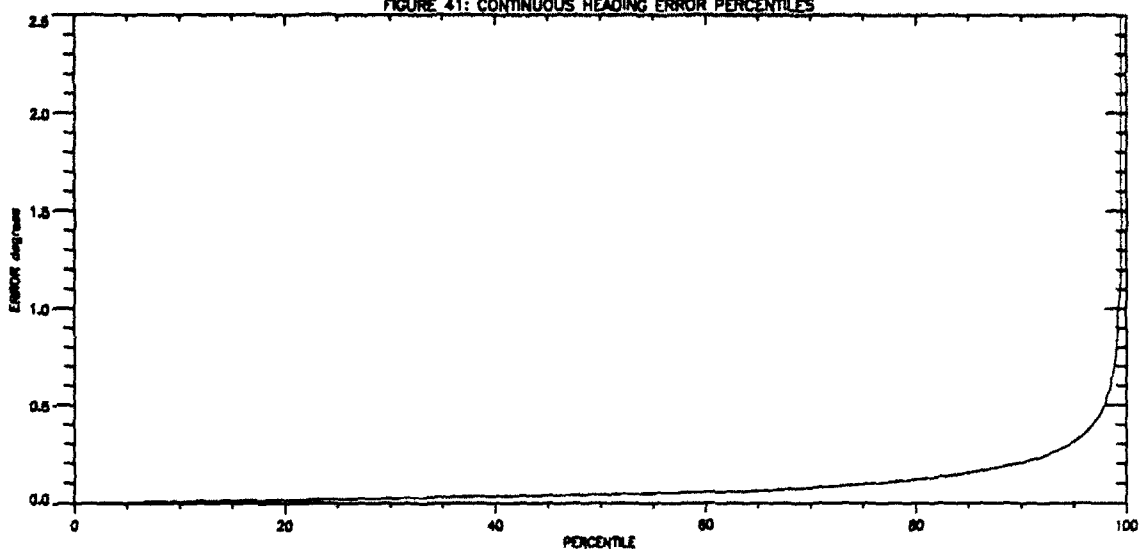


FIGURE 42: CONTINUOUS PITCH ERROR PERCENTILES

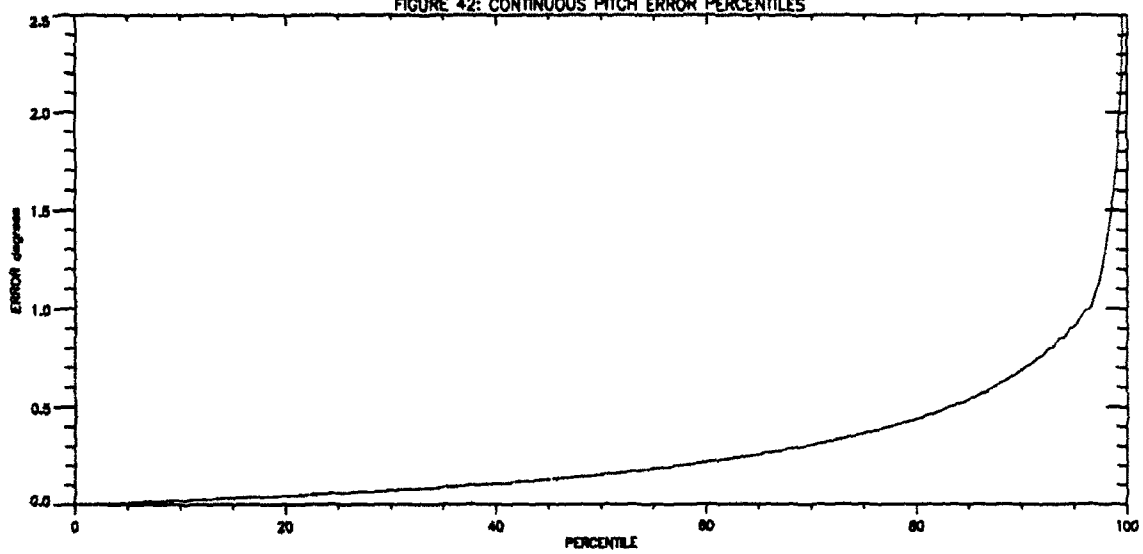


FIGURE 43: CONTINUOUS ROLL ERROR PERCENTILES

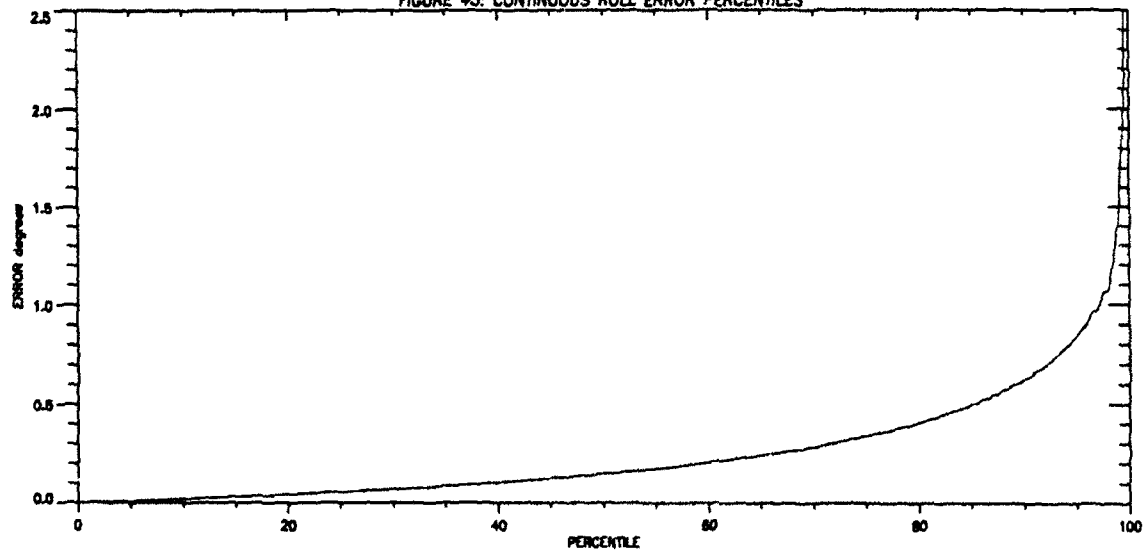


FIGURE 44: CONTINUOUS HEADING ERROR PERCENTILES

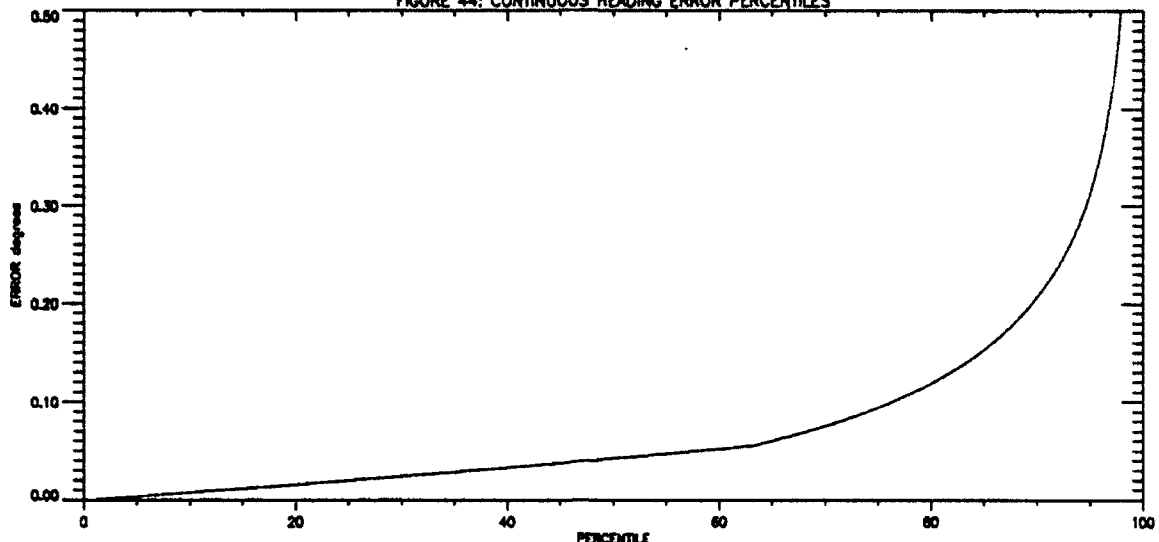


FIGURE 45: CONTINUOUS PITCH ERROR PERCENTILES

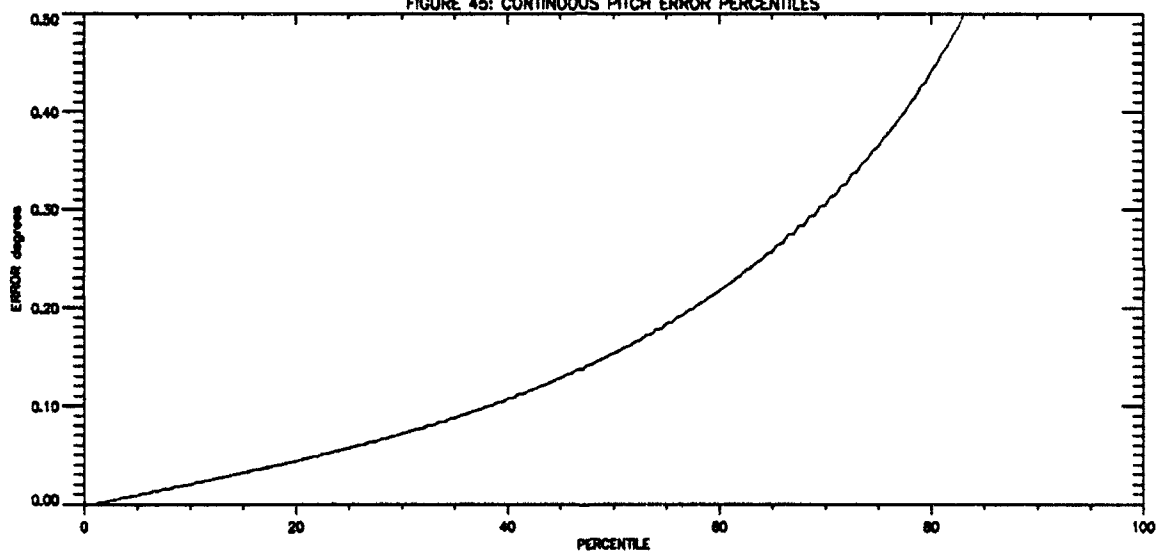
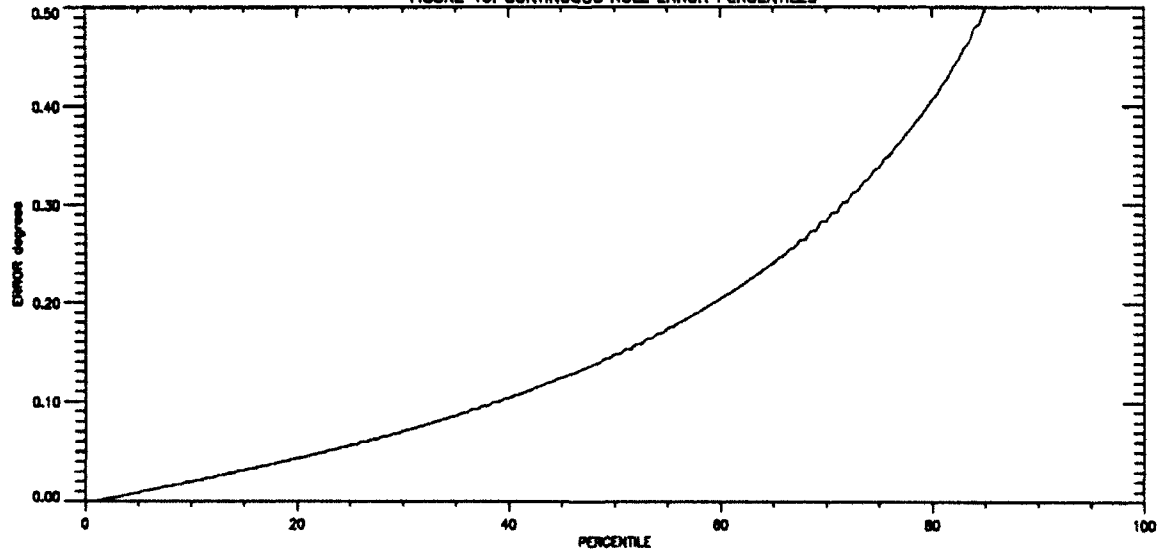


FIGURE 46: CONTINUOUS ROLL ERROR PERCENTILES



6. STOCHASTIC ERROR MODEL

In this section a specific stochastic error model will be developed for each of the 3DF attitude error components. Besides offering insight into the error behaviour of the 3DF attitude measurements, these models will be in a form suitable for use by a Kalman filter. As expected, these errors will be shown to have characteristics which are complementary to the error characteristics of an inertial system, making a Kalman filter integration of the two an attractive option.

The stochastic models normally used by Kalman filter designers to describe random variables $x(t)$, are relatively simple linear models such as random biases, white noise processes, first order Markov processes, random walks or periodic processes. These are adequately described in reference [14]. They are usually distinguished by their distinctive autocorrelation functions $\phi(\Delta t)$. The autocorrelation function $\phi_{xx}(\Delta t)$, of a random variable $x(t)$, is defined to be the expected correlation between values of $x(t)$ separated in time by Δt seconds:

$$\phi_{xx}(\Delta t) = E\{x(t)x(t+\Delta t)\} \quad (11)$$

Perhaps the most useful stochastic model is the first order Markov process, since the random bias and white noise are both, in some sense, a special case of this Markov process. The Markov process $x(t)$ is described by two parameters: its root mean square value σ and its autocorrelation time τ . It has the following autocorrelation function:

$$\phi_{xx}(\Delta t) = \sigma^2 e^{-\Delta t/\tau} \quad (12)$$

For obvious reasons this type of process is often referred to as an "exponentially correlated process". If the correlation time τ is made very large, this Markov process will be so strongly correlated that it will essentially behave as a random bias, and if the correlation time τ is made very small (much smaller than the sample time), then it will be so weakly correlated that it will essentially behave as uncorrelated white noise. Equation 12 therefore provides an ideal "template" to use in extracting the error model parameters (σ and τ) from an autocorrelation function.

Now the definition given by equation 11 can be used to obtain a "sample autocorrelation function" from the measured $x(t)$ (the 3DF attitude errors in this case). Then by matching the plot of this autocorrelation function ϕ_{xx} to the template of equation 12, the model parameters σ and τ can be easily extracted as follows. The initial value is σ :

$$\sigma^2 = \phi_{xx}(0) \quad (13)$$

and the point at which ϕ_{xx} drops to $1/e$ of its initial value is τ :

$$\phi_{xx}(\tau) = \sigma^2 e^{-1} \quad (14)$$

or alternately, the slope of ϕ_{xx} at the origin is $-\phi_{xx}(0)/\tau$:

$$\left. \frac{\partial \phi_{xx}(t)}{\partial t} \right|_{t=0} = \frac{-\phi_{xx}(0)}{\tau} \quad (15)$$

Therefore, in order to match the 3DF errors to the appropriate model(s), it is useful to examine the sample autocorrelation functions.

6.1 Autocorrelation Functions

As described in reference [14], the sample autocorrelation function ϕ_{xx} of the variable x_n , $n=1\dots N$ (discrete samples of a stochastic process $x(t)$ at times $n\Delta t$ where $x(t)$ may be a vector) is defined to be:

$$\phi_{xx}(n\Delta t) = \frac{1}{N-n-1} \sum_{i=1}^{N-n} (x_i - m)(x_{i+n} - m)^T \quad n=0,1,\dots,N-2 \quad (16)$$

where m is the sample mean:

$$m = \frac{1}{N} \sum_{i=1}^N x_i \quad (17)$$

where it can be seen from equation 16 that, as expected, $\phi_{xx}(0)$ is the mean square value. The relationship between this sample autocorrelation function and the true autocorrelation function is discussed in reference [14] (page 89), where it is indicated that the sample function is a very good approximation of the true function provided that the sample length is much longer than the correlation time of the process. In fact, for a Markov process, the uncertainty in the mean $\hat{\sigma}$ and correlation time $\hat{\tau}$, as derived from the sample autocorrelation function is:

$$E\left\{(\hat{\sigma}^2 - \sigma^2)^2\right\} = \frac{\sigma^4}{N} \quad (18)$$

and

$$E\left\{(\hat{\tau} - \tau)^2\right\} = \tau^2 \frac{\left(e^{2\Delta t/\tau} - 1\right)}{N(\Delta t/\tau)^2} \quad (19)$$

For small $\Delta t/\tau$ ($\ll 1$), as will usually be the case, this can be simplified to:

$$E\left\{(\hat{\tau} - \tau)^2\right\} \approx \frac{2\tau^3}{N\Delta t} \quad (20)$$

In this case the sample period is $\Delta t = 1$ and $N = 469,577$. Therefore if $\tau \geq 600$ seconds and $\sigma \geq .04$ degrees (and if the process really is a first order Markov process) then using the sample autocorrelation function to estimate σ and τ introduces only about 0.00015 degrees (4%) error in the case of $\hat{\sigma}$ and 30 seconds (5%) in the case of $\hat{\tau}$, which are not significant for most purposes.

For modeling purposes it is most appropriate to first model the discrete-dynamic errors, since the continuous-dynamic error model can be obtained from this by simply adding the expected errors due to platform dynamics. The complete sample autocorrelation functions of the discrete attitude errors, (with the biases removed and the worst 1% of errors removed) are therefore shown in Figures 47 to 49.

Now any values of ϕ less than the square of the rms accuracy of the reference system are not significant and should be ignored. In this case, based on INS/DGPS reference accuracy from Table 3, any correlation values below about 0.0001 degrees² should be ignored. Based on INS1 reference data alone, these limits are much higher, and recourse must be taken to the known correlation characteristics of the INS. However, from Figures 47 to 49 it can be seen that there is no significant heading error autocorrelation for $n\Delta t > 10,000$ seconds and no significant pitch and roll error autocorrelation for $n\Delta t > 3,000$ seconds.

Figures 50 to 52 show the first 8,000 seconds of these functions, from which it can be seen that there is at least some temporally correlated error, and in the case of heading a substantial amount. In fact, ignoring for the moment the smaller structure beyond 8,000 seconds (which will be briefly discussed below), these sample autocorrelation function plots appear to be very closely matched to the correlation function of a first order Markov process (exponentially decaying as in equation 12). Closer examination however, reveals that there are strong peaks at $\Delta t = 0$, as is perhaps more apparent in Figures 53 to 55 which show the first 800 seconds. The small fine structure at $0 < \Delta t < 50$ seconds will also be explained below. For the moment we will focus on modeling the dominant error components: the white noise and the Markov processes.

If each of these 3DF attitude errors (heading, pitch and roll) is assumed to be the sum of two stationary processes:

$$\delta\theta = \delta\theta_1 + \delta\theta_2 \quad (21)$$

where $\delta\theta_1$ is white noise and $\delta\theta_2$ is a Markov process, then if these are independent (*uncorrelated* with each other) it can be shown that the autocorrelation function for $\delta\theta$ is simply the sum of the autocorrelation functions of $\delta\theta_1$ and $\delta\theta_2$. Of course this generalizes to the sum of n independent processes, so that the autocorrelation function can be used to decompose the error into component parts. It should be noted that if errors come from independent sources, such as for example receiver noise and multipath, then they are almost certainly independent.

Since the autocorrelation function of a white noise process is zero except at $\Delta t = 0$, the peaks at $\Delta t = 0$ are due to the white noise components and can be removed to find the model

parameters for the Markov component. The magnitude of the peaks *above the exponentially decaying portion*, in Figures 47 to 55, are therefore the mean square of the white noise component. Unfortunately these peak values at $\Delta t = 0$ cannot actually be seen from the data plots (since they drop off so sharply at $\Delta t = 1$, which at these scales is not clearly visible). However the numerical values can of course be easily obtained from the corresponding data files. This error model parameter extraction process is discussed below, and the results are summarized in Table 6.

Pitch

From the sample autocorrelation data file, the total σ^2 for the pitch error is $\phi_{\phi\phi}(0) = 0.0028$ degrees². From Figure 54 the Markov σ_2^2 can be estimated at 0.0012 degrees². This puts the white noise σ_1^2 estimate at 0.0016 degrees². The Markov correlation time is the point where the Markov ϕ drops below $\phi_{\phi\phi}(0)/e = 0.0012/2.718 = 0.00044$, which appears to be at about $\tau_2 = 620$ seconds.

Roll

From the sample autocorrelation data, the total σ^2 for the roll error is $\phi_{\psi\psi}(0) = 0.0028$ degrees². From Figure 55 the Markov σ_2^2 can be estimated at 0.0012 degrees² which puts the white noise σ_1^2 estimate at 0.0016 degrees². The Markov correlation time is the point where the Markov ϕ drops below $\phi_{\psi\psi}(0)/e = 0.0012/2.718 = 0.00044$, which appears to be at about $\tau_2 = 550$ seconds.

Heading

The heading error, as seen in Figure 47, has a somewhat more complicated autocorrelation function, as should perhaps be expected (and as will be discussed below). In this case there seems to be a dominant longer correlation time Markov process plus several smaller processes, none of which can be considered significant. (They consist of small periodic processes with 12 hour, 24 hour and 84 minute periods, and perhaps a very small, short correlation time Markov process (these last two are only visible by close examination of Figure 50). Because these are of questionable statistical significance, only the white noise and long term Markov process will be modeled here.

From the sample autocorrelation data, the total σ^2 for the heading error is $\phi_{\theta\theta}(0) = 0.0013$ degrees². From Figure 53 the Markov σ_2^2 can be estimated at 0.0005 degrees² which puts the white noise σ_1^2 estimate at 0.0008 degrees². The Markov correlation time is the point where the Markov ϕ drops below $\phi_{\theta\theta}(0)/e = 0.0005/2.718 = 0.0002$, which appears to be at about $\tau_2 = 4,000$ seconds. To see this, one should remove the very small "Schuler bump" (due to inertial errors) at about 84 minutes (5,040 seconds) by matching a straight line to the sample autocorrelation function on both sides of this bump. According to equation 19, there should be an uncertainty in τ_2 of about 500 seconds.

The biases, which have been removed from the data prior to these calculations, are installation dependent and therefore more difficult to model in this way. Since only one

installation was done for this trial, the bias model parameters in Table 6 are based on a sample of one and represent an order-of-magnitude estimate only. They must therefore be treated carefully.

It should also be kept in mind that these models are based on data from which the spurious data (worst 1% of errors) have been removed. While this spurious data had a significant effect on the performance statistics (as shown in Table 4 above) they could presumably be rejected by an integrated system. In a stand alone GPS system however, these spurious points cannot be ignored. It should also be kept in mind that these *discrete* errors do not include the latency or interpolation errors which would be present (and very significant) in the continuous dynamic situation with a stand alone GPS system.

TABLE 6. DISCRETE 3DF ERROR MODEL PARAMETERS

	BIAS*	WHITE NOISE	MARKOV	
			σ_2 (degrees)	τ_2 (seconds)
HEADING $\delta\theta$	0.1	0.03	0.022	4,000
PITCH $\delta\phi$	1.0	0.04	0.035	600
ROLL $\delta\psi$	1.0	0.04	0.035	600

* order of magnitude only

A simple interpretation of this model would be that the Markov components were due to multipath errors, the white noise components due to receiver noise and the bias due to installation alignment (calibration) error.

The receiver noise, which should introduce the same level of phase error in each measurement, should therefore produce a slightly smaller heading error, due to the geometric effect mentioned in Section 2. This is consistent with the measured noise components shown in Table 6.

The multipath error, on the other hand, may not introduce the same phase error in each measurement. In fact it seems plausible that low satellite elevation angle signals, which contribute primarily to the heading measurement, would be much more susceptible to multipath errors than high angle signals, which contribute primarily to the pitch and roll. This is consistent with the measured Markov components shown in Table 6. There in fact seems to be strong circumstantial evidence that a large portion of the correlated heading error is due to multipath. There are various times where a sudden shift in heading error takes place, corresponding exactly with a sudden change in ship heading, as seen at time 40,000 sec. in Figure B1, time 26,000 sec. in Figure B2, time 70,000 sec. in Figure B5 and time 46,000 sec.

in Figure B6. Furthermore, the 4,000 second correlation time of the heading Markov error corresponds roughly to the expected correlation time of the multipath error, which changes with satellite geometry. The satellites, in 12 hour orbits, move through about 33 degrees in 4,000 seconds, which corresponds roughly to a "significant" change in geometry (enough to substantially change the multipath errors).

Because of these maneuver-induced discontinuities in the heading error, this multipath error does not truly behave as a pure Markov process. These discontinuities could be modeled as a Poisson process (see reference [15]) which can also be modeled within a Kalman filter as described in reference [16], but this degree of modeling fidelity is likely unnecessary. One might expect this error to have a periodic component as well as the Markov component, since the GPS geometry repeats every 12 hours (provided the platform does not move a great distance). The platform orientation relative to the GPS constellation would not generally repeat in the same way, but since this trial used primarily cardinal headings (north, south, east and west, with some north-west and south-east), there was a significant probability of coincident geometry from one period to the next.

Another factor which may affect heading differently than pitch and roll is ionospheric and atmospheric refraction, which will be much greater for low elevation satellites than high. While the effect on time of arrival of the signal is removed by the double differencing technique used to obtain attitude, the (possible) effect of this refraction on the direction of incidence will be relevant. The correlation function for this type of error would be expected to also have a 12-hour periodic component plus a Markov component. A full analysis of this effect is beyond the scope of this report.

Various other error sources could also contribute to a lesser extent, and could be modeled for some special applications. For example, a data registration error (due to an unknown data latency, as discussed in Section 3.3 above) would introduce a periodic error, with the period being that of the platform dynamics, which was about 10 seconds in this case. This would introduce a decaying periodic component to the autocorrelation function, with the same period. Indeed such a component can be clearly seen in all three of the sample autocorrelation functions in Figures 53 to 55. The small magnitude of these periodic components (about 0.01 degrees), when compared to the observed 3DF error components, shows that the data registration was adequate for this purpose.

Another factor to consider is the internal Kalman filtering within the 3DF receiver, as mentioned in reference [6]. This could have the effect of reducing the white noise component of the error at the expense of the Markov component. The filter gains used will determine the correlation time of the resulting "error" (higher gain leading to shorter correlation time). Hopefully this correlation time is very short.

Finally the errors in the reference system must also be carefully considered. Reference [13] provides an excellent description of inertial system error behaviour. The inertial error would explain the 24-hour (86,400 second) periodic component in the sample heading autocorrelation function as well as the very small Shuler periodic components (5040 seconds) in all three sample autocorrelation functions.

6.2 Cross-Correlation Functions

For use as measurements in a Kalman filter, the cross-correlation is also important. The cross-correlation function of two processes is defined by the obvious generalization of equation (11):

$$\varphi_{xy}(\Delta t) \equiv E\{x(t)y(t+\Delta t)\} \quad (22)$$

and the sample cross-correlation function is the corresponding generalization of equation (16):

$$\varphi_{xy}(n\Delta t) \equiv \frac{1}{N-n-1} \sum_{i=1}^{N-n} (x_i - m_x)(y_{i+n} - m_y)^T \quad n=0,1,\dots,N-2 \quad (23)$$

The Markov processes would be expected to be cross-correlated since they arise from different projections of the same carrier phase errors. (This will be properly accounted for if the phase errors are modeled.) It is the cross-correlation of the measurement noise that is primarily of interest, since negligible cross-correlation here will simplify the Kalman filter.

Figures 56 to 61 show these three cross-correlation functions at different scales. From these it can be seen that the three measurement noise components do not have any significant cross-correlation beyond a few seconds, as would be expected. However, the important error model parameters here (from a Kalman filter perspective) are the *cross-covariance* values:

$$\varphi_{xy}(0) \equiv E\{x(t)y(t)\} \quad (24)$$

and the *correlation coefficients*:

$$\rho_{xy} \equiv \frac{E\{x(t)y(t)\} - E\{x(t)\}E\{y(t)\}}{\sigma_x \sigma_y} \quad (25)$$

From the data shown in Figures 59 to 61, and using equation 24 we have the sample cross-covariance values:

$$\begin{aligned} E\{\delta\theta \delta\phi\} &= 0.000023 \text{ degrees}^2 \\ E\{\delta\theta \delta\psi\} &= -0.00018 \text{ degrees}^2 \\ E\{\delta\phi \delta\psi\} &= -0.00058 \text{ degrees}^2 \end{aligned} \quad (26)$$

which imply the following correlation coefficients:

$$\rho_{\theta\phi} \equiv \frac{E\{\delta\theta \delta\phi\} - E\{\delta\theta\}E\{\delta\phi\}}{\sigma_\theta \sigma_\phi}$$

$$\begin{aligned}
&= \frac{0.000023 - 0}{\sqrt{0.0013 \times 0.0028}} \\
&= 0.012 \\
\rho_{\theta\psi} &= \frac{E\{\delta\theta \delta\psi\} - E\{\delta\theta\}E\{\delta\psi\}}{\sigma_\theta \sigma_\psi} \\
&= \frac{-0.00018 - 0}{\sqrt{0.0013 \times 0.0028}} \tag{27} \\
&= -0.094 \\
\rho_{\phi\psi} &= \frac{E\{\delta\phi \delta\psi\} - E\{\delta\phi\}E\{\delta\psi\}}{\sigma_\phi \sigma_\psi} \\
&= \frac{-0.00058 - 0}{0.0028} \\
&= -0.21
\end{aligned}$$

These correlation coefficients (which can in general range from -1 to 1) suggest that there is a significant degree of cross-correlation, especially between the pitch and roll errors.

6.3 Kalman Filter Model

With this understanding of the error sources, one can begin to formulate an error model suitable for use in a Kalman filter based integrated system. The biases can be modeled as independent random constants (or very long correlation time Markov processes) in the state vector. The white noise component is more appropriately modeled as measurement noise, outside the state vector. Whether the Markov components should be modeled explicitly in the state vector or more simply absorbed into the noise, is dependent on the application and is beyond the scope of this report.

If these Markov states were used, it may be preferable to model them at their source, as independent carrier phase errors, rather than as attitude errors, since the carrier phase errors will be independent to a much greater extent. This is because the phase errors from each receiver channel (noise and multipath etc.) will generally contribute, in varying degrees, to all three components of the attitude error. This will introduce cross-correlations into the attitude errors which can be properly accounted for only by modeling the phase errors. If the GPS position errors were already being modeled as pseudo-range errors, then this should not be overly difficult.

FIGURE 47: HEADING ERROR AUTOCORRELATION FUNCTION

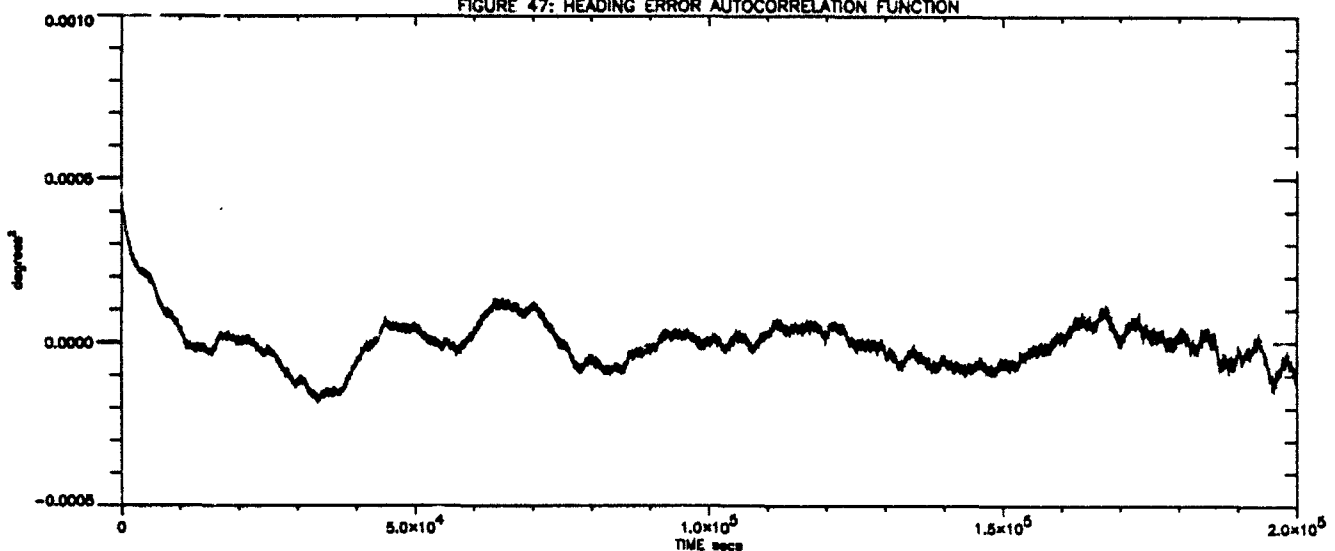


FIGURE 48: PITCH ERROR AUTOCORRELATION FUNCTION

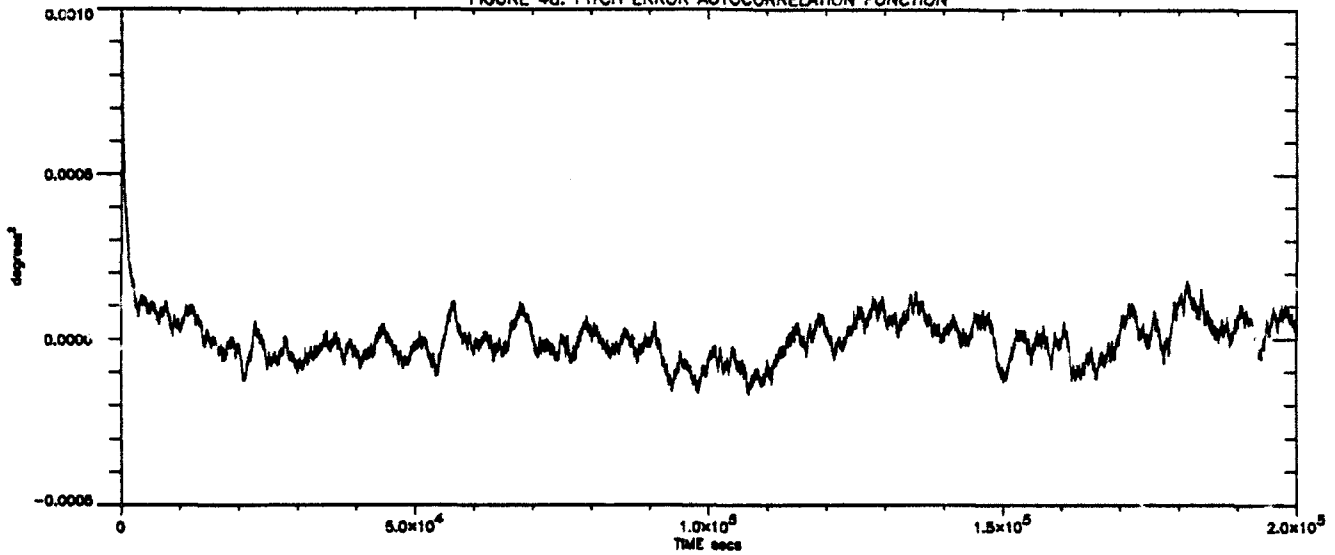


FIGURE 49: ROLL ERROR AUTOCORRELATION FUNCTION

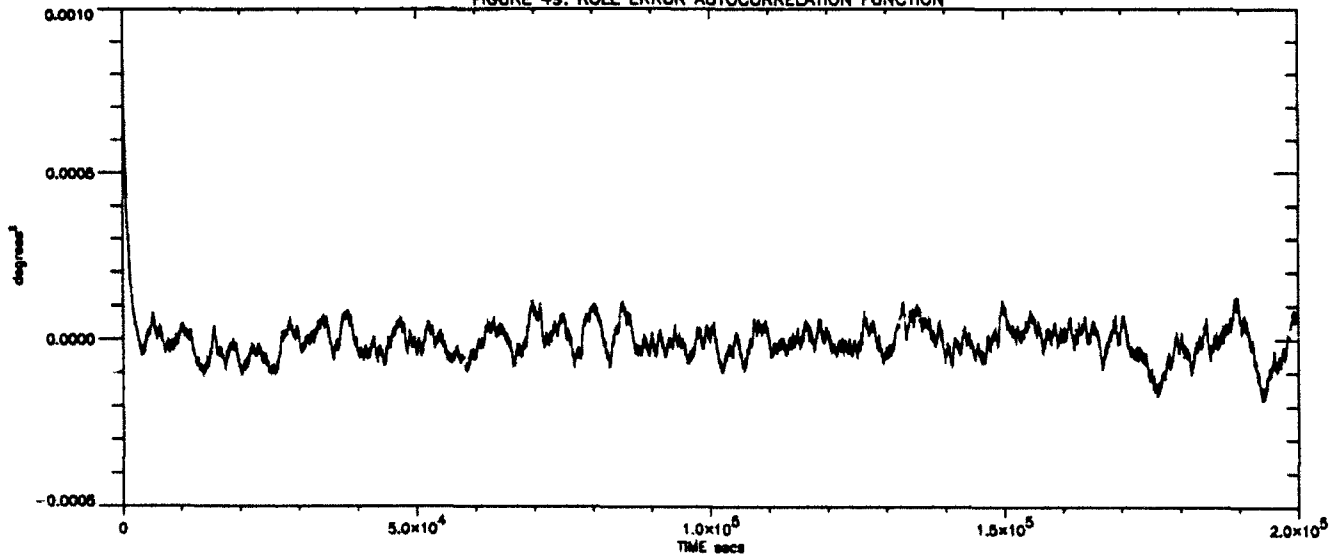


FIGURE 50: HEADING ERROR AUTOCORRELATION FUNCTION DETAIL

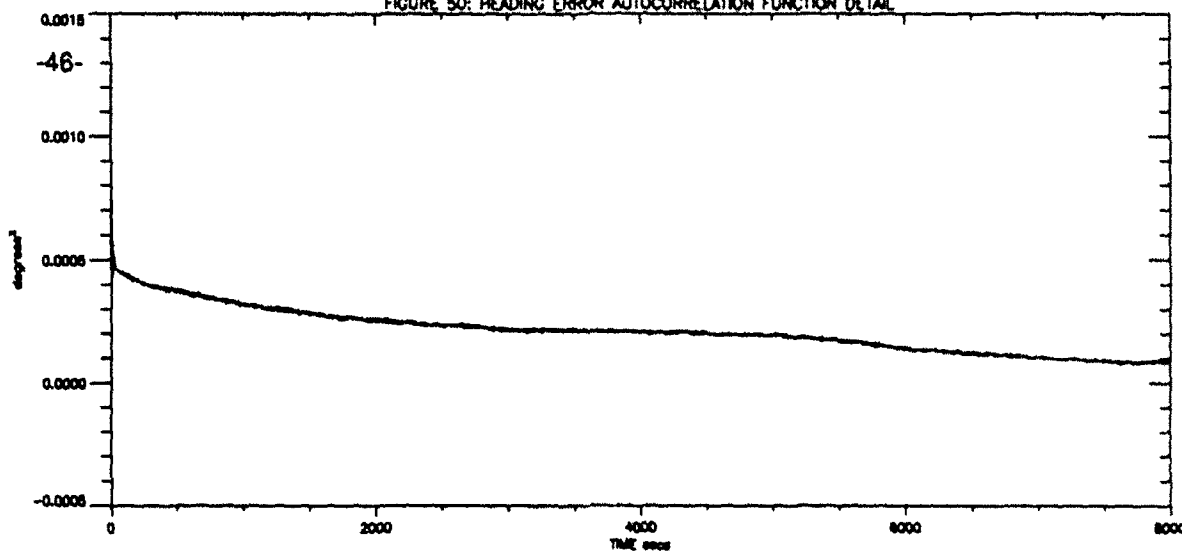


FIGURE 51: PITCH ERROR AUTOCORRELATION FUNCTION DETAIL

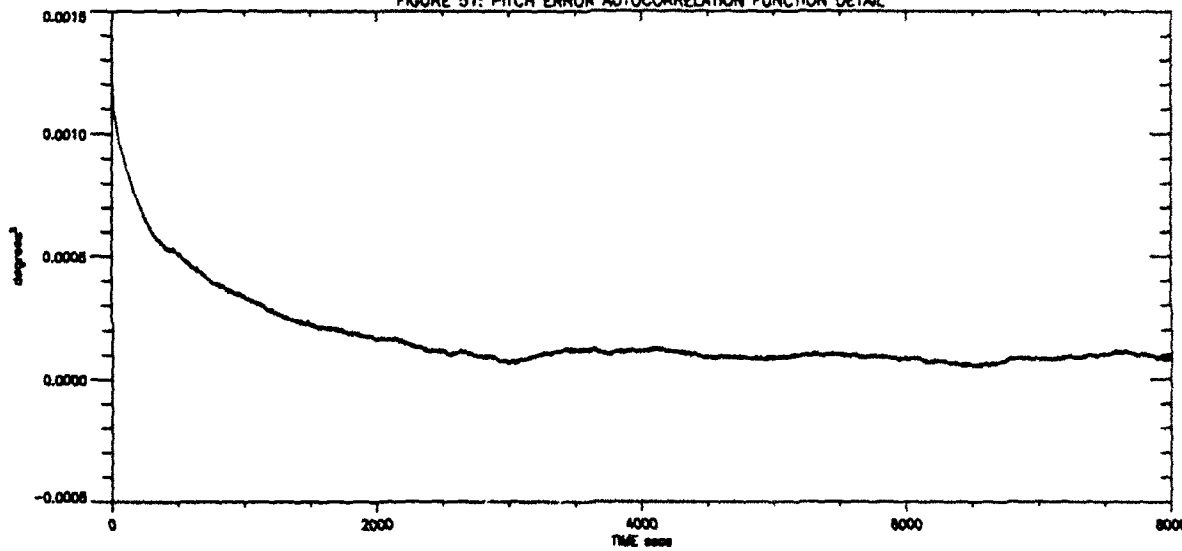


FIGURE 52: ROLL ERROR AUTOCORRELATION FUNCTION DETAIL

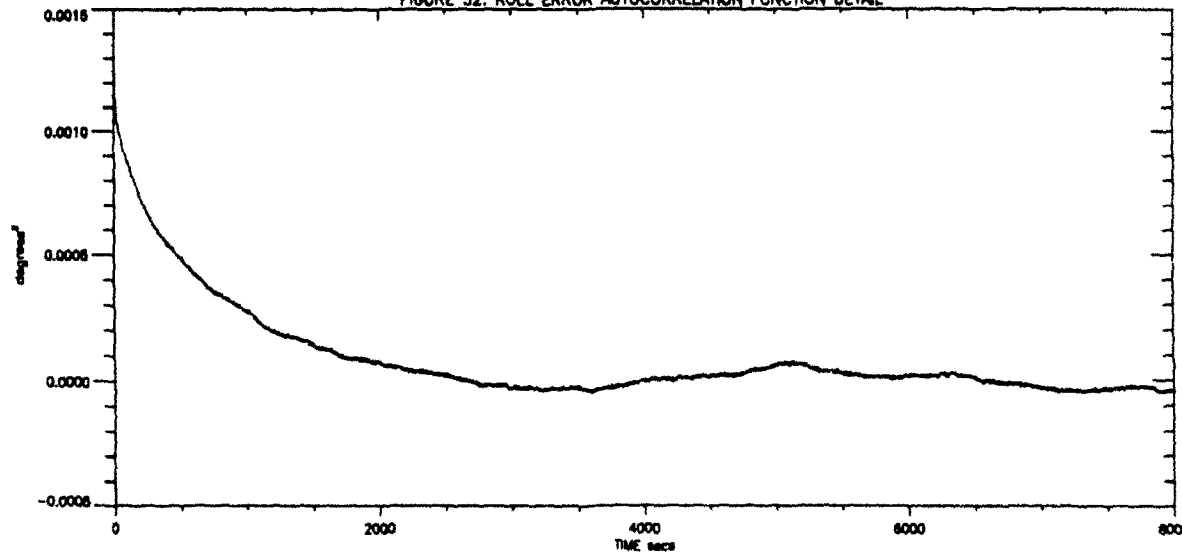


FIGURE 53: HEADING ERROR AUTOCORRELATION (FINE DETAIL)

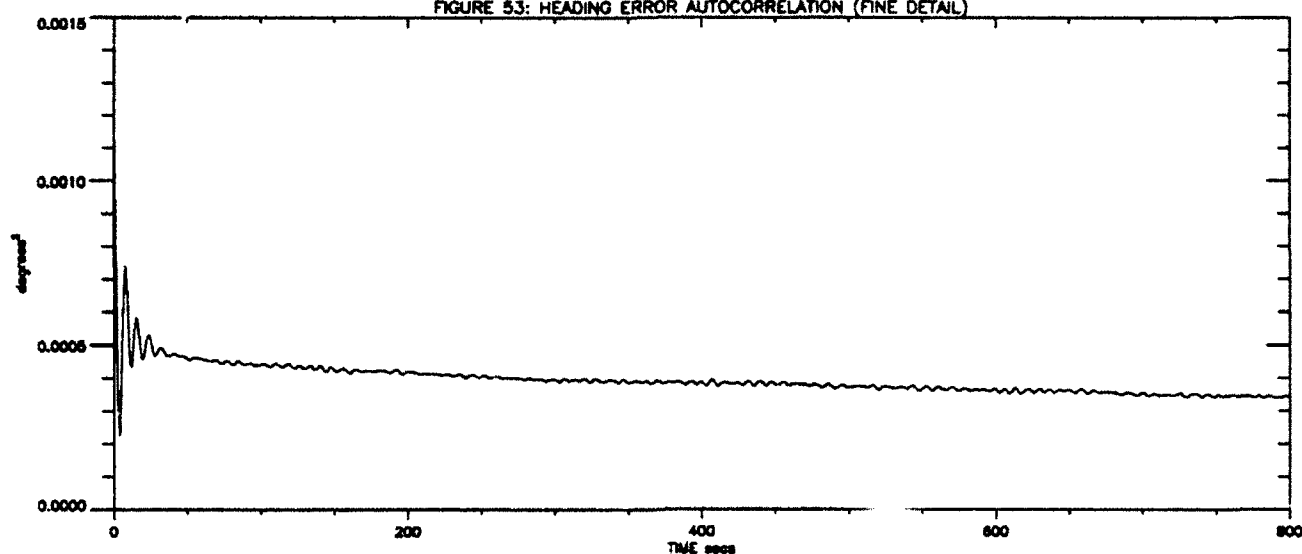


FIGURE 54: PITCH ERROR AUTOCORRELATION (FINE DETAIL)

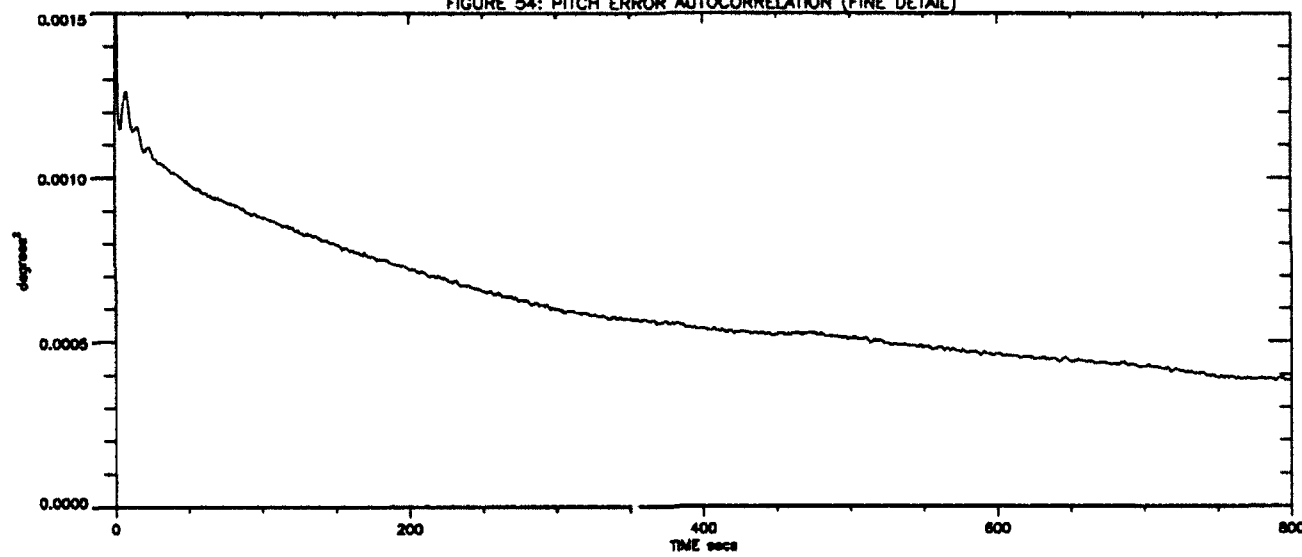


FIGURE 55: ROLL ERROR AUTOCORRELATION FUNCTION (FINE DETAIL)

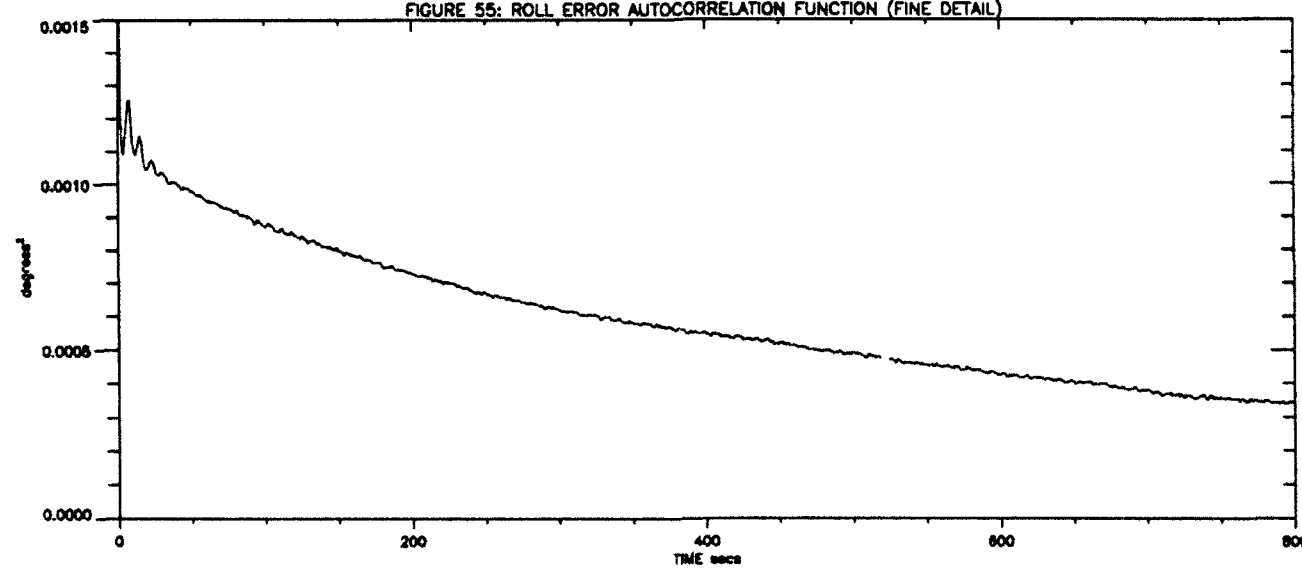


FIGURE 56: HEADING/PITCH CROSS-CORRELATION FUNCTION

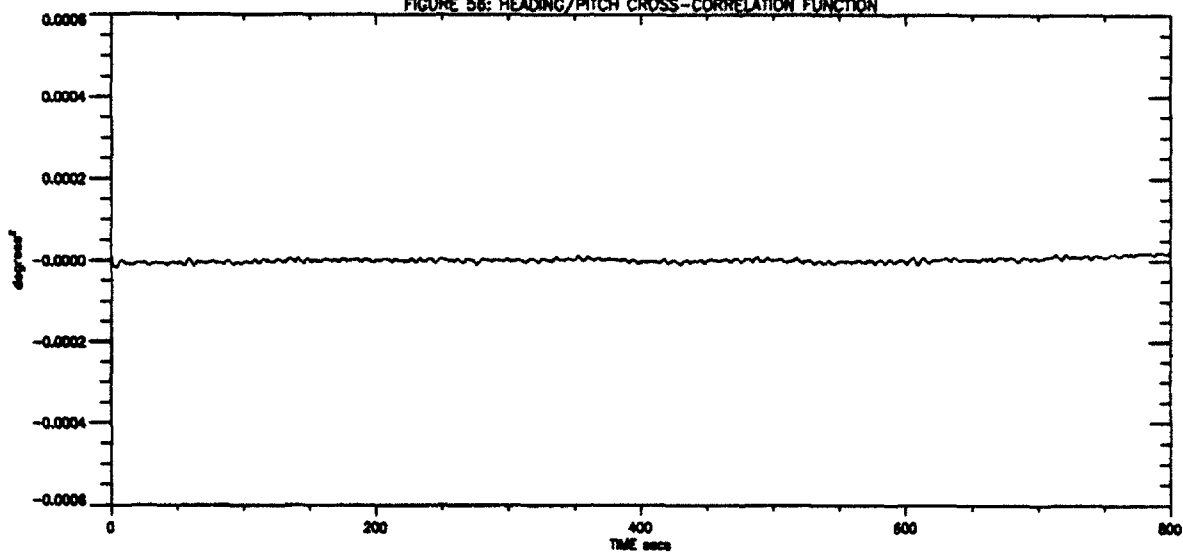


FIGURE 57: HEADING/ROLL CROSS-CORRELATION FUNCTION

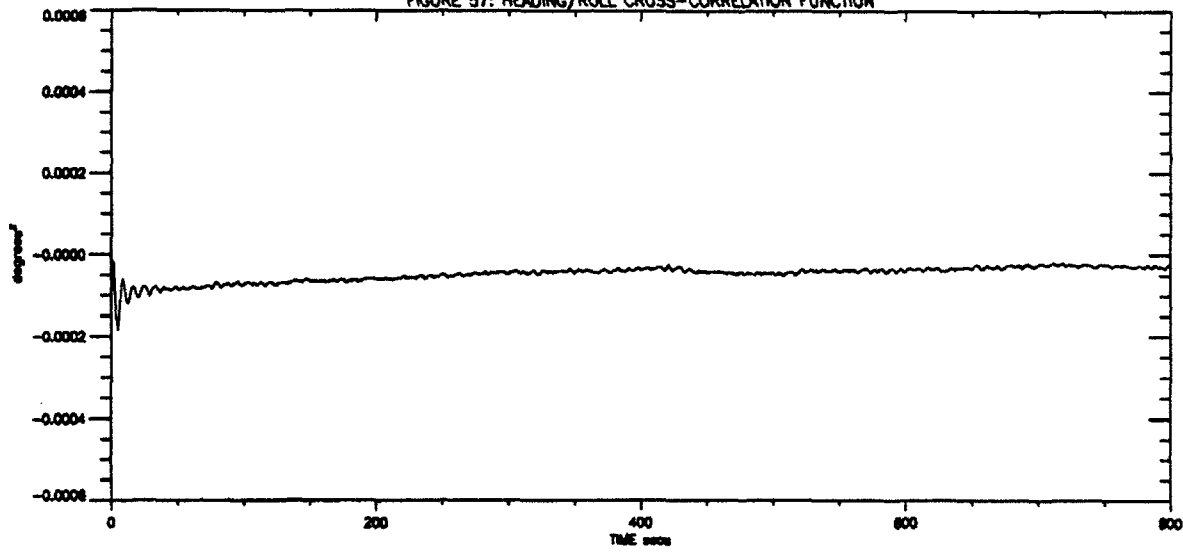


FIGURE 58: PITCH/ROLL CROSS-CORRELATION FUNCTION

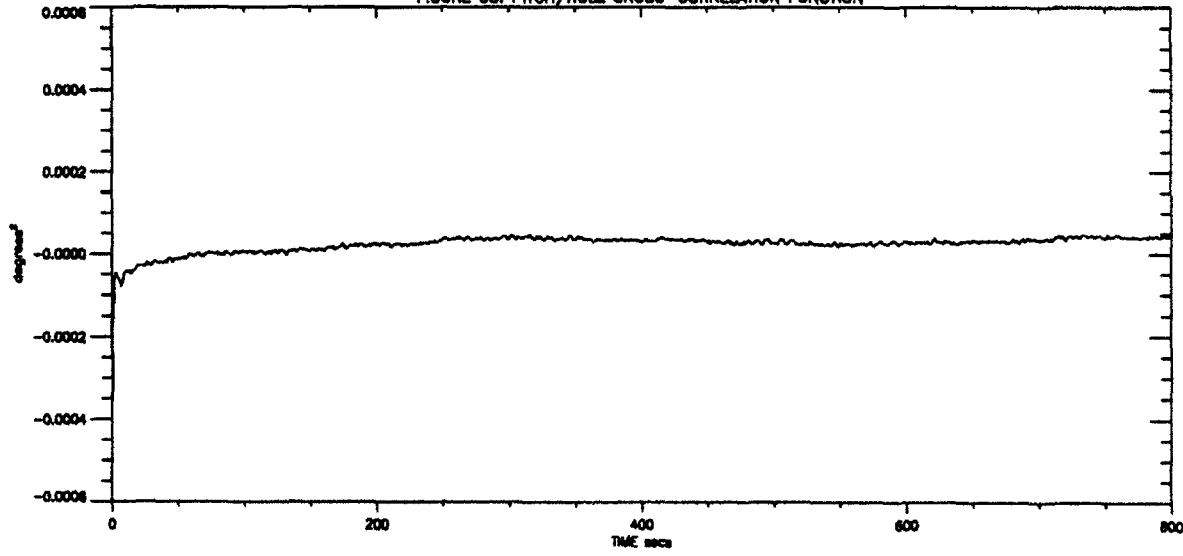


FIGURE 59: HEADING/PITCH CROSS-CORRELATION FUNCTION (DETAIL)

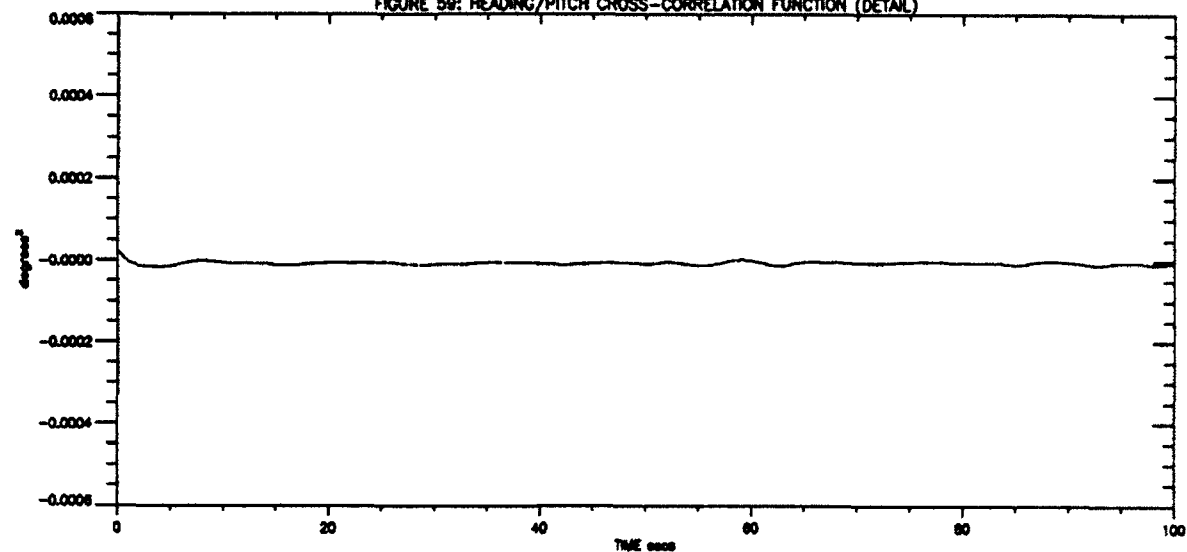


FIGURE 60: HEADING/ROLL CROSS-CORRELATION FUNCTION (DETAIL)

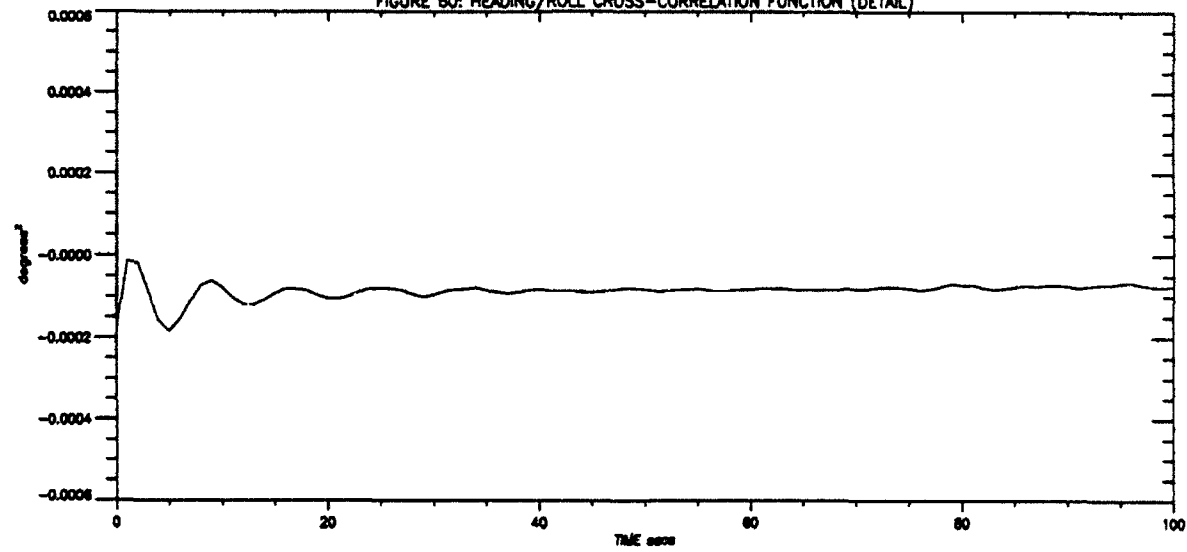
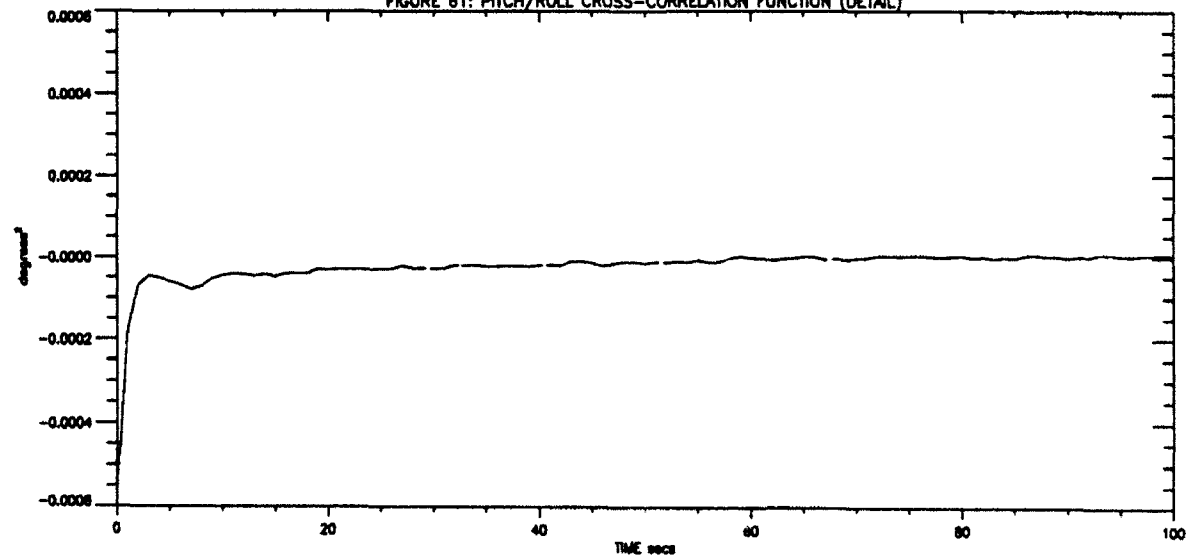


FIGURE 61: PITCH/ROLL CROSS-CORRELATION FUNCTION (DETAIL)



7. ACKNOWLEDGMENTS

This investigation was carried out with financial support from DMCS 6-5, in support of the MINS (Marine Integrated Navigation System) project. The marine inertial system data was collected primarily for the DIINS (Dual Inertial Integrated Navigation System) project, which is also partially sponsored by DMCS. The Ashtech 3DF receiver was provided on loan by EDO Canada Ltd. of Calgary. The differential GPS reference data was provided under contract by McElhanney Surveying and Engineering Ltd. of Vancouver.

The data collection sea trial itself was conducted using the DREP (Defence Research Establishment Pacific) research vessel Endeavour. The post processing and analysis of the data was done using the DREO Navigation Group's integrated systems software development simulation facilities.

8. CONCLUSIONS

This data clearly demonstrates that this type of GPS receiver has the potential to provide very useful dynamic attitude information at a reasonable cost. This is especially true in the static case if multipath can be avoided and in the dynamic case if inertial aiding is available. The data collected on this trial demonstrates that this receiver can provide high quality attitude, at a one Hz rate, with 80% availability, over a seven day period.

The statistics for the discrete-dynamic attitude errors (errors at the 3DF one second data points) are given in Table 4, repeated here:

TABLE 4. DISCRETE-DYNAMIC 3DF ATTITUDE ERRORS

SOURCE	RMS ERROR (degrees)	STANDARD DEVIATION (degrees)	PERCENTILE (degrees)				
			raw		bias removed		
			68%	95%	68%	95%	100%
HEADING	0.47	0.47	0.08	0.13	0.04	0.08	56.7
PITCH	1.14	0.27	1.13	1.20	0.05	0.11	4.5
ROLL	1.28	0.26	1.27	1.34	0.05	0.11	6.5

Perhaps the most significant statistics here are the 95% errors with bias removed. For the heading error this was only 0.08 degrees (1.4 milliradians) and for the pitch and roll it was 0.11 degrees (1.9 milliradians). Although the bias errors were much more significant, they likely could have been removed by a more careful installation/calibration procedure. The larger RMS and standard deviation values are due to a small amount (1%) of spurious data.

The dominant stochastic error model parameters, derived from the valid 3DF data with bias and spurious points removed, are shown in Table 6, repeated here:

TABLE 6. DISCRETE 3DF ERROR MODEL PARAMETERS

	BIAS*	σ_0 (degrees)	WHITE NOISE	MARKOV	
				σ_2 (degrees)	τ_2 (seconds)
HEADING $\delta\theta$	0.1		0.03	0.022	4,000
PITCH $\delta\phi$	1.0		0.04	0.035	600
ROLL $\delta\psi$	1.0		0.04	0.035	600

* order of magnitude only

There were also various other smaller components identified in Section 6 above, but the most important, from a Kalman filtering point of view, are the white noise and Markov components. These important components are all about the same magnitude, between 0.022 and 0.04 degrees (0.4 and 0.7 milliradians). The correlation time for the pitch and roll Markov errors was about ten minutes, and for the heading was about one hour. Integration with an inertial system should easily remove the white noise component, and also part of the Markov components (especially for pitch and roll, which have short correlation times).

There were some significant discontinuities in the heading error corresponding to ship maneuvers, suggesting that multipath was a problem. Also, about 1% of the data was "spurious" (errors in excess of 0.2 degrees).

These observations can be given with confidence, since they are such that the errors of the inertially based reference system could not have significantly influenced them. This is because the stochastic behaviour of an inertial system is well known and occupies a different part of the autocorrelation spectrum. This complementary nature of the error characteristics in fact bodes well for the prospects of obtaining a synergistic improvement in performance through the Kalman filter integration of these two types of system.

It should also be mentioned that the cost of this type of receiver is expected to come down in the future. In fact other models of this type of attitude measuring GPS receiver are already available, at substantially lower cost. For example the Trimble "Tans Vector" is being offered for less than \$20K. If the performance of these lower cost receivers is comparable to that of the Ashtech 3DF, as determined here, then they will make very attractive sensors, to complement or replace inertially based systems.

Of course significant advances are also being made in fiber optic gyro technology, which could improve the cost/performance ratio of the inertial systems as well. Since the two technologies are so complementary, this leads one to believe that more combined systems will be used in the future. There are already various inertial systems available with built-in GPS positioning receivers, some of which are even tightly coupled (optimally integrated).

References

- [1] J. Kilvington, "A Proposal for a Navstar Interferometric Attitude Reference System," Royal Aircraft Establishment Tech Memo: Rad-Nav 51, April 1977.
- [2] A.S. Brown, W.M. Bowles, T.P. Thorvaldsen, "Interferometric Attitude Determination Using Global Positioning System: A New Gyrotheodolite," Unknown Conference Proceedings circa 1981.
- [3] P. Rodgers, "Interim Technical Report, Phase I Task I, Proof of Concept for Azimuth Determination Using Transit Satellite System," prepared for the Defence Research Establishment Ottawa, May 1983.
- [4] B.R. Hermann, "A Simulation of the Navigation and Orientation Potential of the Geostar Receiver," Naval Surface Weapons Centre Report: NSWC TR 83-377, Dahlgren, VA, USA, October 1983.
- [5] Starnav Report #144 Final Report to National Research Council PILP Committee (Program for Industry/Laboratory Projects), January 1987.
- [6] K. Ferguson, S. Gourevitch, M. Kuhl, X. Qin, "Attitude Determination with the Ashtech Three-Dimensional Direction Finding System," Ashtech publication, 1991.
- [7] R.D. Jurgens, C.E. Rodgers, L.C. Fan, "Advances in GPS Attitude Determining Technology as Developed for the Strategic Defence Command," Proceedings of the 4th International Technical Meeting of the Institute of Navigation ION-GPS 91, Albuquerque, N. Mexico, September 1991.
- [8] K.P. Schwarz, A. El-Moaawafy, M. Wei, "Testing a GPS Attitude System in Kinematic Mode," Proceedings of the 5th International Technical Meeting of the Institute of Navigation ION-GPS 92, Albuquerque, N. Mexico, September 1992.
- [9] C.R. Johnson, P.W. Ward, C.H. Turner, S.D. Roemeran, "Applications of a Multiplexed GPS User Set," presented to the Institute of Navigation, Summer 1981.
- [10] X. Qin, S. Gourevitch, K. Ferguson, M. Kuhl, J. Ladd, "Dynamic Short Baseline Calibration & Attitude Determination Using Ashtech 3DF System," Proceedings of the 6th International Geodetic Symposium On Satellite Positioning, Columbus, Ohio, March 1992.
- [11] M. Vinnins, "Conduct of the Navigation Systems Sea Trial 92-01," DREO Tech Note, March 1993.
- [12] J.C. McMillan, J.S. Bird, D.A.G. Arden, "An Hierarchic Alliance of Filters for Fault Tolerant Navigation Using Two Inertial Systems with Aiding Sensors," Proceedings of AGARD Specialists Meeting on Integrated And Multi-Function Navigation, Ottawa, May 92.
- [13] K.R. Britting, *Inertial Navigation Systems Analysis*, John Wiley & Sons, Inc, Toronto, 1971.
- [14] *Applied Optimal Estimation*, edited by A. Gelb, M.I.T. Press, Massachusetts Institute of

Technology, 1974.

- [15] A. Papoulis, *Probability, Random Variables, and Stochastic Processes*, McGraw-Hill Book Company, Toronto, 1965.
- [16] T.E. Dabbous, J.C. McMillan, D.F. Liang and N.U. Ahmed, "Filtering of Discontinuous Processes Arising in Marine Integrated Navigation Systems," IEEE Transactions on Aerospace and Electronic Systems, Vol. 24, No. 1, January 1988.

APPENDIX A. PLATFORM DYNAMICS

Since we are only interested in the angular velocity and acceleration, to place limits on the data latency and interpolation errors, we shall assume that *for short periods of time* the local angular behaviour can be approximated by a sinusoidal variation in attitude θ , (heading, pitch or roll) presumably induced primarily by interactions with ocean waves. That this is so can be clearly seen from the detailed plots of Figures 12 to 14. Therefore we shall model the attitude angle θ as:

$$\theta = \theta_0 + A \sin(\omega t + \phi) \quad (A1)$$

where A is the local angular amplitude and ω is the phase rate (in radians/second). Then the angular rate $\partial\theta/\partial t$ will then be

$$\frac{\partial\theta}{\partial t} = \omega A \cos(\omega t + \phi) \quad (A2)$$

and the acceleration $\partial^2\theta/\partial t^2$ will be

$$\frac{\partial^2\theta}{\partial t^2} = -\omega^2 A \sin(\omega t + \phi) \quad (A3)$$

Thus we can place limits on the platform dynamics of:

$$\left| \frac{\partial\theta}{\partial t} \right| \leq |\omega A| \quad (A4)$$

and

$$\left| \frac{\partial^2\theta}{\partial t^2} \right| \leq |\omega^2 A| \quad (A5)$$

We can see from the data (Figures 9 to 14, for example) that the local angular amplitude, A , during this trial was less than about 4 degrees (and largely less than 2 degrees):

$$|A| < 4 \text{ degrees} \quad (A6)$$

and that the period was about 6 seconds. Therefore the phase rate ω was at most about

$$\begin{aligned} \omega &\approx 2\pi/6 \\ &= 1.05 \text{ radians/second} \end{aligned} \quad (A7)$$

which from A4 and A5 place limits on the angular rate and acceleration:

$$\left| \frac{\partial \theta}{\partial t} \right| < (1.05 \text{ radians/sec}) (4 \text{ degrees}) \\ = 4.2 \text{ degrees/sec.} \quad (A8)$$

and

$$\left| \frac{\partial^2 \theta}{\partial t^2} \right| < (1.05 \text{ radians/sec})^2 (4 \text{ degrees}) \\ \approx 4.4 \text{ degrees/sec.}^2 \quad (A9)$$

APPENDIX B. DAILY ERROR PLOTS

This appendix simply shows the discrete attitude errors, with biases removed, of the valid 3DF data throughout the sea trial. This is the same data as shown in Figures 20 to 22, but is shown here in 24 hour segments so that the temporal behaviour can be more clearly seen.

For the heading errors of Figures B1 to B7, a second plot is presented in which the noise has been suppressed, using a simple moving-window-averager, to more clearly illustrate the Markov component and the discontinuities.

FIGURE B1: DAY1 DISCRETE HEADING ERROR VS TIME

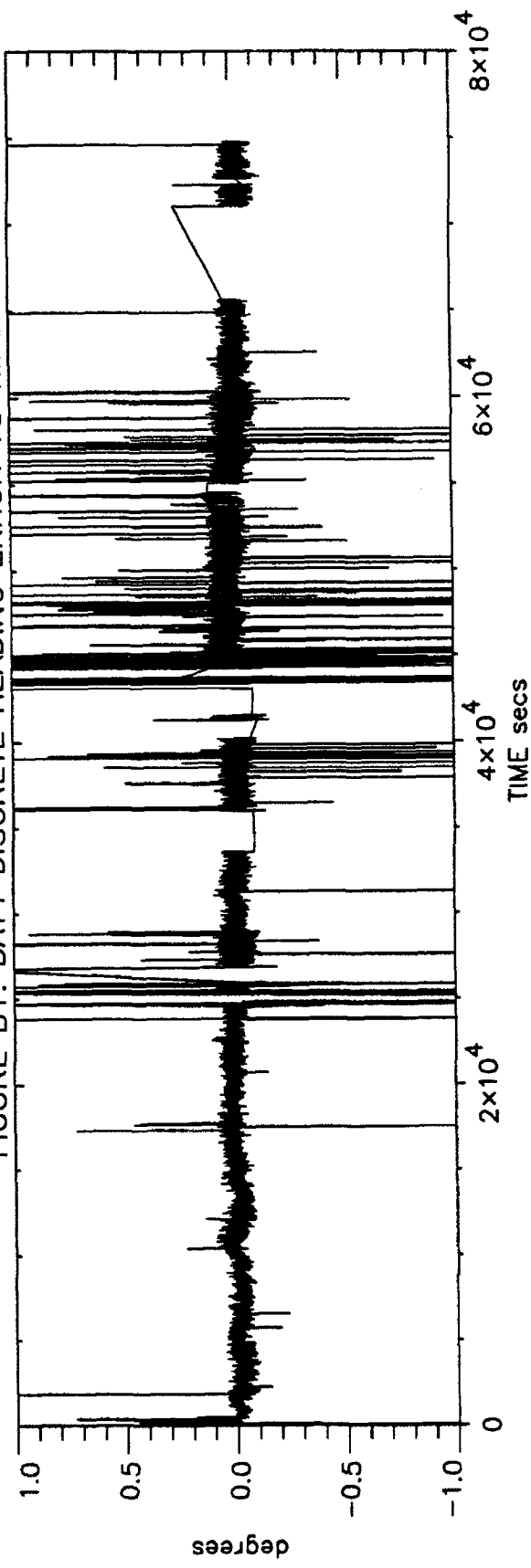


FIGURE B1: DAY1 DISCRETE HEADING ERROR VS TIME

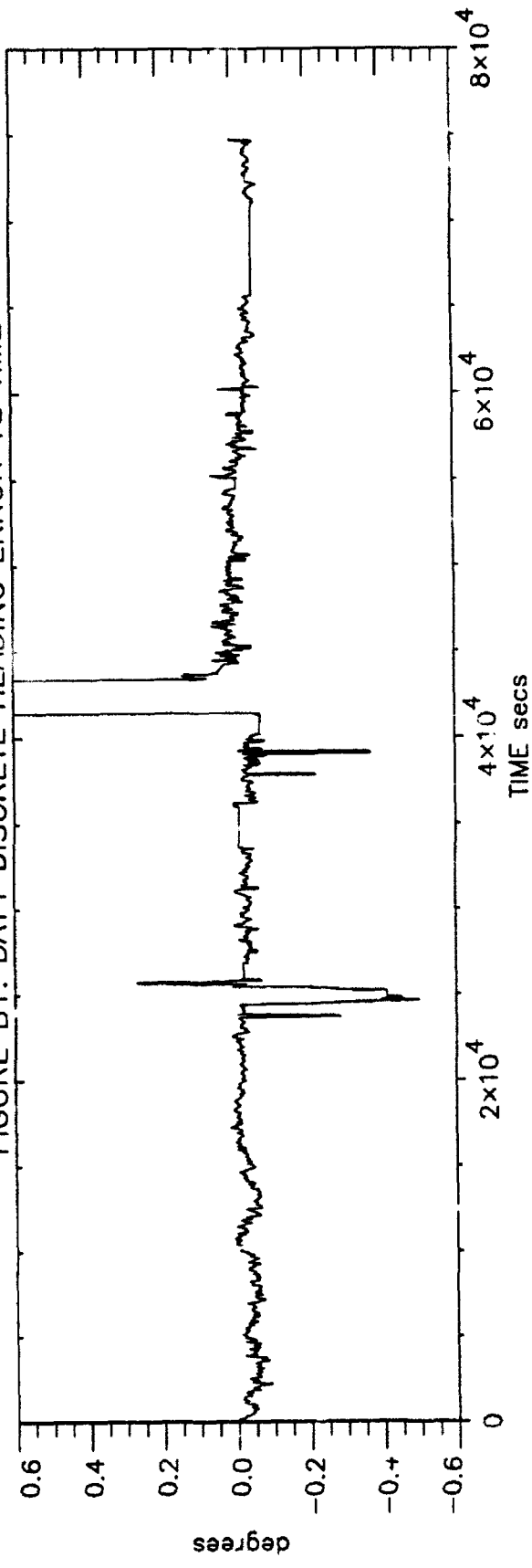


FIGURE B2: DAY2 DISCRETE HEADING ERROR VS TIME

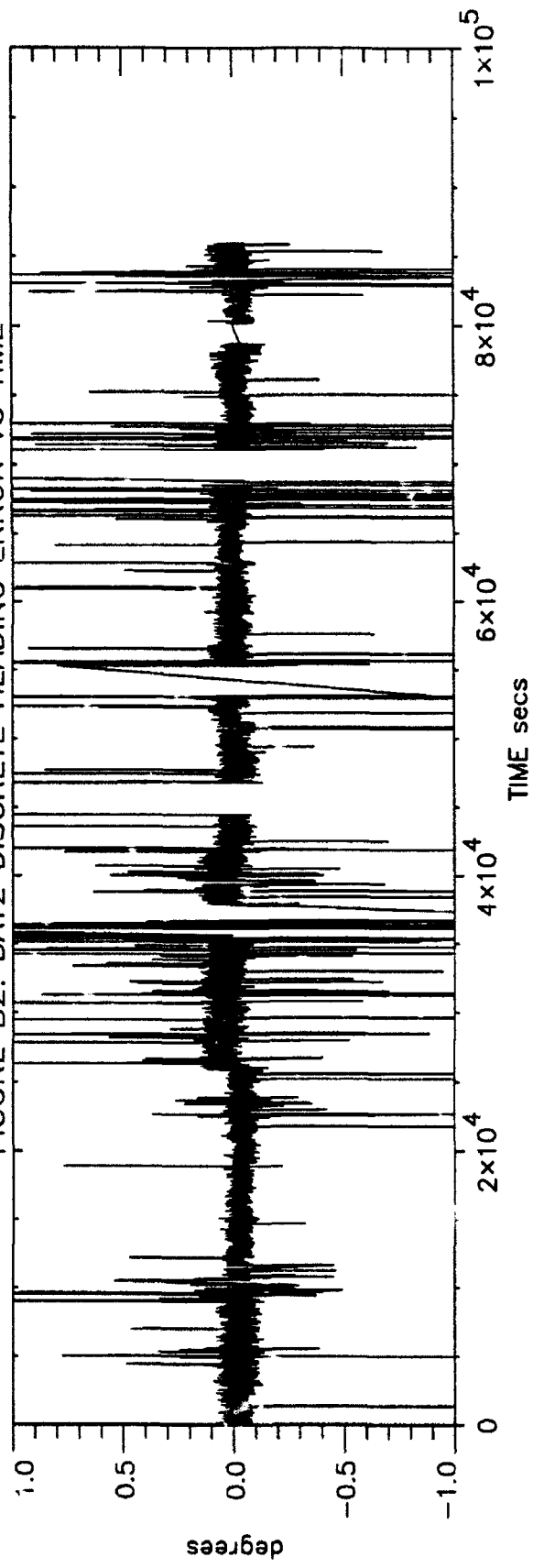


FIGURE B2: DAY2 DISCRETE HEADING ERROR VS TIME

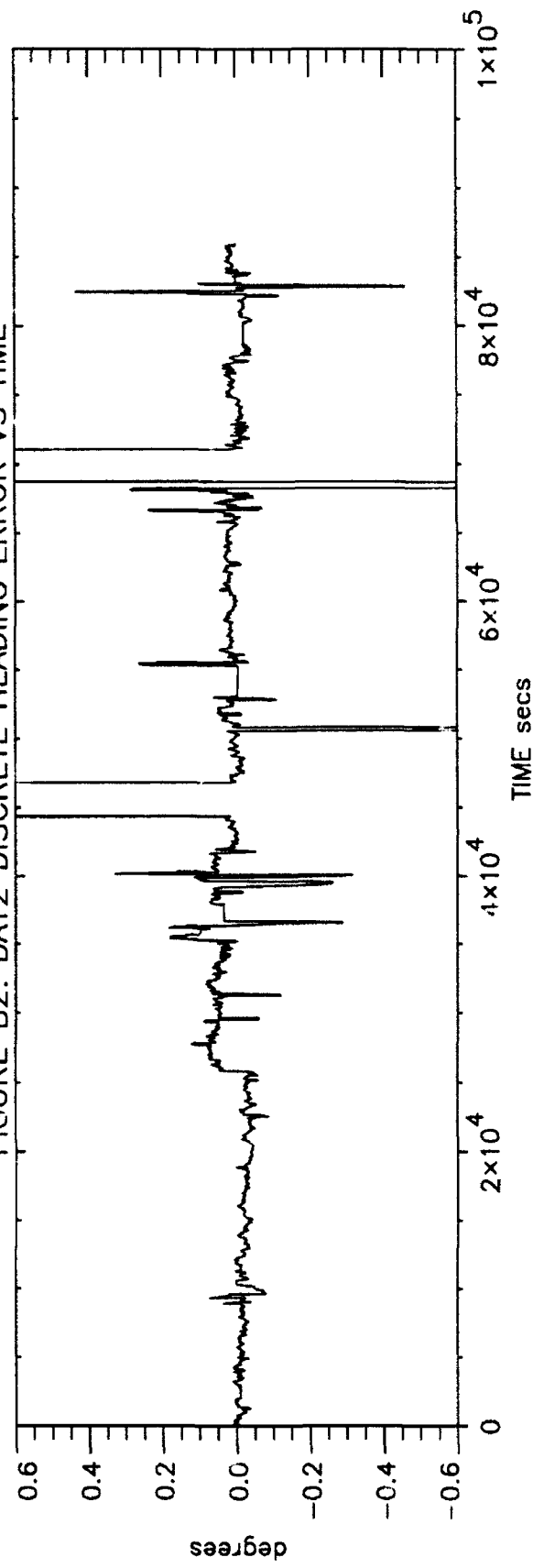


FIGURE B3: DAY3 DISCRETE HEADING ERROR VS TIME

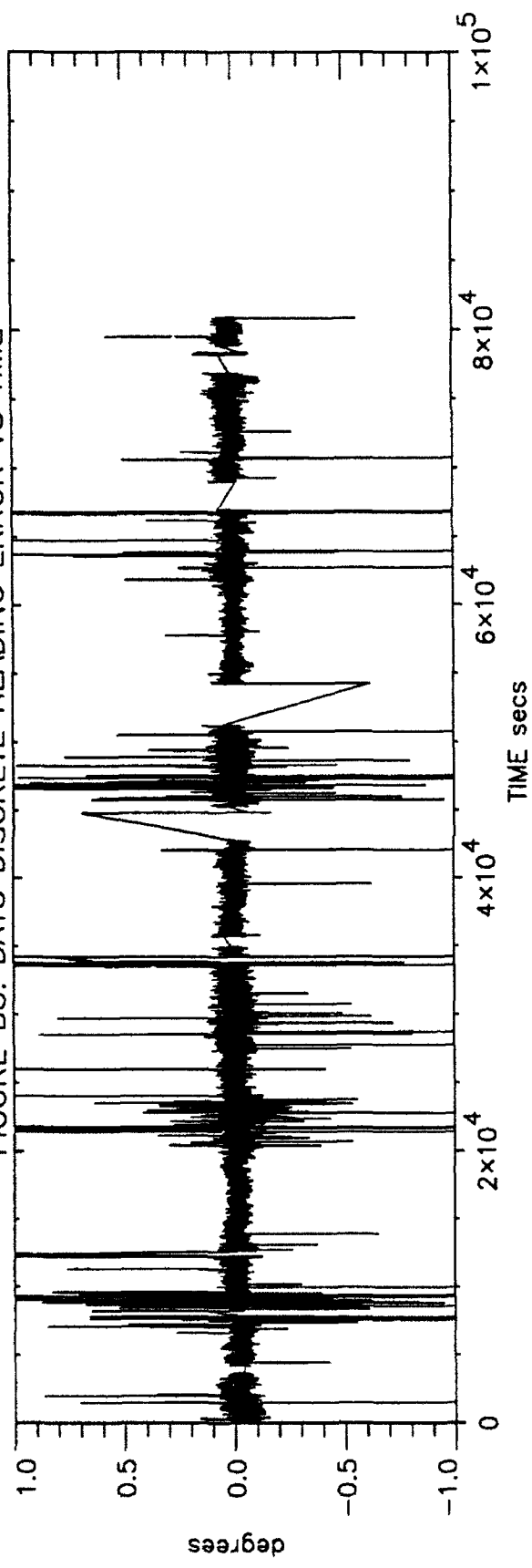


FIGURE B3: DAY3 DISCRETE HEADING ERROR VS TIME

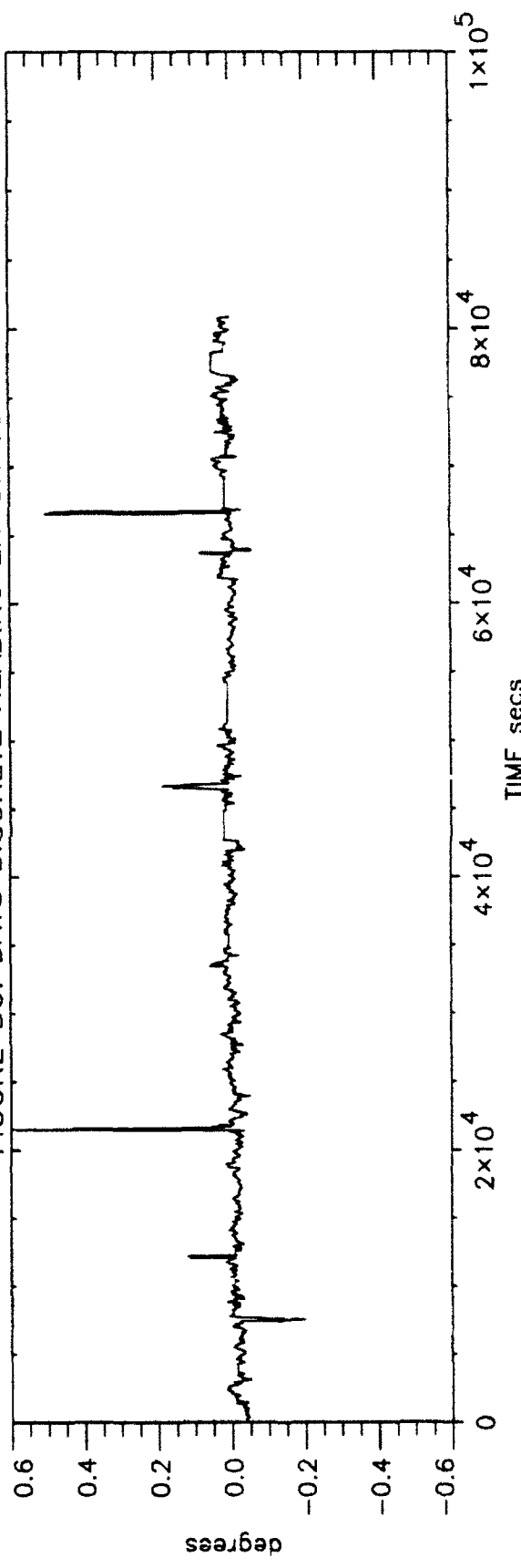


FIGURE B4: DAY4 DISCRETE HEADING ERROR VS TIME

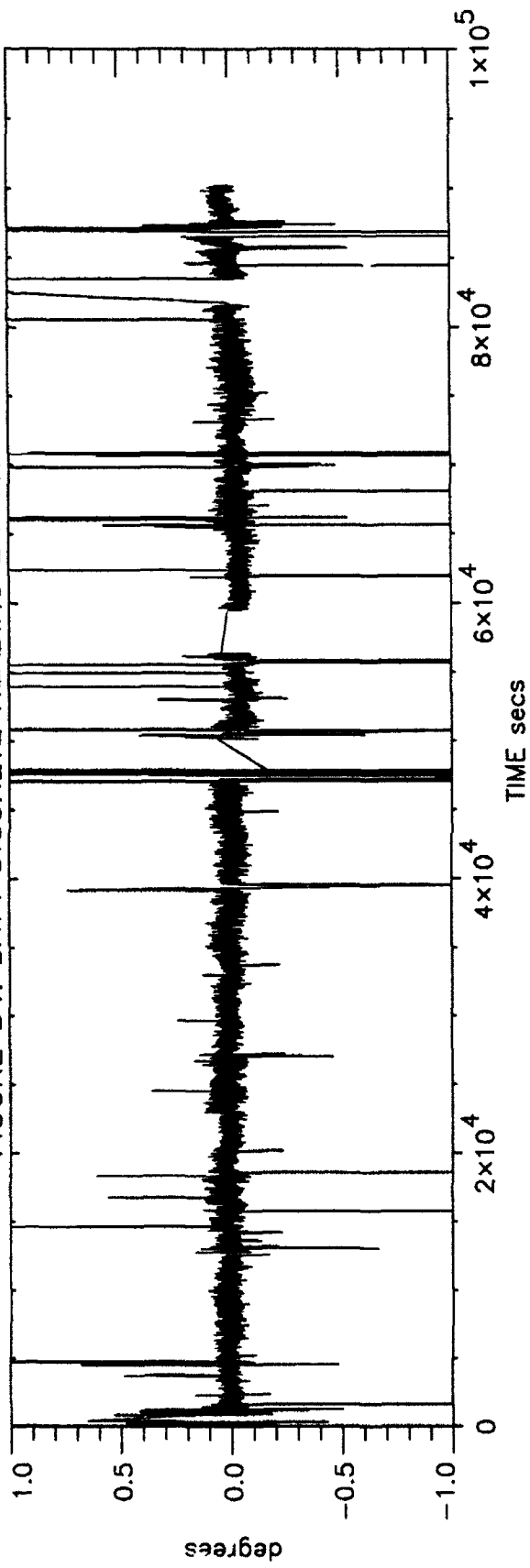


FIGURE B4: DAY4 DISCRETE HEADING ERROR VS TIME

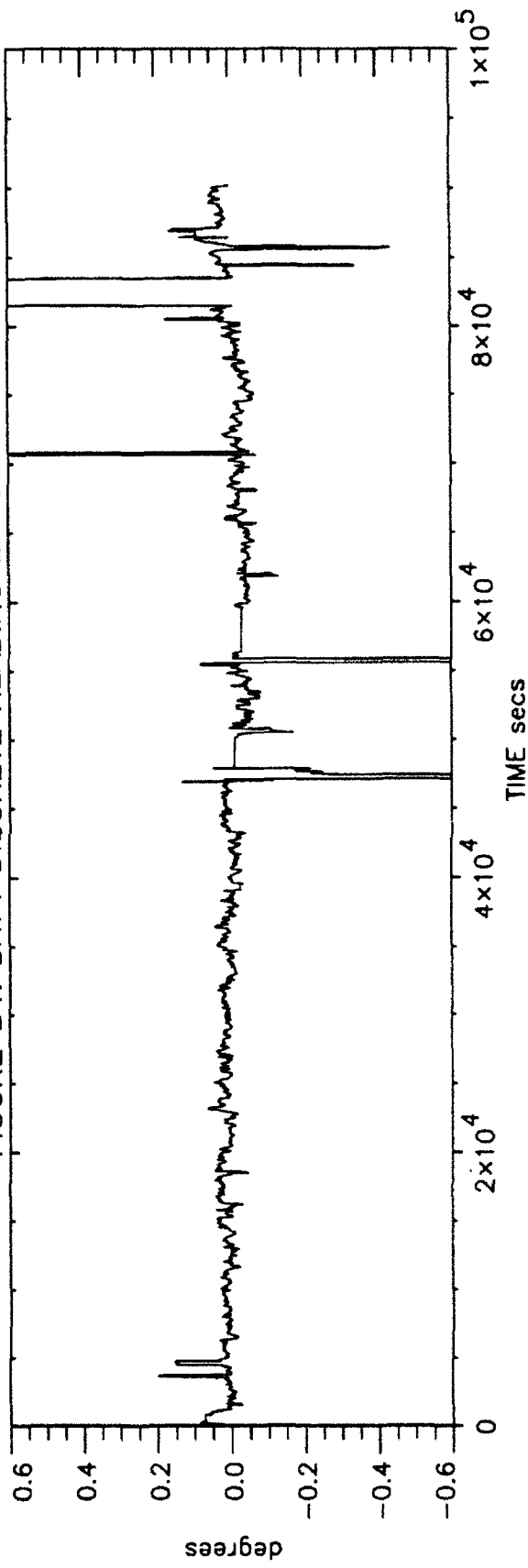


FIGURE B5: DAY5 DISCRETE HEADING ERROR VS TIME

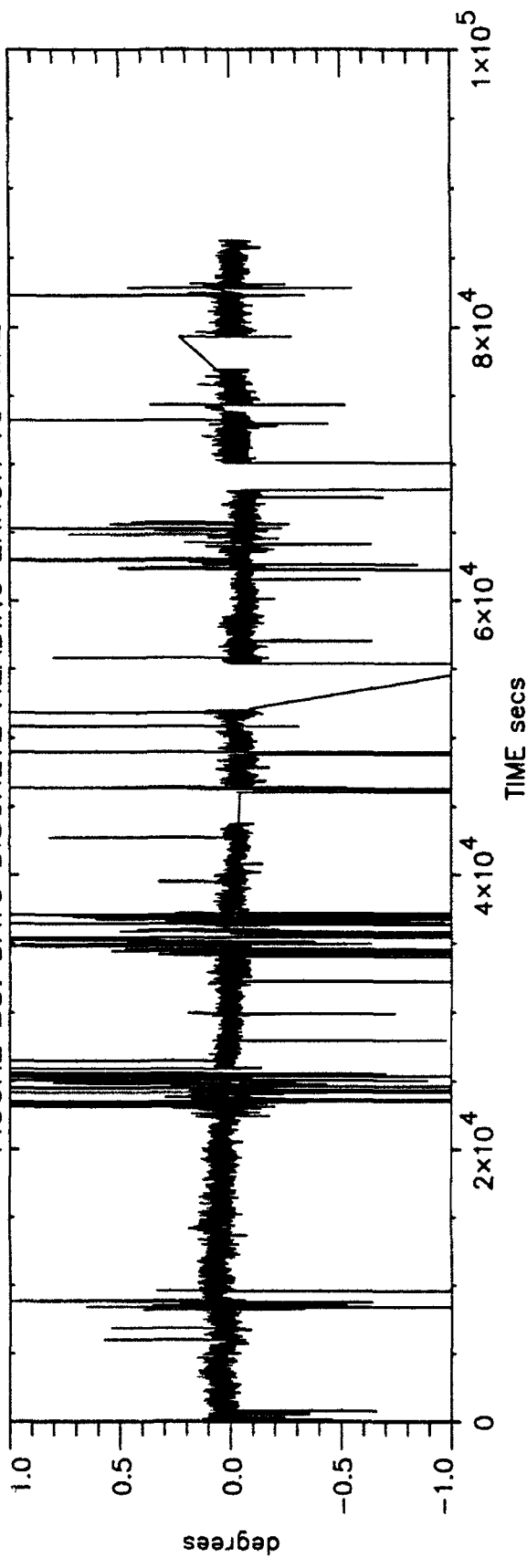


FIGURE B5: DAY5 DISCRETE HEADING ERROR VS TIME

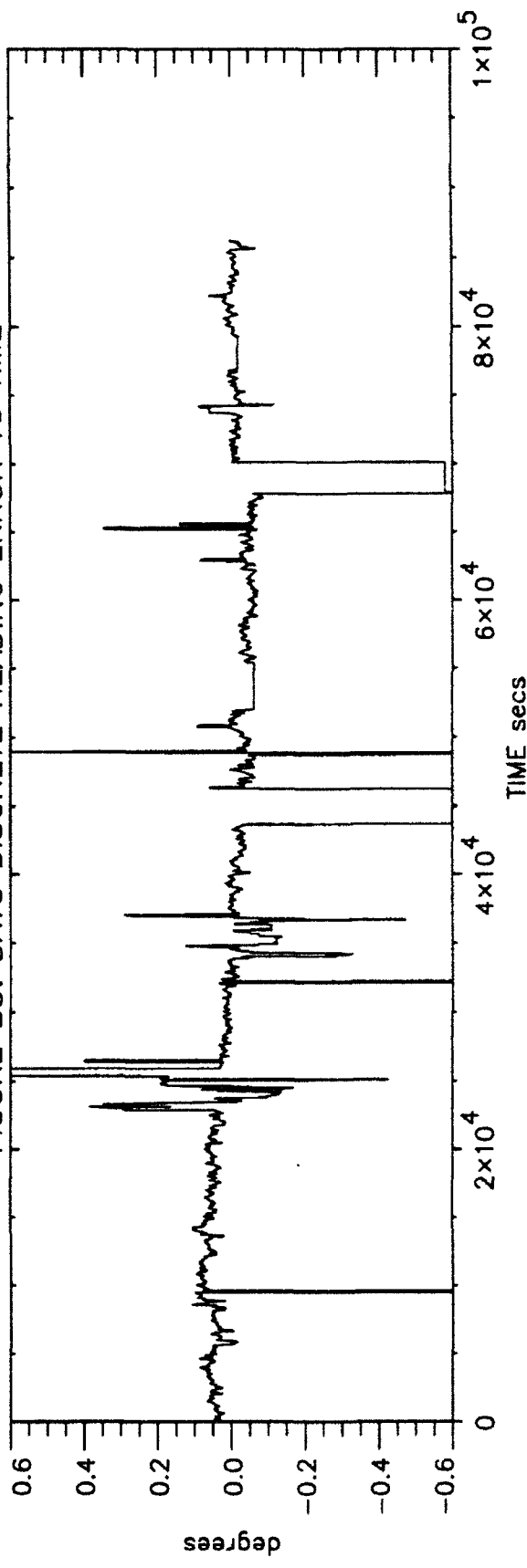


FIGURE B6: DAY6-7 DISCRETE HEADING ERROR VS TIME

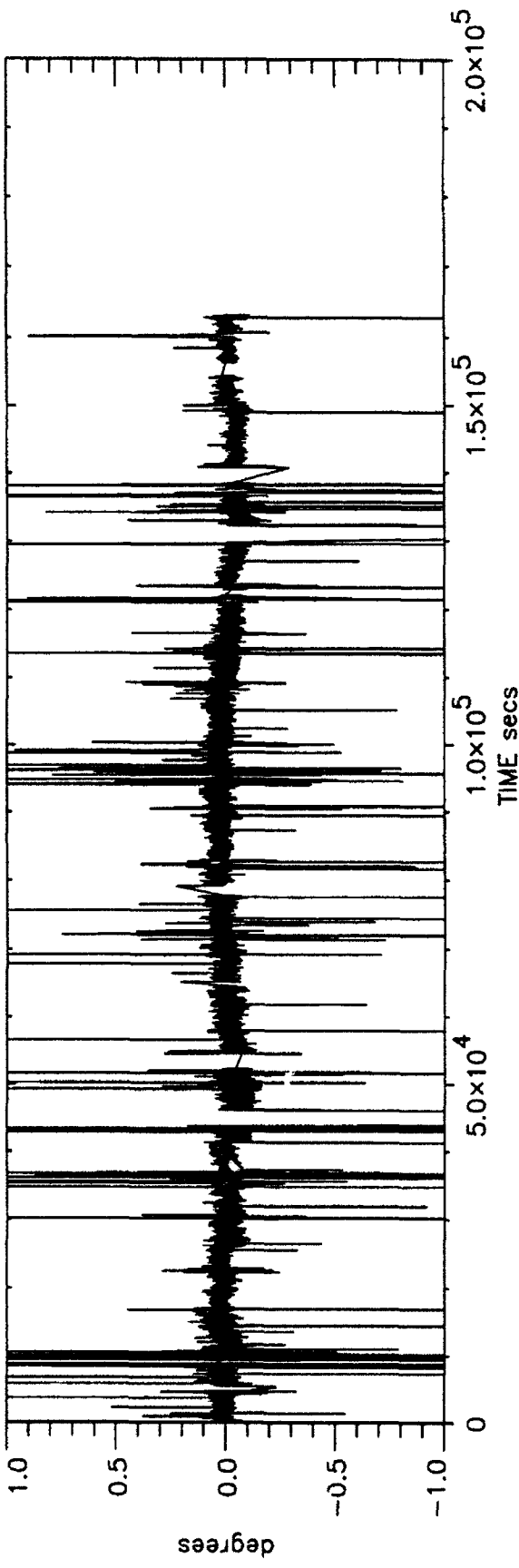


FIGURE B6: DAY6-7 DISCRETE HEADING ERROR VS TIME

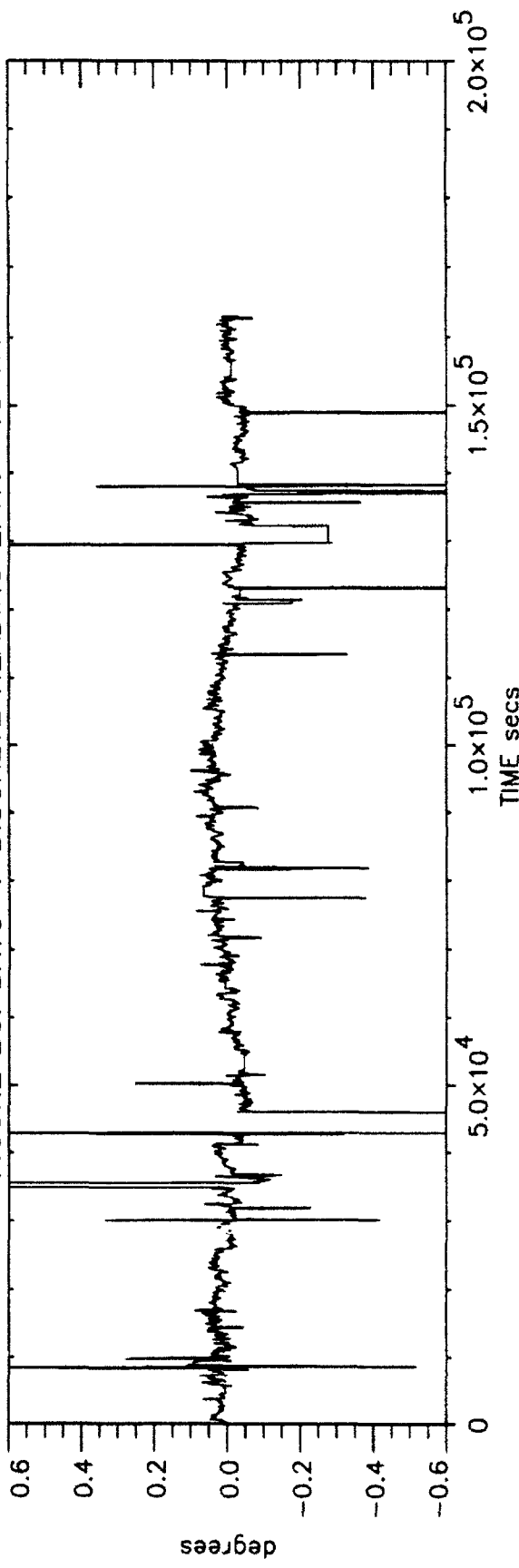


FIGURE B7: DAY1 DISCRETE PITCH ERROR VS TIME

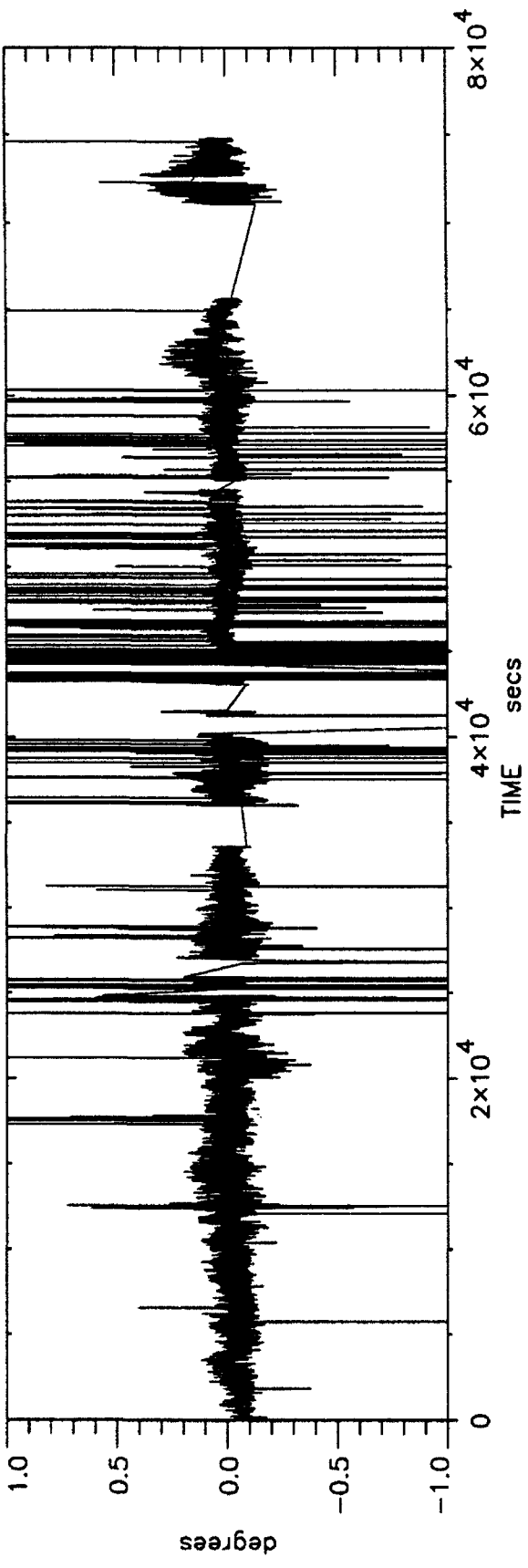


FIGURE B8: DAY1 DISCRETE ROLL ERROR VS TIME

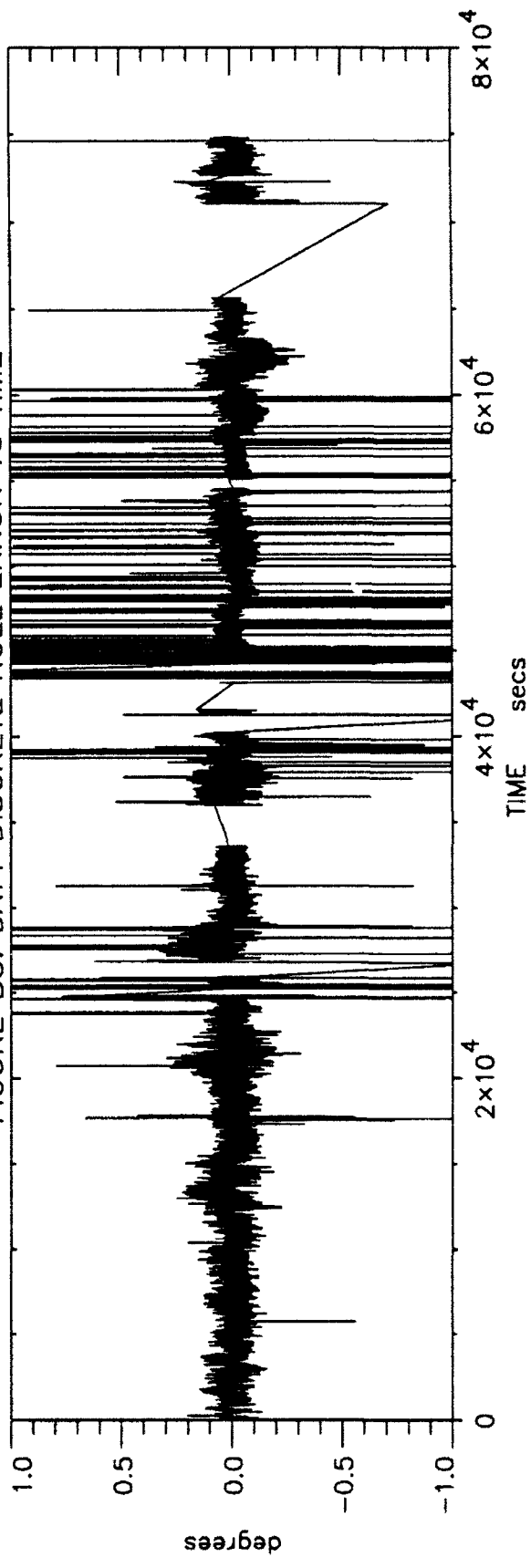


FIGURE B9: DAY2 DISCRETE PITCH ERROR VS TIME

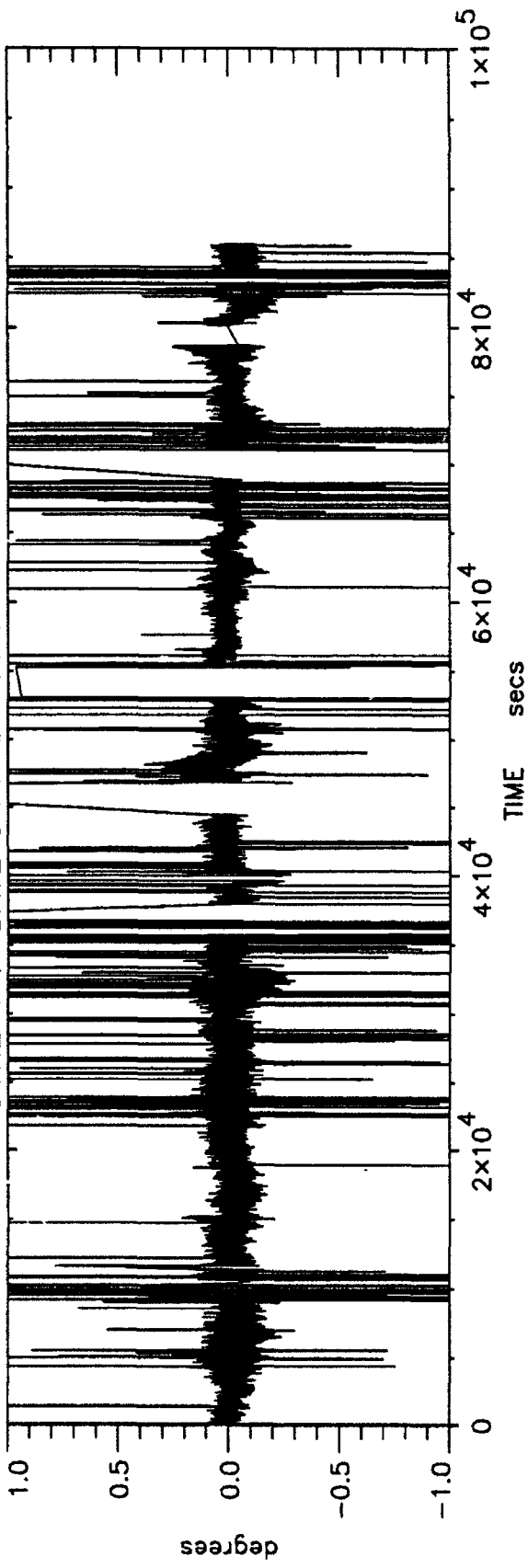


FIGURE B10: DAY2 DISCRETE ROLL ERROR VS TIME

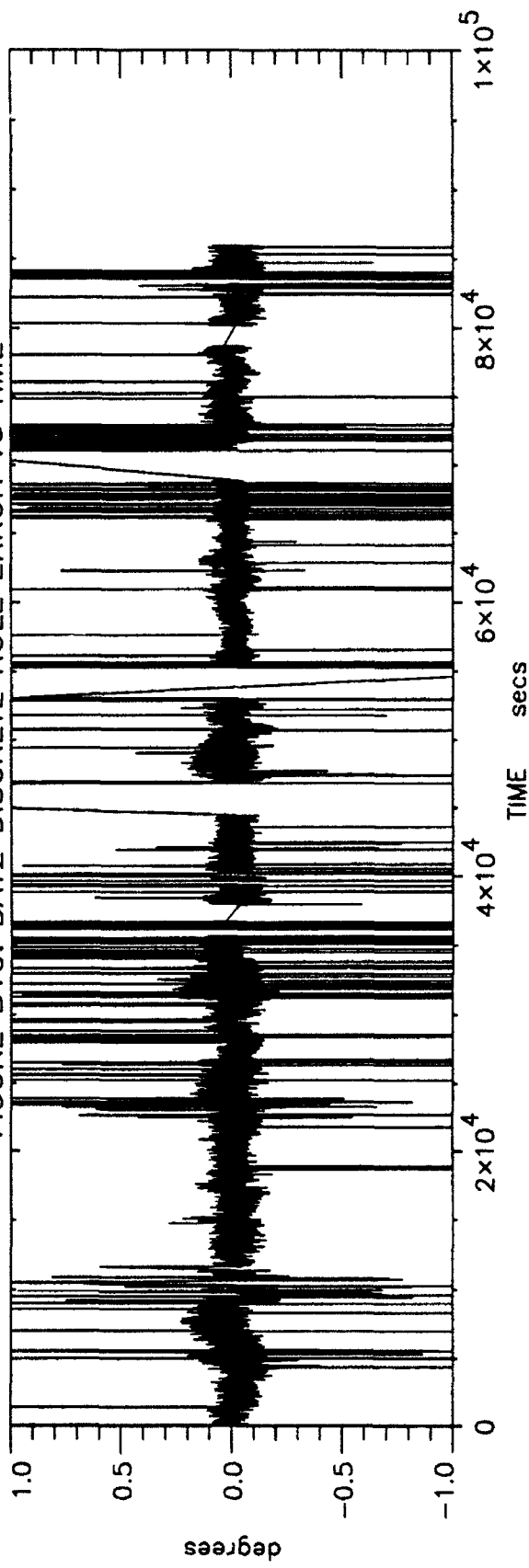


FIGURE B11: DAY3 DISCRETE PITCH ERROR VS TIME

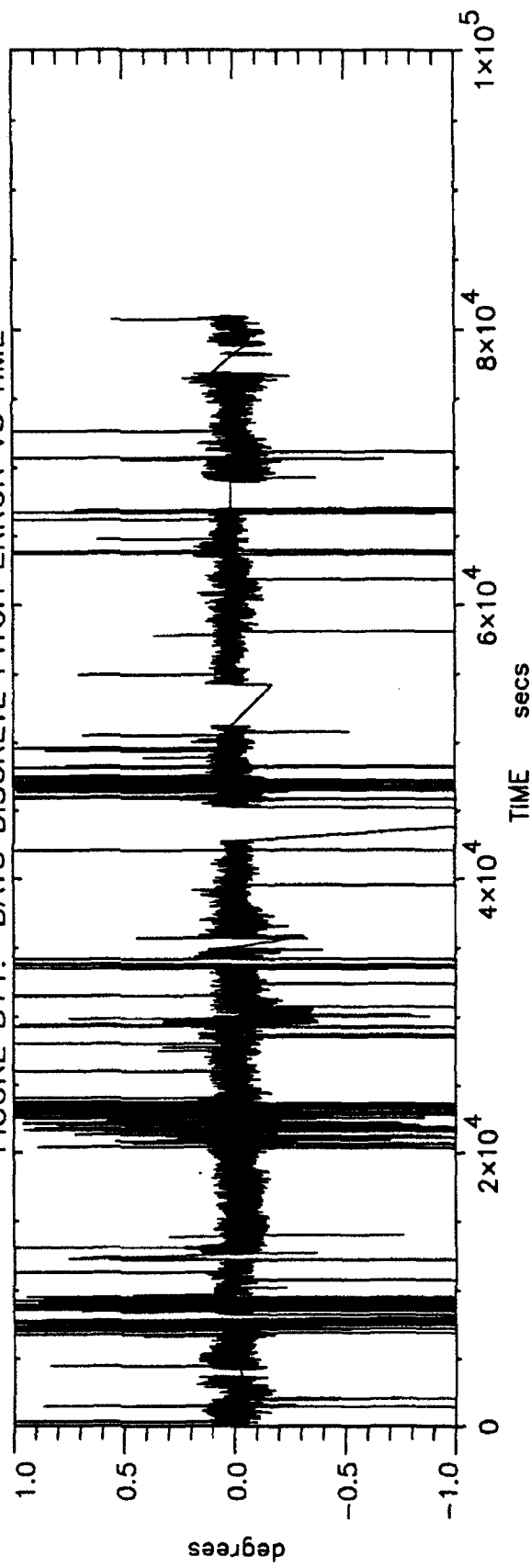


FIGURE B12: DAY3 DISCRETE ROLL ERROR VS TIME

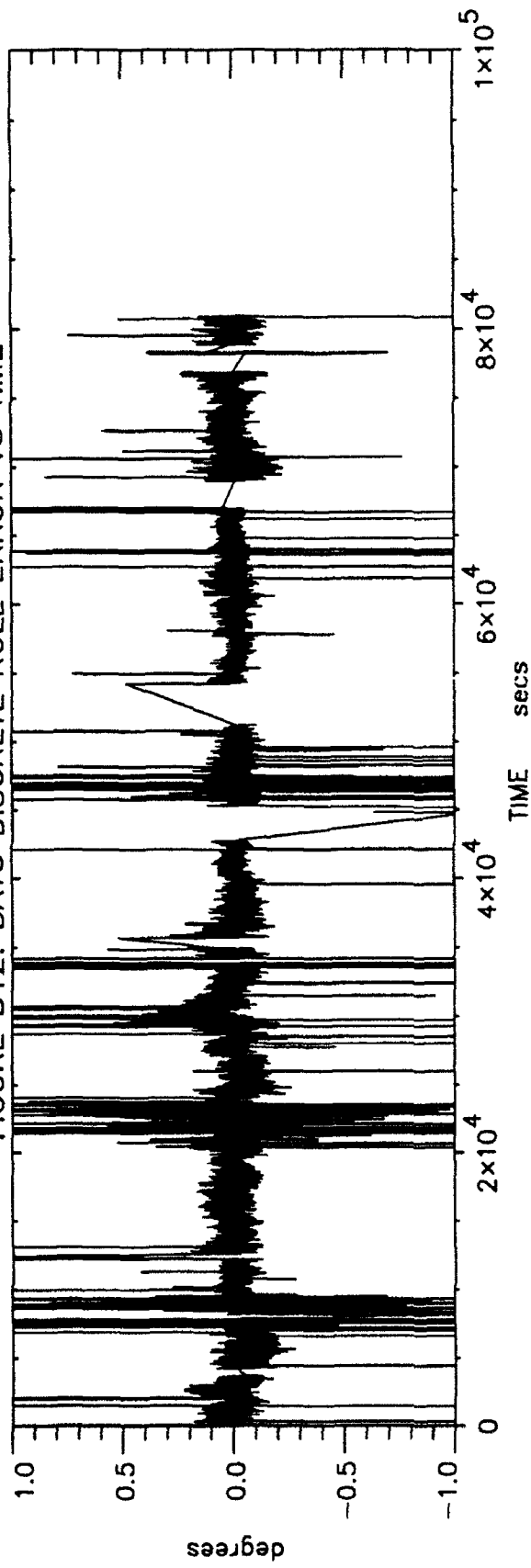


FIGURE B13: DAY4 DISCRETE PITCH ERROR VS TIME

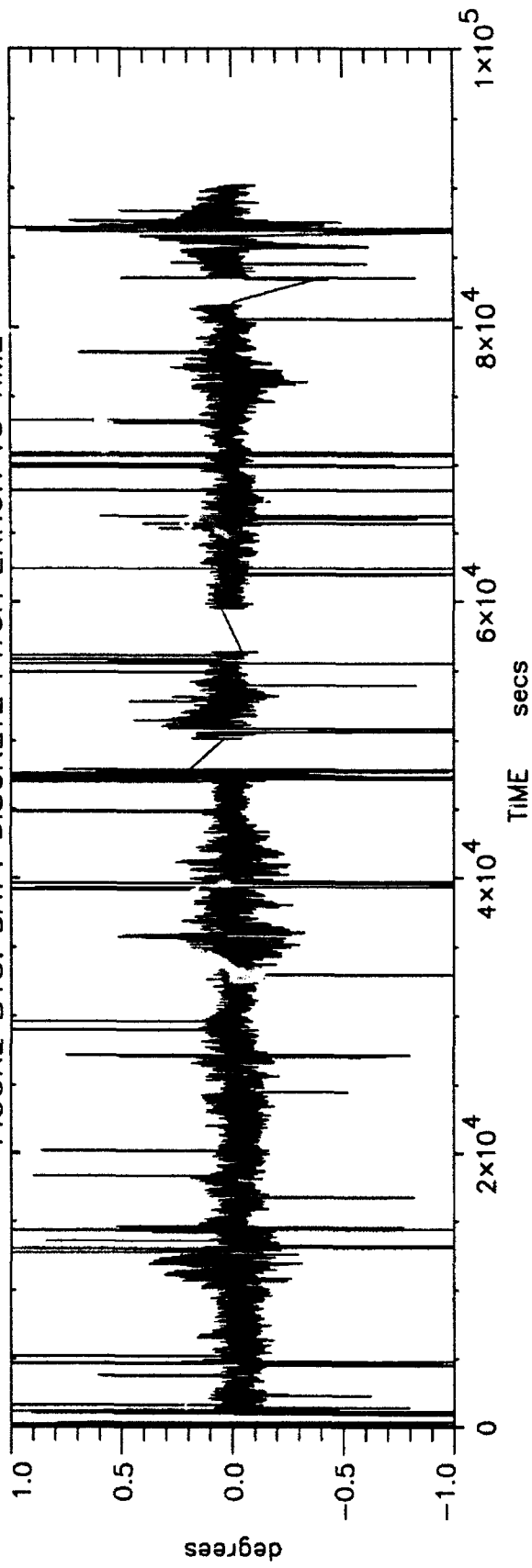


FIGURE B14: DAY4 DISCRETE ROLL ERROR VS TIME

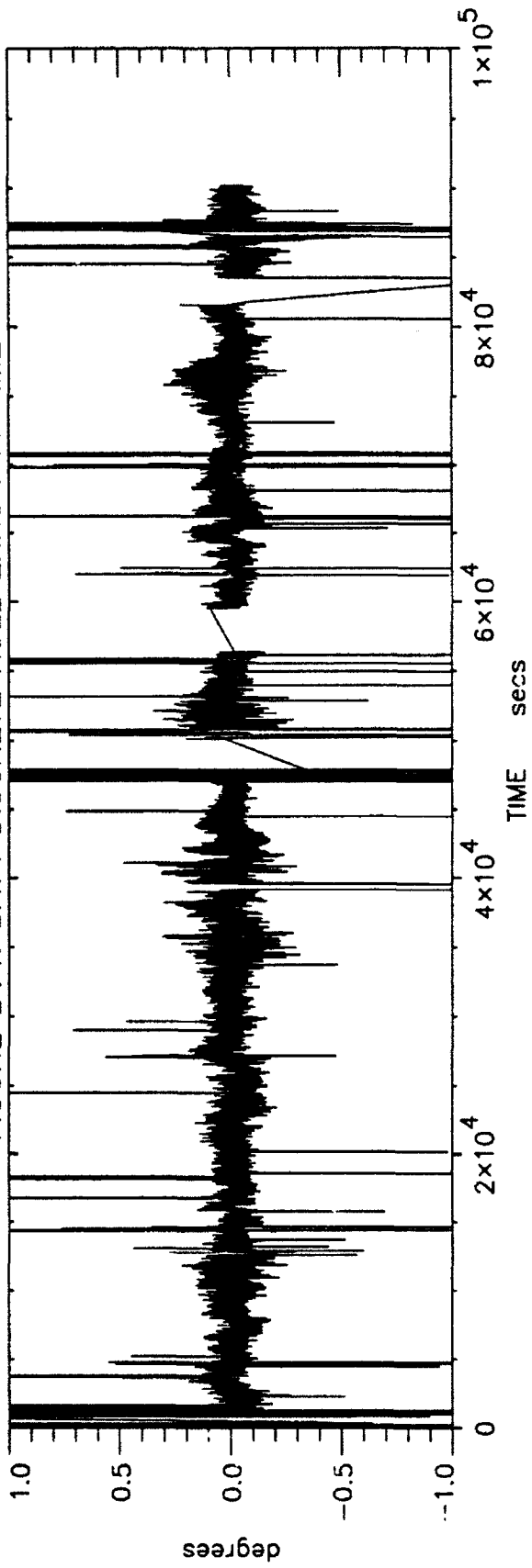


FIGURE B15: DAY5 DISCRETE PITCH ERROR VS TIME

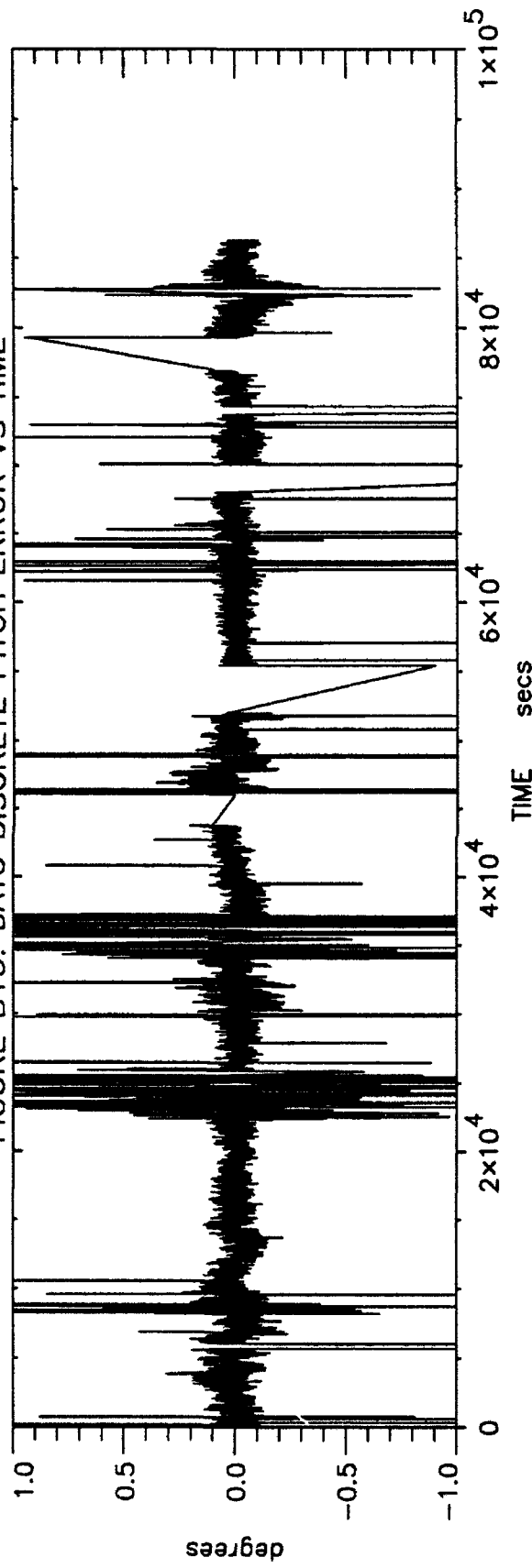


FIGURE B16: DAY5 DISCRETE ROLL ERROR VS TIME

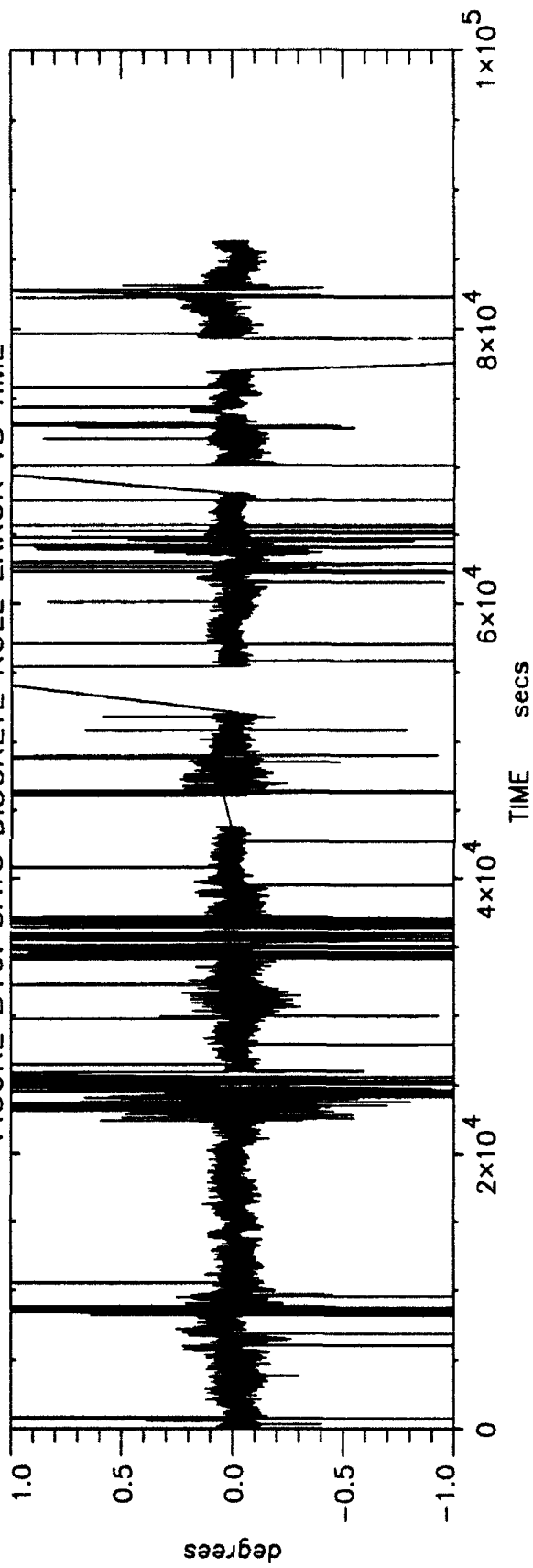


FIGURE B17: DAY6-7 DISCRETE PITCH ERROR VS TIME

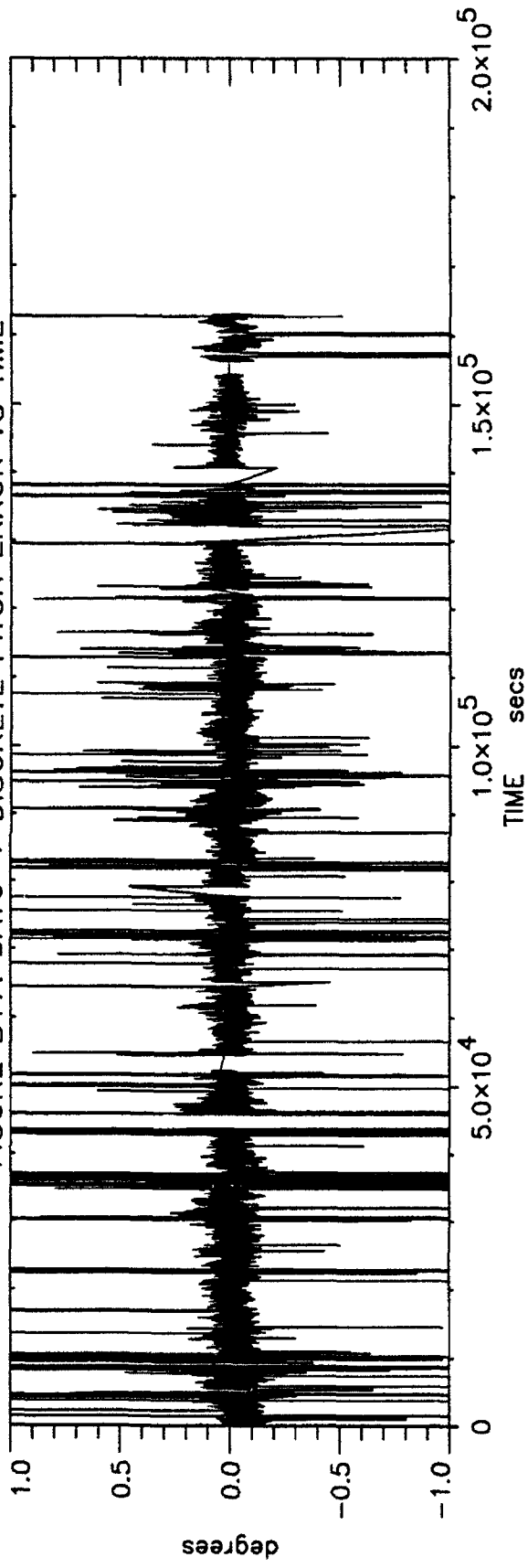
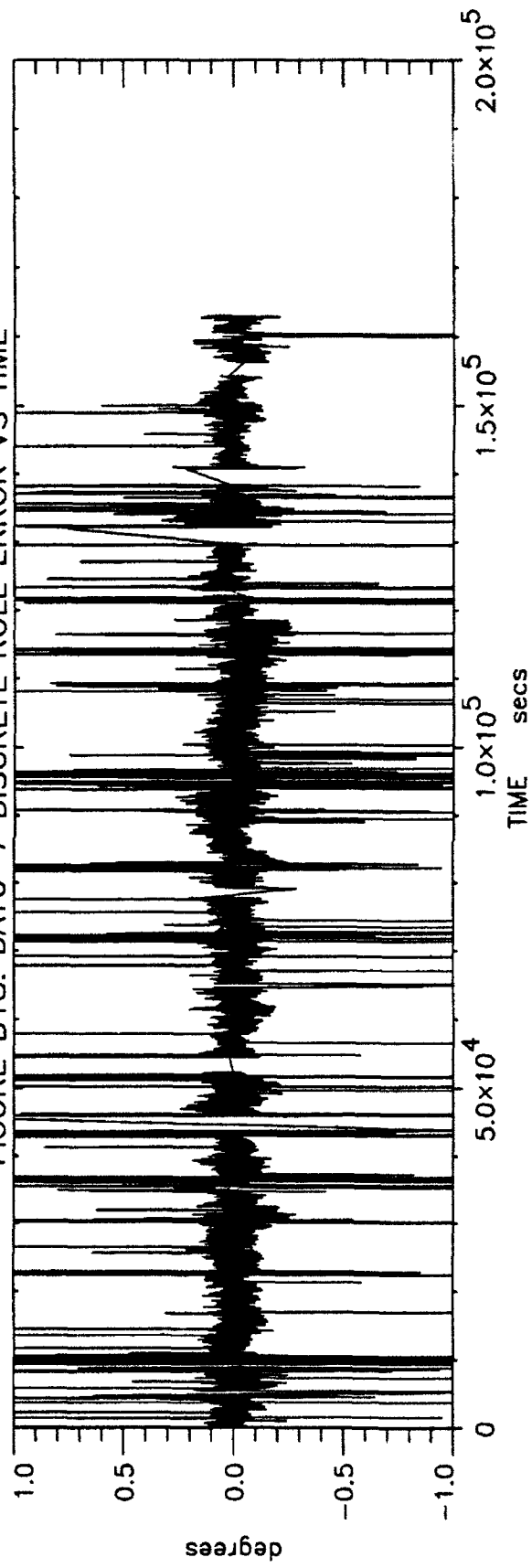


FIGURE B18: DAY6-7 DISCRETE ROLL ERROR VS TIME



UNCLASSIFIED**-71-**

SECURITY CLASSIFICATION OF FORM
(highest classification of Title, Abstract, Keywords)

DOCUMENT CONTROL DATA

(Security classification of title, body of abstract and indexing annotation must be entered when the overall document is classified)

<p>1. ORIGINATOR (the name and address of the organization preparing the document. Organizations for whom the document was prepared, e.g. Establishment sponsoring a contractor's report, or tasking agency, are entered in section 8.) Defence Research Establishment Ottawa Ottawa, Ontario K1A 0K2 </p>	<p>2. SECURITY CLASSIFICATION (overall security classification of the document including special warning terms if applicable) UNCLASSIFIED</p>	
<p>3. TITLE (the complete document title as indicated on the title page. Its classification should be indicated by the appropriate abbreviation (S,C or U) in parentheses after the title.) INTERFEROMETRIC GPS ATTITUDE: A STOCHASTIC ERROR MODEL (U) </p>		
<p>4. AUTHORS (Last name, first name, middle initial) McMillan, J. Chris </p>		
<p>5. DATE OF PUBLICATION (month and year of publication of document) February 1993 </p>	<p>6a. NO. OF PAGES (total containing information. Include Annexes, Appendices, etc.) 77 </p>	<p>6b. NO. OF REFS (total cited in document) 16 </p>
<p>7. DESCRIPTIVE NOTES (the category of the document, e.g. technical report, technical note or memorandum. If appropriate, enter the type of report, e.g. interim, progress, summary, annual or final. Give the inclusive dates when a specific reporting period is covered.) DREO Report </p>		
<p>8. SPONSORING ACTIVITY (the name of the department project office or laboratory sponsoring the research and development. Include the address. Dept of National Defence Ottawa, Ontario K1A 0K2 Attention: DMCS-6 </p>		
<p>9a. PROJECT OR GRANT NO. (if appropriate, the applicable research and development project or grant number under which the document was written. Please specify whether project or grant) 0411J </p>	<p>9b. CONTRACT NO. (if appropriate, the applicable number under which the document was written)</p>	
<p>10a. ORIGINATOR'S DOCUMENT NUMBER (the official document number by which the document is identified by the originating activity. This number must be unique to this document.) DREO Report 1168 </p>	<p>10b. OTHER DOCUMENT NOS. (Any other numbers which may be assigned this document either by the originator or by the sponsor)</p>	
<p>11. DOCUMENT AVAILABILITY (any limitations on further dissemination of the document, other than those imposed by security classification)</p> <p>(X) Unlimited distribution <input type="checkbox"/> Distribution limited to defence departments and defence contractors; further distribution only as approved <input type="checkbox"/> Distribution limited to defence departments and Canadian defence contractors; further distribution only as approved <input type="checkbox"/> Distribution limited to government departments and agencies; further distribution only as approved <input type="checkbox"/> Distribution limited to defence departments; further distribution only as approved <input type="checkbox"/> Other (please specify):</p>		
<p>12. DOCUMENT ANNOUNCEMENT (any limitation to the bibliographic announcement of this document. This will normally correspond to the Document Availability (11). However, where further distribution (beyond the audience specified in 11) is possible, a wider announcement audience may be selected.) Unlimited Announcement </p>		

UNCLASSIFIED

SECURITY CLASSIFICATION OF FORM

RA.W : 17 Dec 90

UNCLASSIFIED

SECURITY CLASSIFICATION OF FORM

13. **ABSTRACT** (a brief and factual summary of the document. It may also appear elsewhere in the body of the document itself. It is highly desirable that the abstract of classified documents be unclassified. Each paragraph of the abstract shall begin with an indication of the security classification of the information in the paragraph (unless the document itself is unclassified) represented as (S), (C), or (U). It is not necessary to include here abstracts in both official languages unless the text is bilingual).

During the August 1992 sea trial off the west coast of Vancouver Island, onboard the CFAV Endeavour, data was collected from a relatively new type of GPS (Global Positioning System) receiver which measures attitude (heading, pitch and roll) as well as the usual GPS measurements of position and velocity. GPS attitude has the potential to provide rapid and precise attitude for a relatively low cost. Attitude is conventionally determined using inertial equipment, which for precise work is very expensive, large and requires a long "settling time" after turn-on. The receiver being evaluated on this sea trial was an Ashtech Three-Dimensional Direction Finding System (3DF). This report provides some general background on GPS attitude technology, presents the attitude errors observed during this sea trial and characterizes these errors as stochastic processes.

14. **KEYWORDS, DESCRIPTORS or IDENTIFIERS** (technically meaningful terms or short phrases that characterize a document and could be helpful in cataloguing the document. They should be selected so that no security classification is required. Identifiers, such as equipment model designation, trade name, military project code name, geographic location may also be included. If possible keywords should be selected from a published thesaurus, e.g. Thesaurus of Engineering and Scientific Terms (TEST) and that thesaurus-identified. If it is not possible to select indexing terms which are Unclassified, the classification of each should be indicated as with the title.)

NAVIGATION
GLOBAL POSITIONING SYSTEM
GPS
ATTITUDE
INTERFEROMETRIC
SEA TRIAL
ERROR MODEL

UNCLASSIFIED

SECURITY CLASSIFICATION OF FORM